Very high-temperature impact melt products as evidence for cosmic airbursts and impacts 12,900 years ago

Ted E. Bunch[a,1], Robert E. Hermes[b], Andrew M.T. Moore[c], Douglas J. Kennett[d], James C. Weaver[e], James H. Wittke[a], Paul S. DeCarli[f], James L. Bischoff[g], Gordon C. Hillman[h], George A. Howard[i], David R. Kimbel[j], Gunther Kletetschka[k,l], Carl P. Lipo[m], Sachiko Sakai[m], Zsolt Revay[n], Allen West[o], Richard B. Firestone[p], and James P. Kennett[q]

[a]Geology Program, School of Earth Science and Environmental Sustainability, Northern Arizona University, Flagstaff, AZ 86011; [b]Los Alamos National Laboratory (retired), Los Alamos, NM 87545; [c]College of Liberal Arts, Rochester Institute of Technology, Rochester, NY 14623; [d]Department of Anthropology, Pennsylvania State University, University Park, PA 16802; [e]Wyss Institute for Biologically Inspired Engineering, Harvard University, Cambridge, MA 02138; [f]SRI International, Menlo Park, CA 94025; [g]US Geological Survey, Menlo Park, CA 94025; [h]Institute of Archaeology, University College London, London, United Kingdom; [i]Restoration Systems, LLC, Raleigh, NC 27604; [j]Kimstar Research, Fayetteville, NC 28312; [k]Faculty of Science, Charles University in Prague, and [l]Institute of Geology, Czech Academy of Science of the Czech Republic, v.v.i., Prague, Czech Republic; [m]Institute for Integrated Research in Materials, Environments, and Society (IIRMES), California State University, Long Beach, CA 90840; [n]Forschungsneutronenquelle Heinz Maier-Leibnitz (FRM II), Technische Universität München, Munich, Germany; [o]GeoScience Consulting, Dewey, AZ 86327; [p]Lawrence Berkeley National Laboratory, Berkeley, CA 94720; and [q]Department of Earth Science and Marine Science Instititute, University of California, Santa Barbara, CA 93106

Edited by* Steven M. Stanley, University of Hawaii, Honolulu, HI, and approved April 30, 2012 (received for review March 19, 2012)

It has been proposed that fragments of an asteroid or comet impacted Earth, deposited silica-and iron-rich microspherules and other proxies across several continents, and triggered the Younger Dryas cooling episode 12,900 years ago. Although many independent groups have confirmed the impact evidence, the hypothesis remains controversial because some groups have failed to do so. We examined sediment sequences from 18 dated Younger Dryas boundary (YDB) sites across three continents (North America, Europe, and Asia), spanning 12,000 km around nearly one-third of the planet. All sites display abundant microspherules in the YDB with none or few above and below. In addition, three sites (Abu Hureyra, Syria; Melrose, Pennsylvania; and Blackville, South Carolina) display vesicular, high-temperature, siliceous scoria-like objects, or SLOs, that match the spherules geochemically. We compared YDB objects with melt products from a known cosmic impact (Meteor Crater, Arizona) and from the 1945 Trinity nuclear airburst in Socorro, New Mexico, and found that all of these high-energy events produced material that is geochemically and morphologically comparable, including: (*i*) high-temperature, rapidly quenched microspherules and SLOs; (*ii*) corundum, mullite, and suessite (Fe_3Si), a rare meteoritic mineral that forms under high temperatures; (*iii*) melted SiO_2 glass, or lechatelierite, with flow textures (or schlieren) that form at >2,200 °C; and (*iv*) particles with features indicative of high-energy interparticle collisions. These results are inconsistent with anthropogenic, volcanic, authigenic, and cosmic materials, yet consistent with cosmic ejecta, supporting the hypothesis of extraterrestrial airbursts/impacts 12,900 years ago. The wide geographic distribution of SLOs is consistent with multiple impactors.

tektite | microcraters | oxygen fugacity | trinitite

Manuscript Text

The discovery of anomalous materials in a thin sedimentary layer up to a few cm thick and broadly distributed across several continents led Firestone et al. (1) to propose that a cosmic impact (note that "impact" denotes a collision by a cosmic object either with Earth's surface, producing a crater, or with its atmosphere, producing an airburst) occurred at 12.9 kiloannum (ka; all dates are in calendar or calibrated ka, unless otherwise indicated) near the onset of the Younger Dryas (YD) cooling episode. This stratum, called the YD boundary layer, or YDB, often occurs directly beneath an organic-rich layer, referred to as a black mat (2), that is distributed widely over North America and parts of South America, Europe, and Syria. Black mats also occur less frequently in quaternary deposits that are younger and older than 12.9 ka (2). The YDB layer contains elevated abundances of iron- and silica-rich microspherules (collectively called "spherules") that are interpreted to have originated by cosmic impact because of their unique properties, as discussed below. Other markers include sediment and magnetic grains with elevated iridium concentrations and exotic carbon forms, such as nanodiamonds, glass-like carbon, aciniform soot, fullerenes, carbon onions, and carbon spherules (3, 4). The Greenland Ice Sheet also contains high concentrations of atmospheric ammonium and nitrates at 12.9 ka, indicative of biomass burning at the YD onset and/or high-temperature, impact-related chemical synthesis (5). Although these proxies are not unique to the YDB layer, the combined assemblage is highly unusual because these YDB markers are typically present in abundances that are substantially above background, and the assemblage serves as a datum layer for the YD onset at 12.9 ka. The wide range of proxies is considered here to represent evidence for a cosmic impact that caused airbursts/impacts (the YDB event may have produced ground impacts and atmospheric airbursts) across several continents.

Since the publication of Firestone et al. (1), numerous independent researchers have undertaken to replicate the results. Two groups were unable to confirm YDB peaks in spherules (6, 7), whereas seven other groups have confirmed them (*, †, ‡,

Author contributions: T.E.B., R.E.H., A.M.M., D.J.K., J.H.W., G.K., A.W., R.B.F., and J.P.K. designed research; T.E.B., R.E.H., A.M.M., D.J.K., J.C.W., J.H.W., J.L.B., G.C.H., G.A.H., D.R.K., G.K., C.P.L., S.S., Z.R., A.W., R.B.F., and J.P.K. performed research; T.E.B., R.E.H., A.M.M., D.J.K., J.C.W., J.H.W., P.S.D., J.L.B., D.R.K., G.K., C.P.L., S.S., Z.R., A.W., R.B.F., and J.P.K. analyzed data; and T.E.B., R.E.H., A.M.M., J.H.W., P.S.D., J.L.B., A.W., R.B.F., and J.P.K. wrote the paper.

The authors declare no conflict of interest.

*This Direct Submission article had a prearranged editor.

Freely available online through the PNAS open access option.

*LeCompte MA, et al., Unusual material in early Younger Dryas age sediments and their potential relevance to the YD cosmic impact hypothesis, XVIII INQUA-Congress, July 21–27, 2011, Bern, Switzerland, paper 1813.

†Baker DW, Miranda PJ, Gibbs KE, Montana evidence for extra-terrestrial impact event that caused Ice-Age mammal die-off, American Geophysical Union, Spring Meeting, 2008, abstr P41A-05.

‡Scruggs MA, Raab LM, Murowchick JS, Stone MW, Niemi TM, Investigation of sediment containing evidence of the Younger Dryas Boundary (YPB) Impact Event, El Carrizal, Baja California Sur, Mexico, Geological Society of America Abstracts with Programs, Vol 42, no. 2, p 101 (abstr).

[1]To whom correspondence should be addressed. E-mail: tbear1@cableone.net.

See Author Summary on page 11066 (volume 109, number 28).

This article contains supporting information online at www.pnas.org/lookup/suppl/doi:10.1073/pnas.1204453109/-/DCSupplemental.

8–14), with most but not all agreeing that their evidence is consistent with a cosmic impact. Of these workers, Fayek et al. (8) initially observed nonspherulitic melted glass in the well-dated YDB layer at Murray Springs, Arizona, reporting "iron oxide spherules (framboids) in a glassy iron–silica matrix, which is one indicator of a possible meteorite impact…. Such a high formation temperature is only consistent with impact… conditions." Similar materials were found in the YDB layer in Venezuela by Mahaney et al. (12), who observed "welded microspherules,… brecciated/impacted quartz and feldspar grains, fused metallic Fe and Al, and… aluminosilicate glass," all of which are consistent with a cosmic impact.

Proxies in High-Temperature Impact Plumes. Firestone et al. (1) proposed that YDB microspherules resulted from ablation of the impactor and/or from high-temperature, impact-related melting of terrestrial target rocks. In this paper, we explore evidence for the latter possibility. Such an extraterrestrial (ET) impact event produces a turbulent impact plume or fireball cloud containing vapor, melted rock, shocked and unshocked rock debris, breccias, microspherules, and other target and impactor materials. One of the most prominent impact materials is melted siliceous glass (lechatelierite), which forms within the impact plume at temperatures of up to 2,200 °C, the boiling point of quartz. Lechatelierite cannot be produced volcanically, but can form during lightning strikes as distinctive melt products called fulgurites that typically have unique tubular morphologies (15). It is also common in cratering events, such as Meteor Crater, AZ (16), and Haughton Crater, Canada[§], as well as in probable high-temperature aerial bursts that produced melt rocks, such as Australasian tektites (17), Libyan Desert Glass (LDG) (17), Dakhleh Glass (18), and potential, but unconfirmed, melt glass from Tunguska, Siberia (19). Similar lechatelierite-rich material formed in the Trinity nuclear detonation, in which surface materials were drawn up and melted within the plume (20).

After the formation of an impact fireball, convective cells form at temperatures higher than at the surface of the sun (>4,700 °C), and materials in these cells interact during the short lifetime of the plume. Some cells will contain solidified or still-plastic impactites, whereas in other cells, the material remains molten. Some impactites are rapidly ejected from the plume to form proximal and distal ejecta depending on their mass and velocity, whereas others are drawn into the denser parts of the plume, where they may collide repeatedly, producing multiple accretionary and collisional features. Some features, such as microcraters, are unique to impacts and cosmic ablation and do not result from volcanic or anthropogenic processes[¶].

For ground impacts, such as Meteor Crater (16), most melting occurred during the formation of the crater. Some of the molten rock was ejected at high angles, subsequently interacting with the rising hot gas/particulate cloud. Most of this material ultimately fell back onto the rim as proximal ejecta, and molten material ejected at lower angles became distal ejecta. Cosmic impacts also include atmospheric impacts called airbursts, which produce some material that is similar to that produced in a ground impact. Aerial bursts differ from ground impacts in that mechanically shocked rocks are not formed, and impact markers are primarily limited to materials melted on the surface or within the plume. Glassy spherules and angular melted objects also are produced by the hot hypervelocity jet descending to the ground from the atmospheric explosion. The coupling of the airburst fireball with the upper soil layer of Earth's surface causes major melting of material to a depth of a few cm. Svetsov and Wasson (2007) [‖] calculated that the thickness of the melted layer was a function of time and flux density, so that for $T_e > 4{,}700$ °C at a duration of several seconds, the thickness of melt is 1–1.5 cm. Calculations show that for higher fluxes, more soil is melted, forming thicker layers, as exemplified by Australasian tektite layered melts.

The results of an aerial detonation of an atomic bomb are similar to those of a cosmic airburst (e.g., lofting, mixing, collisions, and entrainment), although the method of heating is somewhat different because of radioactive byproducts (*SI Appendix*). The first atomic airburst occurred atop a 30-m tower at the Alamogordo Bombing Range, New Mexico, in 1945, and on detonation, the thermal blast wave melted 1–3 cm of the desert soils up to approximately 150 m in radius. The blast did not form a typical impact-type crater; instead, the shock wave excavated a shallow depression 1.4 m deep and 80 m in diameter, lifting molten and unmelted material into the rising, hot detonation plume. Other melted material was ejected at lower angles, forming distal ejecta. For Trinity, Hermes and Strickfaden (20) estimated an average plume temperature of 8,000 °C at a duration of 3 s and an energy yield of up to 18 kilotons (kt) trinitrotoluene (TNT) equivalent. Fallback of the molten material, referred to as trinitite, littered the surface for a diameter of 600 m, in some places forming green glass puddles (similar to Australasian layered tektites). The ejecta includes irregularly shaped fragments and aerodynamically shaped teardrops, beads, and dumbbell glasses, many of which show collision and accretion features resulting from interactions in the plume (similar to Australasian splash-form tektites). These results are identical to those from known cosmic airbursts. *SI Appendix*, Table S1 provide a comparison of YDB objects with impact products from Meteor Crater, the Australasian tektite field, and the Trinity nuclear airburst.

Scope of Study. We investigated YDB markers at 18 dated sites, spanning 12,000 km across seven countries on three continents (*SI Appendix*, Fig. S1), greatly expanding the extent of the YDB marker field beyond earlier studies (1). Currently, there are no known limits to the field. Using both deductive and inductive approaches, we searched for and analyzed YDB spherules and melted siliceous glass, called scoria-like objects (SLOs), both referred to below as YDB objects. The YDB layer at all 18 sites contains microspherules, but SLOs were found at only three sites: Blackville, South Carolina; Abu Hureyra, Syria; and Melrose, Pennsylvania. Here, we focus primarily on abundances, morphology, and geochemistry of the YDB SLOs. Secondarily, we discuss YDB microspherules with regard to their geochemical similarity and co-occurrence with SLOs. We also compare compositions of YDB objects to compositions: (*i*) of materials resulting from meteoritic ablation and from terrestrial processes, such as volcanism, anthropogenesis, and geological processes; and (*ii*) from Meteor Crater, the Trinity nuclear detonation, and four ET aerial bursts at Tunguska, Siberia; Dakhleh Oasis, Egypt; Libyan Desert Glass Field, Egypt; and the Australasian tektite strewnfield, SE Asia.

For any investigation into the origin of YDB objects, the question arises as to whether these objects formed by cosmic impact or by some other process. This is crucial, because sedimentary spherules are found throughout the geological record and can result from nonimpact processes, such as cosmic influx, meteoritic ablation, anthropogenesis, lightning, and volcanism. However, although microspherules with widely varying origins can appear superficially similar, their origins may be determined with reasonably high confidence by a combination of various analyses—e.g., scanning electron microscopy with energy dispersive spectroscopy

[§]Osinski GF, Bunch TE, Wittke J, Evidence for shock melting of carbonates from Meteor Crater, Arizona, Annual Meeting of the Meteoritical Society, July 28–August 1, 2003, abstr 5070.

[¶]Buchner E, Schmeider M, Strasser A, Krochert L, Impacts on spherules, 40th Lunar and Planetary Science Conference. March 26, 2009, abstr 1017.

[‖]Svetsov VV, Wasson JT, Melting of soil rich in quartz by radiation from aerial bursts—A possible cause of the formation for Libyan Desert Glass and layered Australasian tektites, 38th Lunar and Planetary Science Conference. March 13, 2007, abstr 1499.

(SEM-EDS) and wavelength-dispersive spectroscopy (WDS) by electron microprobe—to examine evidence for microcratering, dendritic surface patterns produced during rapid melting—quenching **, and geochemical composition. Results and discussion are below and in the *SI Appendix*.

SLOs at YDB Sites. ***Abu Hureyra, Syria.*** This is one of a few archaeological sites that record the transition from nomadic hunter—gatherers to farmer—hunters living in permanent villages (21). Occupied from the late Epipalaeolithic through the Early Neolithic (13.4–7.5 ka), the site is located close to the Euphrates River on well-developed, highly calcareous soils containing platy flint (chert) fragments, and the regional valley sides are composed of chalk with thin beds of very fine-grained flint. The dominant lithology is limestone within a few km, whereas gypsum deposits are prominent 40 km away, and basalt is found 80 km distant. Much of this part of northern Syria consists of highly calcareous Mediterranean, steppe, and desert soils. To the east of Abu Hureyra, there are desert soils marked by wind-polished flint fragments forming a pediment on top of marls (calcareous and clayey mudstones). Thus, surface sediments and rocks of the entire region are enriched in CaO and SiO_2. Moore and co-workers excavated the site in 1972 and 1973, and obtained 13 radiocarbon dates ranging from 13.37 ± 0.30 to 9.26 ± 0.13 cal ka B.P., including five that ranged from 13.04 ± 0.15 to 12.78 ± 0.14 ka, crossing the YDB interval (21) (*SI Appendix*, Table S2). Linear interpolation places the date of the YDB layer at 12.9 ± 0.2 ka (1σ probability) at a depth of 3.6 m below surface (mbs) at 284.7 m above sea level (m asl) (*SI Appendix*, Figs. S2*D* and S3). The location of the YDB layer is further supported by evidence of 12.9-ka climatic cooling and drying based on the palynological and macrobotanical record that reveal a sudden decline of 60–100% in the abundance of charred seed remains of several major groups of food plants from Abu Hureyra. Altogether, more than 150 species of plants showed the distinct effects of the transition from warmer, moister conditions during the Bølling-Allerød (14.5–12.9 ka) to cooler, dryer condition during the Younger Dryas (12.9–11.5 ka).

Blackville, South Carolina. This dated site is in the rim of a Carolina Bay, one of a group of >50,000 elliptical and often overlapping depressions with raised rims scattered across the Atlantic Coastal Plain from New Jersey to Alabama (*SI Appendix*, Fig. S4). For this study, samples were cored by hand auger at the thickest part of the bay rim, raised 2 m above the surrounding terrain. The sediment sequence is represented by eolian and alluvial sediments composed of variable loamy to silty red clays down to an apparent unconformity at 190 cm below surface (cmbs). Below this there is massive, variegated red clay, interpreted as a paleosol predating bay rim formation (Miocene marine clay >1 million years old) (*SI Appendix*, Fig. S4). A peak in both SLOs and spherules occurs in a 15 cm—thick interval beginning at 190 cmbs above the clay section, extending up to 175 cmbs (*SI Appendix*, Table S3). Three optically stimulated luminescence (OSL) dates were obtained at 183, 152, and 107 cmbs, and the OSL date of 12.96 ± 1.2 ka in the proxy-rich layer at 183 cmbs is consistent with Firestone et al. (1) (*SI Appendix*, Fig. S4 and Table S2).

Melrose, Pennsylvania. During the Last Glacial Maximum, the Melrose area in NE Pennsylvania lay beneath 0.5–1 km of glacial ice, which began to retreat rapidly after 18 ka (*SI Appendix*, Fig. S5). Continuous samples were taken from the surface to a depth of 48 cmbs, and the sedimentary profile consists of fine-grained, humic colluvium down to 38 cmbs, resting on sharply defined end-Pleistocene glacial till (diamicton), containing 40 wt% angular clasts >2 mm in diameter. Major abundance peaks in SLOs and spherules were encountered above the till at a depth of 15–28 cmbs, consistent with emplacement after 18 ka. An OSL date was acquired at 28 cmbs, yielding an age of 16.4 ± 1.6 ka, and, assuming a modern age for the surface layer, linear interpolation dates the proxy-rich YDB layer at a depth of 21 cmbs to 12.9 ± 1.6 ka (*SI Appendix*, Fig. S5 and Table S2).

YDB sites lacking SLOs. The other 15 sites, displaying spherules but no SLOs, are distributed across six countries on three continents, representing a wide range of climatic regimes, biomes, depositional environments, sediment compositions, elevations (2–1,833 m), and depths to the YDB layer (13 cm–14.0 m) (*SI Appendix*, Fig. S1). YDB spherules and other proxies have been previously reported at seven of the 18 sites (1). The 12.9-ka YDB layers were dated using accelerator mass spectrometry (AMS) radiocarbon dating, OSL, and/or thermal luminescence (TL).

Results and Discussion

Impact-Related Spherules Description. The YDB layer at 18 sites displays peaks in Fe-and/or Si-rich magnetic spherules that usually appear as highly reflective, black-to-clear spheroids (Fig. 1 and *SI Appendix*, Fig. S6 *A–C*), although 10% display more complex shapes, including teardrops and dumbbells (*SI Appendix* Fig. S6 *D–H*). Spherules range from 10 μm to 5.5 mm in diameter (mean, 240 μm; median, 40 μm), and concentrations range from 5–4,900 spherules/kg (mean, 940/kg; median, 180/kg) (Fig. 2 and *SI Appendix*, Table S3). Above and below the YDB layer, concentrations are zero to low. SEM imaging reveals that the outer surfaces of most spherules exhibit distinctive skeletal (or dendritic) textures indicative of rapid quenching producing varying levels of coarseness (*SI Appendix*, Fig. S7). This texture makes them easily distinguishable from detrital magnetite, which is typically fine-grained and monocrystalline, and from framboidal grains, which are rounded aggregates of blocky crystals. It is crucial to note that these other types of grains cannot be easily differentiated from impact spherules by light microscopy and instead require investigation by SEM. Textures and morphologies of YDB spherules correspond to those observed in known impact events, such as at the 65-million-year-old Cretaceous—Paleogene boundary, the 50-ka Meteor Crater impact, and the Tunguska airburst in 1908 (*SI Appendix*, Fig. S7).

SLOs Description. Three sites contained conspicuous assemblages of both spherules and SLOs that are composed of shock-fused vesicular siliceous glass, texturally similar to volcanic scoria. Most SLOs are irregularly shaped, although frequently they are com-

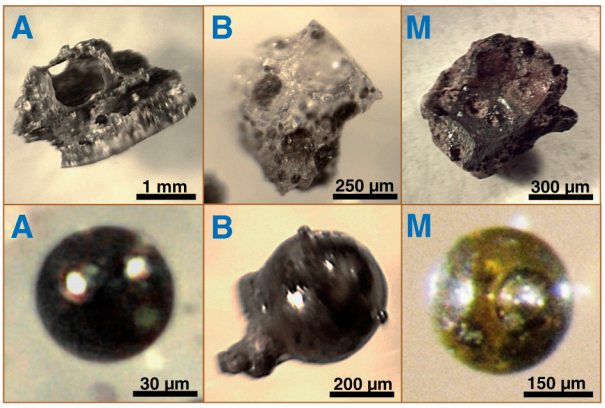

Fig. 1. Light photomicrographs of YDB objects. (*Upper*) SLOs and (*Lower*) magnetic spherules. **A** = Abu Hureyra, **B** = Blackville, **M** = Melrose.

**Petaev ML, Jacobsen SB, Basu AR, Becker L, Magnetic Fe,Si,Al-rich impact spherules from the P-T Boundary Layer at Graphite Peak, Antarctica, 35th Lunar and Planetary Science Conference. March 16, 2004, abstr 1216.

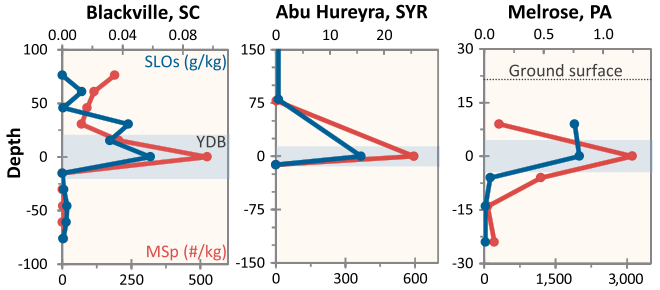

Fig. 2. Site graphs for three key sites. SLOs and microspherules exhibit significant peaks in YDB layer. Depth is relative to YDB layer, represented by the light blue bar.

posed of several fused, subrounded glassy objects. As compared to spherules, most SLOs contain higher concentrations of Si, Al, and Ca, along with lower Fe, and they rarely display the dendritic textures characteristic of most Fe-rich spherules. They are nearly identical in shape and texture to high-temperature materials from the Trinity nuclear detonation, Meteor Crater, and other impact craters (*SI Appendix*, Fig. S8). Like spherules, SLOs are generally dark brown, black, green, or white, and may be clear, translucent, or opaque. They are commonly larger than spherules, ranging from 300 μm to 5.5 mm long (mean, 1.8 mm; median, 1.4 mm) with abundances ranging from 0.06–15.76 g/kg for the magnetic fraction that is >250 μm. At the three sites, spherules and SLOs co-occur in the YDB layer dating to 12.9 ka. Concentrations are low to zero above and below the YDB layer.

Geochemistry of YDB Objects. ***Comparison to cosmic spherules and micrometeorites.*** We compared Mg, total Fe, and Al abundances for 70 SLOs and 340 spherules with >700 cosmic spherules and micrometeorites from 83 sites, mostly in Antarctica and Greenland (Fig. 3*A*). Glassy Si-rich extraterrestrial material typically exhibits MgO enrichment of 17× (avg 25 wt%) (23) relative to YDB spherules and SLOs from all sites (avg 1.7 wt%), the same as YDB magnetic grains (avg 1.7 wt%). For Al_2O_3 content, extraterrestrial material is depleted 3× (avg 2.7 wt%) relative to YDB spherules and SLOs from all sites (avg 9.2 wt%), as well as YDB magnetic grains (avg 9.2 wt%). These results indicate >90% of YDB objects are geochemically distinct from cosmic material.

Comparison to anthropogenic materials. We also compared the compositions of the YDB objects to >270 anthropogenic spherules and fly ash collected from 48 sites in 28 countries on five continents (Fig. 3*B* and *SI Appendix*, Table S5), primarily produced by one of the most prolific sources of atmospheric contamination: coal-fired power plants (24). The fly ash is 3× enriched in Al_2O_3 (avg 25.8 wt%) relative to YDB objects and magnetic grains (avg 9.1 wt%) and depleted 2.5× in P_2O_5 (0.55 vs. 1.39 wt%, respectively). The result is that 75% of YDB objects have compositions different from anthropogenic objects. Furthermore, the potential for anthropogenic contamination is unlikely for YDB sites, because most are buried 2–14 mbs.

Comparison to volcanic glasses. We compared YDB objects with >10,000 volcanic samples (glass, tephra, and spherules) from 205 sites in four oceans and on four continents (*SI Appendix*, Table S5). Volcanic material is enriched 2× in the alkalis, $Na_2O + K_2O$ (avg 3 wt%), compared with YDB objects (avg 1.5 wt%) and magnetic grains (avg 1.2 wt%). Also, the Fe concentrations for YDB objects (avg 55 wt%) are enriched 5.5× compared to volcanic material (avg 10 wt%) (Fig. 3*C*), which tends to be silica-rich (>40 wt%) with lower Fe. Approximately 85% of YDB objects exhibit compositions dissimilar to silica-rich volcanic material. Furthermore, the YDB assemblages lack typical volcanic markers, including volcanic ash and tephra.

Melt temperatures. A FeO^T–Al_2O_3–SiO_2 phase diagram reveals three general groups of YDB objects (Fig. 3*D*). A Fe-rich group, dominated by the mineral magnetite, forms at temperatures of approximately 1,200–1,700 °C. The high-Si/low-Al group is dominated by quartz, plagioclase, and orthoclase and has liquidus temperatures of 1,200–1,700 °C. An Al—Si-rich group is dominated by mullite and corundum with liquidus temperatures of 1,400–2,050 °C. Because YDB objects contain more than the three oxides shown, potentially including H_2O, and are not in equilibrium, the liquidus temperatures are almost certainly lower than indicated. On the other hand, in order for high-silica material to produce low-viscosity flow bands (schlieren), as observed in many SLOs, final temperatures of >2,200 °C are probable, thus eliminating normal terrestrial processes. Additional temperatures diagrams are shown in *SI Appendix*, Fig. S9.

Comparison to impact-related materials. Geochemical compositions of YDB objects are presented in a Al_2O_3 – CaO – FeO^T ternary diagram used to plot compositional variability in metamorphic rocks (Fig. 4*A*). The diagram demonstrates that the composition of YDB objects is heterogeneous, spanning all metamorphic rock types (including pelitic, quartzofeldspathic, basic, and calcareous). From 12 craters and tektite strewnfields on six continents, we compiled compositions of >1,000 impact-related markers (spherules, ejecta, and tektites, which are melted glassy objects), as well as 40 samples of melted terrestrial sediments from two nuclear aerial detonations: Trinity (22) and Yucca Flat (25) (Fig. 4*B* and *SI Appendix*, Table S5). The compositions of YDB impact markers are heterogeneous, corresponding well with heterogeneous nuclear melt material and impact proxies.

Comparison to terrestrial sediments. We also used the acriflavine system to analyze >1,000 samples of bulk surface sediment, such as clay, mud, and shale, and a wide range of terrestrial metamorphic rocks. YDB objects (Fig. 4*A*) are similar in composition to surface sediments, such as clay, silt, and mud (25) (Fig. 4*C*),

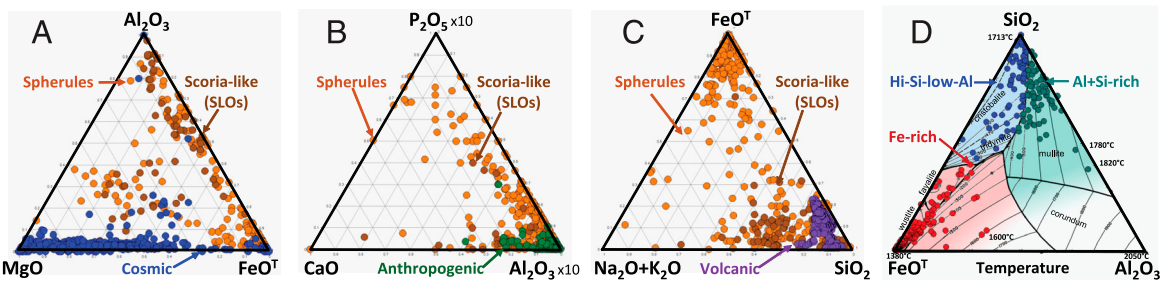

Fig. 3. Ternary diagrams comparing molar oxide wt% of YDB SLOs (dark orange) and magnetic spherules (orange) to (*A*) cosmic material, (*B*) anthropogenic material, and (*C*) volcanic material. (*D*) Inferred temperatures of YDB objects, ranging up to 1,800 °C. Spherules and SLOs are compositionally similar; both are dissimilar to cosmic, anthropogenic, and volcanic materials.

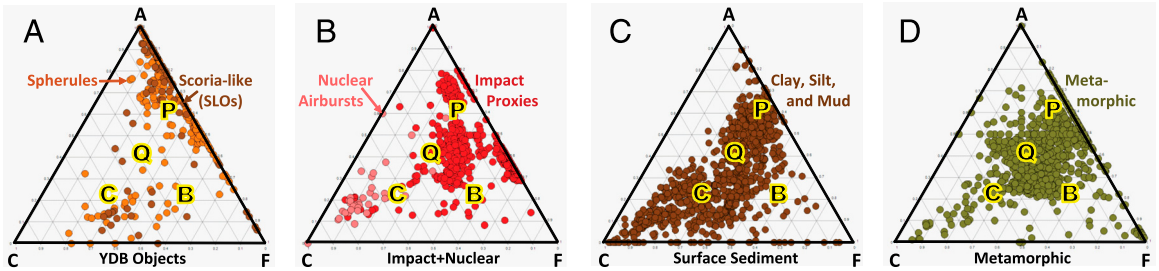

Fig. 4. Compositional ternary diagrams. (*A*) YDB objects: Spherules (orange) and SLOs (dark orange) are heterogeneous. Letters indicate plot areas typical of specific metamorphic rock types: P = pelitic (e.g., clayey mudstones and shales), Q = quartzofeldspathic (e.g., gneiss and schist), B = basic (e.g., amphibolite), and C = calcareous (e.g., marble) (40). (*B*) Cosmic impact materials in red ($N > 1{,}000$) with nuclear material in light red. (*C*) Surface sediments, such as clay, silt, and mud (41). (*D*) Metamorphic rocks. Formula for diagrams: A = $(Al_2O_3 + Fe_2O_3)$-$(Na_2O + K_2O)$; C = $[CaO\text{-}(3.33 \times P_2O_5)]$; F = $(FeO + MgO + MnO)$.

and to metamorphic rocks, including mudstone, schist, and gneiss (25) (Fig. 4*D*).

In addition, rare earth element (REE) compositions of the YDB objects acquired by instrumental neutron activation analysis (INAA) and prompt gamma activation analysis (PGAA) are similar to bulk crust and compositions from several types of tektites, composed of melted terrestrial sediments (*SI Appendix*, Fig. S10*A*). In contrast, REE compositions differ from those of chondritic meteorites, further confirming that YDB objects are not typical cosmic material. Furthermore, relative abundances of La, Th, and Sc confirm that the material is not meteoritic, but rather is of terrestrial origin (*SI Appendix*, Fig. S10*B*). Likewise, Ni and Cr concentrations in YDB objects are generally unlike those of chondrites and iron meteorites, but are an excellent match for terrestrial materials (*SI Appendix*, Fig. S10*C*). Overall, these results indicate SLOs and spherules are terrestrial in origin, rather than extraterrestrial, and closely match known cosmic impact material formed from terrestrial sediments.

We investigated whether SLOs formed from local or nonlocal material. Using SEM-EDS percentages of nine major oxides (97 wt%, total) for Abu Hureyra, Blackville, and Melrose, we compared SLOs to the composition of local bulk sediments, acquired with NAA and PGAA (*SI Appendix*, Table S4). The results for each site show little significant difference between SLOs and bulk sediment (*SI Appendix*, Fig. S11), consistent with the hypothesis that SLOs are melted local sediment. The results demonstrate that SLOs from Blackville and Melrose are geochemically similar, but are distinct from SLOs at Abu Hureyra, suggesting that there are at least two sources of melted terrestrial material for SLOs (i.e., two different impacts/airbursts).

We also performed comparative analyses of the YDB object dataset demonstrating that: (*i*) proxy composition is similar regardless of geographical location (North America vs. Europe vs. Asia); (*ii*) compositions are unaffected by method of analysis (SEM-EDS vs. INAA/PGAA); and (*iii*) compositions are comparable regardless of the method of preparation (sectioned vs. whole) (*SI Appendix*, Fig. S12).

Importance of Melted Silica Glass. Lechatelierite is only known to occur as a product of impact events, nuclear detonations, and lightning strikes (15). We observed it in spherules and SLOs from Abu Hureyra, Blackville, and Melrose (Fig. 5), suggesting an origin by one of those causes. Lechatelierite is found in material from Meteor Crater (16), Haughton Crater, the Australasian tektite field (17), Dakhleh Oasis (18), and the Libyan Desert Glass Field (17), having been produced from whole-rock melting of quartzite, sandstones, quartz-rich igneous and metamorphic rocks, and/or loess-like materials. The consensus is that melting begins above 1,700 °C and proceeds to temperatures >2,200 °C, the boiling point of quartz, within a time span of a few seconds depending on the magnitude of the event (26, 27). These temperatures restrict potential formation processes, because these are far higher than peak temperatures observed in magmatic eruptions of <1,300 °C (28), wildfires at <1,454 °C (29), fired soils at <1,500 °C (30), glassy slag from natural biomass combustion at <1,290 °C (31), and coal seam fires at <1,650 °C (31).

Lechatelierite is also common in high-temperature, lightning-produced fulgurites, of which there are two types (for detailed discussion, see *SI Appendix*). First, subsurface fulgurites are glassy tube-like objects (usually <2 cm in diameter) formed from melted sediment at >2,300 °C. Second, exogenic fulgurites include vesicular glassy spherules, droplets, and teardrops (usually <5 cm in diameter) that are only rarely ejected during the formation of subsurface fulgurites. Both types closely resemble melted material from cosmic impact events and nuclear airbursts, but there are recognizable differences: (*i*) no collisions (fulgurites show no high-velocity collisional damage by other particles, unlike YDB SLOs and trinitite); (*ii*) different ultrastructure (subsurface fulgurites are tube-like, and broken pieces typically have highly reflective inner surfaces with sand-coated exterior surfaces, an ultrastructure unlike that of any known YDB SLO); (*iii*) lateral distribution (exogenic fulgurites are typically found <1 m from the point of a lightning strike, whereas the known lateral distribution of impact-related SLOs is 4.5 m at Abu Hureyra, 10 m at Blackville, and 28 m at Melrose); and (*iv*) rarity (at 18 sites investigated, some spanning >16,000 years, we did not observe any fulgurites or fragments in any stratum). Pigati et al. (14) confirmed the presence of YDB spherules and iridium at Murray Springs, AZ, but proposed that cosmic, volcanic, and impact melt products have been concentrated over time beneath black mats and in deflational basins, such as are present at eight of our sites that have wetland-derived black mats. In this study, we did not observe any fulguritic glass or YDB SLOs beneath any wetland black mats, contradicting Pigati et al., who propose that they should concentrate such materials. We further note that the enrichment in spherules reported by Pigati et al. at four non-YDB sites in Chile are most likely caused by volcanism, because their collection sites are located 20–80 km downslope from 22 major active volcanoes in the Andes (14). That group performed no

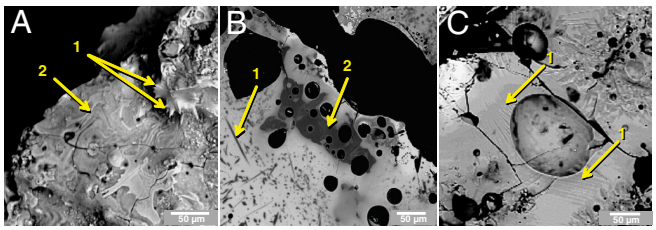

Fig. 5. SEM-BSE images of high-temperature SLOs with lechatelierite. (*A*) Abu Hureyra: portion of a dense 4-mm chunk of lechatelierite. Arrows identify tacky, viscous protrusions (no. 1) and high-temperature flow lines or schlieren (no. 2). (*B*) Blackville: Polished section of SLO displays vesicles, needle-like mullite quench crystals (no. 1), and dark grey lechatelierite (no. 2). (*C*) Melrose: Polished section of a teardrop displays vesicles and lechatelierite with numerous schlieren (no. 1).

SEM or EDS analyses to determine whether their spherules are volcanic, cosmic, or impact-related, as stipulated by Firestone et al. (1) and Israde-Alcántara et al. (4)

Pre-Industrial anthropogenic activities can be eliminated as a source of lechatelierite because temperatures are too low to melt pure SiO_2 at >1,700 °C. For example, pottery-making began at approximately 14 ka but maximum temperatures were <1,050 °C (31); glass-making at 5 ka was at <1,100 °C (32) and copper-smelting at 7 ka was at <1,100 °C (32). Humans have only been able to produce temperatures >1,700 °C since the early 20th century in electric-arc furnaces. Only a cosmic impact event could plausibly have produced the lechatelierite contained in deeply buried sediments that are 12.9 kiloyears (kyrs) old.

SiO_2 glass exhibits very high viscosity even at melt temperatures of >1,700 °C, and flow textures are thus difficult to produce until temperatures rise much higher. For example, Wasson and Moore (33) noted the morphological similarity between Australasian tektites and LDG, and therefore proposed the formation of LDG by a cosmic aerial burst. They calculated that for low-viscosity flow of SiO_2 to have occurred in Australasian tektites and LDG samples, temperatures of 2,500–2,700 °C were required. For tektites with lower SiO_2 content, requisite minimum temperatures for flow production may have been closer to 2,100–2,200 °C. Lechatelierite may form schlieren in mixed glasses (27) when viscosity is low enough. Such flow bands are observed in SLOs from Abu Hureyra and Melrose (Fig. 5) and if the model of Wasson and Moore (33) is correct, then an airburst/impact at the YDB produced high-temperature melting followed by rapid quenching (15). Extreme temperatures in impact materials are corroborated by the identification of frothy lechatelierite in Muong Nong tektites reported by Walter (34), who proposed that some lechatelierite cores displayed those features because of the boiling of quartz at 2,200 °C. We surveyed several hundred such lechatelierite grains in 18 Muong Nong tektites and found similar evidence of boiling; most samples retained outlines of the precursor quartz grains (*SI Appendix*, Fig. S13).

To summarize the evidence, only two natural processes can form lechatelierite: cosmic impacts and lightning strikes. Based on the evidence, we conclude that YDB glasses are not fulgurites. Their most plausible origin is by cosmic impact.

Collision and Accretion Features. Evidence for interparticle collisions is observed in YDB samples from Abu Hureyra, Blackville, and Melrose. These highly diagnostic features occur within an impact plume when melt droplets, rock particles, dust, and partially melted debris collide at widely differing relative velocities. Such features are only known to occur during high-energy atomic detonations and cosmic impacts, and, because differential velocities are too low [††], have never been reported to have been caused by volcanism, lightning, or anthropogenic processes. High-speed collisions can be either constructive, whereby partially molten, plastic spherules grow by the accretion of smaller melt droplets (35), or destructive, whereby collisions result in either annihilation of spherules or surface scarring, leaving small craters (36). In destructive collisions, small objects commonly display three types of collisions (36): (*i*) microcraters that display brittle fracturing; (*ii*) lower-velocity craters that are often elongated, along with very low-impact "furrows" resulting from oblique impacts (Fig. 6); and (*iii*) penetrating collisions between particles that result in melting and deformational damage (Fig. 7). Such destructive damage can occur between impactors of the same or different sizes and compositions, such as carbon impactors colliding with Fe-rich spherules (*SI Appendix*, Fig. S14).

Collisions become constructive, or accretionary, at very low velocities and show characteristics ranging from disrupted projectiles to partial burial and/or flattening of projectiles on the accreting host (Fig. 8 *A* and *B*). The least energetic accretions are marked by gentle welding together of tacky projectiles. Accretionary impacts are the most common type observed in 36 glassy impactites from Meteor Crater and in YDB spherules and SLOs (examples in Fig. 9). Other types of accretion, such as irregular melt drapings and filament splatter (37), are common on YDB objects and melt products from Meteor Crater (Fig. 9*D*). Additional examples of collisions and splash forms are shown in *SI Appendix*, Fig. S15. This collective evidence is too energetic to be consistent with any known terrestrial mechanism and is unique to high-energy cosmic impact events.

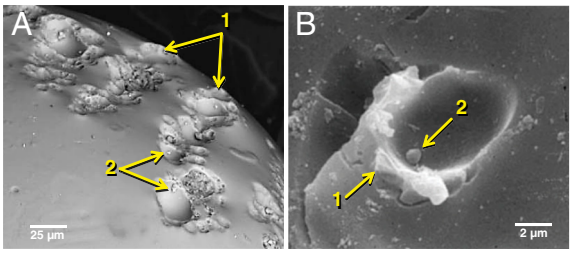

Fig. 6. SEM-BSE images of impact pitting. (*A*) Melrose: cluster of oblique impacts on a SLO that produced raised rims (no. 1). Tiny spherules formed in most impact pits together with irregularly shaped impact debris (no. 2). (*B*) Australasian tektite: Oblique impact produced a raised rim (no. 1). A tiny spherule is in the crater bottom (no. 2) (36).

YDB Objects by Site. ***Blackville, South Carolina.*** High-temperature melt products consisting of SLOs (420–2,700 μm) and glassy spherules (15–1,940 μm) were collected at a depth of 1.75–1.9 m. SLOs range from small, angular, glassy, shard-like particles to large clumps of highly vesiculated glasses, and may contain pockets of partially melted sand, clay, mineral fragments, and carbonaceous matter. Spherules range from solid to vesicular, and some are hollow with thin to thick walls, and the assemblage also includes welded glassy spherules, thermally processed clay clasts, and partially melted clays.

Spherules show a considerable variation in composition and oxygen fugacity, ranging from highly reduced, Al—Si-rich glasses to dendritic, oxidized iron oxide masses. One Blackville spherule (Fig. 10*A*) is composed of Al_2O_3-rich glasses set with lechatelierite, suessite, spheres of native Fe, and quench crystallites of corundum and 2:1 mullite, one of two stoichiometric forms of mullite ($2Al_2O_3{\cdot}SiO_2$, or 2:1 mullite; and $3Al_2O_3{\cdot}2SiO_2$, or 3:2 mullite). This spherule is an example of the most reduced melt with oxygen fugacity (fO_2) along the IW (iron—wustite) buffer. Other highly oxidized objects formed along the H or magnetite—hematite buffer. For example, one hollow spherule contains 38% by volume of dendritic aluminous hematite (*SI Appendix*, Fig. S16) with minor amounts of unidentified iron

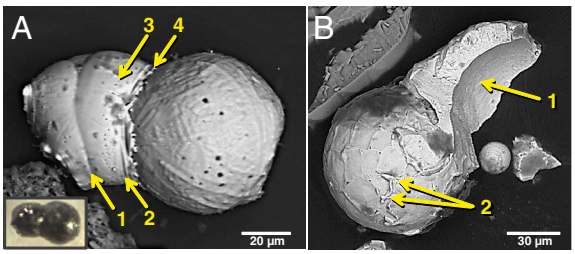

Fig. 7. SEM-BSE images of collisional spherules. (*A*) Lake Cuitzeo, Mexico: collision of two spherules at approximately tens of m/s; left spherule underwent plastic compaction to form compression rings (nos. 1 and 2), a line of gas vesicles (no. 3), and a splash apron (no. 4). (*B*) Kimbel Bay: Collision of two spherules destroyed one spherule (no. 1) and formed a splash apron on the other (no. 2). This destructive collision suggests high differential velocities of tens to hundreds of m/s.

[††]Buchner E, Schmeider M, Strasser A, Krochert L, Impacts on spherules, 40th Lunar and Planetary Science Conference. March 26, 2009, abstr 1017.

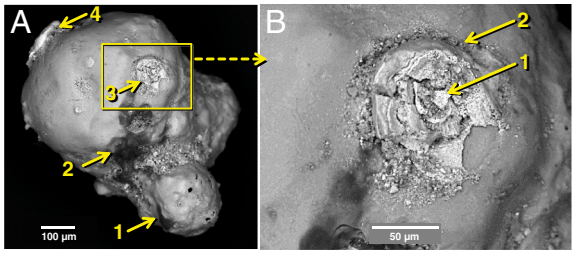

Fig. 8. SEM-BSE images of accretionary features. (*A*) Melrose: lumpy spherule with a subrounded accretion (no. 1), a dark carbon accretion (no. 2), and two hollow, magnetic spherules flattened by impact (nos. 3 and 4). (*B*) Melrose: enlargement of box in *A*, displaying fragmented impacting magnetic spherule (no. 1) forming a debris ring (no. 2) that partially fused with the aluminosilicate host spherule.

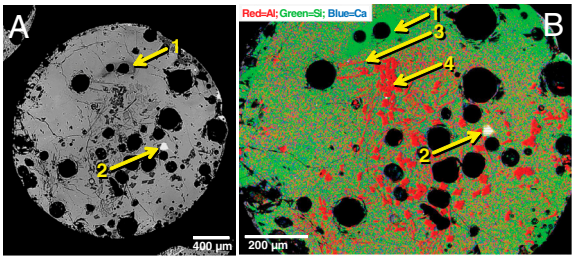

Fig. 10. SEM-BSE images of Blackville spherule. (*A*) Sectioned spherule composed of high-temperature, vesiculated aluminosilicate glass and displaying lechatelierite (no. 1) and reduced-Fe spherules (no. 2). (*B*) False-colored enlargement of same spherule displaying lechatelierite (green, no. 1) and reduced-Fe spherules (white, no. 2) with needle-like mullite quench crystals (red, no. 3) and corundum quench crystals (red, no. 4).

oxides set in Fe-rich glass with no other crystallites. One Blackville SLO is composed of high Al_2O_3–SiO_2 glass with dendritic magnetite crystals and vesicles lined with vapor-deposited magnetite (*SI Appendix*, Fig. S17). In addition to crystallizing from the glass melt, magnetite also crystallized contemporaneously with glassy carbon. These latter samples represent the most oxidized of all objects, having formed along the H or magnetite—hematite buffer, displaying 10-to 20-μm diameter cohenite (Fe_3C) spheres with inclusions of Fe phosphide (Fe_2P–Fe_3P) containing up to 1.10 wt% Ni and 0.78 wt% Co. These occur in the reduced zones of spherules and SLOs, some within tens of μm of highly oxidized Al—hematite. These large variations in composition and oxygen fugacity over short distances, which are also found in Trinity SLOs and spherules, are the result of local temperature and physicochemical heterogeneities in the impact plume. They are consistent with cosmic impacts, but are inconsistent with geological and anthropogenic mechanisms.

Spherules and SLOs from Blackville are mostly aluminosilicate glasses, as shown in the ternary phase diagrams in *SI Appendix*, Fig. S9, and most are depleted in $K_2O + Na_2O$, which may reflect high melting temperatures and concomitant loss of volatile elements that increases the refractoriness of the melts. For most spherules and SLOs, quench crystallites are limited to corundum and mullite, although a few have the Fe—Al spinel, hercynite. These phases, together with glass compositions, limit the compositional field to one with maximum crystallization temperatures ranging from approximately 1,700–2,050 °C. The spherule in Fig. 10*A* is less alumina-rich, but contains suessite (Fe_3Si), which indicates a crystallization temperature of 2,000–2,300 °C (13, 38).

Observations of clay-melt interfaces with mullite or corundum-rich enclaves indicate that the melt glasses are derived from materials enriched in kaolinite with smaller amounts of quartz and iron oxides. Partially melted clay discontinuously coated the surfaces of a few SLOs, after which mullite needles grew across the clay—glass interface. The melt interface also has quench crystals of magnetite set in Fe-poor and Fe-rich glasses (*SI Appendix*, Fig. S18). SLOs also contain carbon-enriched black clay clasts displaying a considerable range of thermal decomposition in concert with increased vesiculation and vitrification of the clay host. The interfaces between mullite-rich glass and thermally decomposed black clay clasts are frequently decorated with suessite spherules.

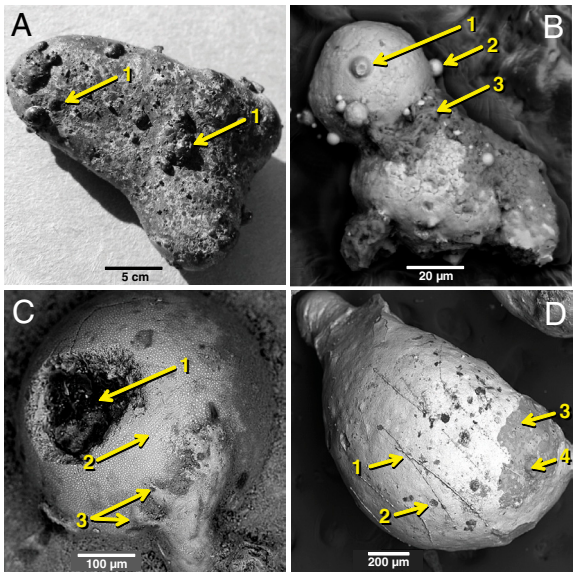

Fig. 9. Accretion textures. (*A*) Meteor Crater: glassy impactite with multiple accretionary objects deformed by collisional impact (no. 1). (*B*) Talega site: cluster of large quenched spherules with smaller partially buried spherules (no. 1), accretion spherules (no. 2), and accreted carbonaceous matter (no. 3). (*C*) Meteor Crater: accretion spherule on larger host with impact pit lined with carbon (no. 1), quenched iron oxide surface crystals (light dots at no. 2), and melt draping (no. 3). (*D*) Melrose: YDB teardrop with a quench crust of aluminosilicate glass and a subcrust interior of SiO_2 and Al-rich glasses, displaying melt drapings (no. 1), microcraters (no. 2), mullite crystals (no. 3), and accretion spherules (no. 4).

Abu Hureyra site, Syria. The YDB layer yielded abundant magnetic and glass spherules and SLOs containing lechatelierite intermixed with CaO-rich glasses. Younger layers contain few or none of those markers (*SI Appendix*, Table S3). The SLOs are large, ranging in size up to 5.5 mm, and are highly vesiculated (*SI Appendix*, Fig. S19); some are hollow and some form accretionary groups of two or more objects. They are compositionally and morphologically similar to melt glasses from Meteor Crater, which, like Abu Hureyra, is located in Ca-rich terrain (*SI Appendix*, Fig. S21). YDB magnetic spherules are smaller than at most sites (20–50 μm). Lechatelierite is abundant in SLOs and exhibits many forms, including sand-size grains and fibrous textured objects with intercalated high-CaO glasses (Fig. 11). This fibrous morphology, which has been observed in material from Meteor Crater and Haughton Crater (*SI Appendix*,

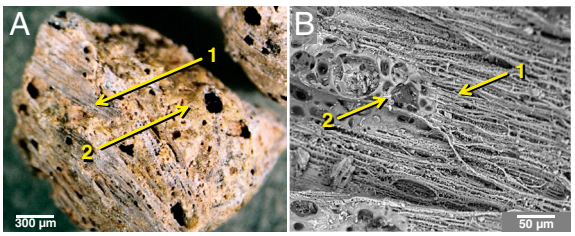

Fig. 11. (*A*) Abu Hureyra: SLO (2 mm wide) with grey tabular lechatelierite grains (no. 1) surrounded by tan CaO-rich melt (no. 2). (*B*) SEM-BSE image showing fibrous lechatelierite (no. 1) and bubbled CaO-rich melt (no. 2).

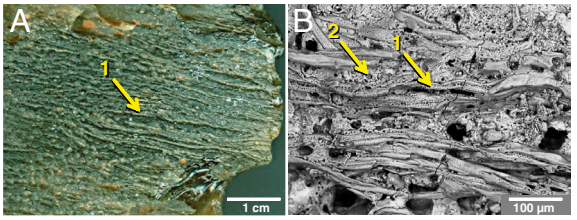

Fig. 12. (*A*) Libyan Desert Glass (7 cm wide) displaying tubular glassy texture (no. 1). (*B*) Abu Hureyra: lechatelierite tubes (no. 1) disturbed by chaotic plastic flow and embedded in a vesicular, CaO-rich matrix (no. 2).

Fig. S22), exhibits highly porous and vesiculated lechatelierite textures, especially along planes of weakness that formed during the shock compression and release stage. During impact, the SiO_2 melted at very high post-shock temperatures (>2,200 °C), produced taffy-like stringers as the shocked rock pulled apart during decompression, and formed many tiny vesicles from vapor outgassing. We also observed distorted layers of hollow vesiculated silica glass tube-like features, similar to some LDG samples (Fig. 12), which are attributed to relic sedimentary bedding structures in the sandstone precursor (39). The Abu Hureyra tubular textures may be relic structures of thin-bedded chert that occurs within the regional chalk deposits. These clusters of aligned micron-sized tubes are morphologically unlike single, centimeter-sized fulgurites, composed of melted glass tubes encased in unmelted sand. The Abu Hureyra tubes are fully melted with no sediment coating, consistent with having formed aerially, rather than below ground.

At Abu Hureyra, glass spherules have compositions comparable to associated SLOs (*SI Appendix*, Table S4) and show accretion and collision features similar to those from other YDB sites. For example, low-velocity elliptical impact pits were observed that formed by low-angle collisions during aerodynamic rotation of a spherule (Fig. 13*A*). The shape and low relief of the rims imply that the spherule was partially molten during impact. It appears that these objects were splattered with melt drapings while rotating within a debris cloud. Linear, subparallel, high-SiO_2 melt strands (94 wt% SiO_2) are mostly embedded within the high-CaO glass host, but some display raised relief on the host surface, thus implying that both were molten. An alternative explanation is that the strands are melt relics of precursor silica similar to fibrous lechatelierite (Fig. 11).

Melrose site, Pennsylvania. As with other sites, the Melrose site displays exotic YDB carbon phases, magnetic and glassy spherules, and coarse-grained SLOs up to 4 mm in size. The SLOs exhibit accretion and collision features consistent with flash melting and interactions within a debris cloud. Teardrop shapes are more common at Melrose than at other sites, and one typical teardrop (Fig. 14 *A* and *B*) displays high-temperature melt glass with mullite quench crystals on the glassy crust and with corundum in the

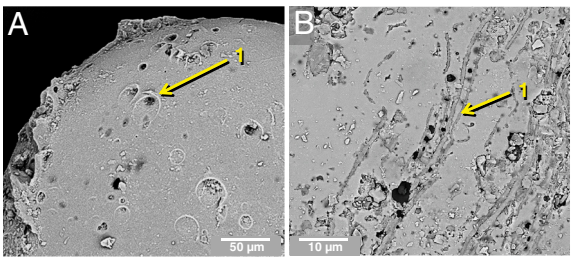

Fig. 13. Abu Hureyra: (*A*) SLO with low-angle impact craters (no. 1); half-formed rims show highest relief in direction of impacts and/or are counter to rotation of spherule. (*B*) Enlargement showing SiO_2 glass strands (no. 1) on and in surface.

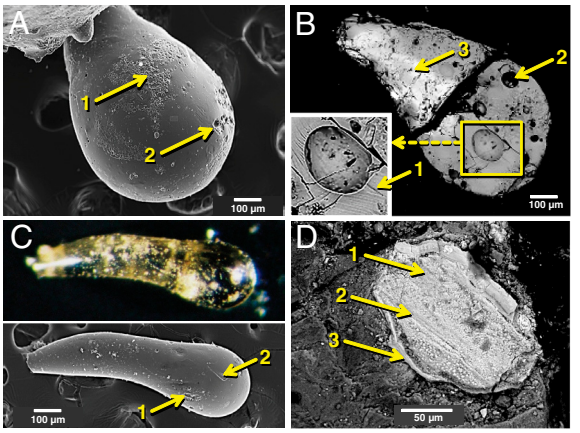

Fig. 14. Melrose. (*A*) Teardrop with aluminosilicate surface glass with mullite quench crystals (no. 1) and impact pits (no. 2). (*B*) Sectioned slide of *A* showing lechatelierite flow lines emanating from the nose (*Inset*, no. 1), vesicles (no. 2), and patches of quenched corundum and mullite crystals. The bright area (no. 3) is area with 30 wt% FeO compared with 15 wt% in darker grey areas. (*C*) Reflected light photomicrograph of *C* teardrop (*Top*) and SEM-BSE image (*Bottom*) of teardrop that is compositionally homogeneous to *A*; displays microcraters (no. 1) and flow marks (no. 2). (*D*) Melted magnetite (no. 1) embedded in glass-like carbon. The magnetite interior is composed of tiny droplets atop massive magnetite melt displaying flow lines (no. 2). The rapidly quenched rim with flow lines appears splash formed (no. 3).

interior. This teardrop is highly vesiculated and compositionally heterogeneous. FeO ranges from 15–30 wt%, SiO_2 from 40–48 wt %, and Al_2O_3 from 21–31 wt%. Longitudinally oriented flow lines suggest the teardrop was molten during flight. These teardrops (Fig. 14 *A*–*C*) are interpreted to have fallen where excavated because they are too fragile to have been transported or reworked by alluvial or glacial processes. If an airburst/impact created them, then these fragile materials suggest that the event occurred near the sampling site.

Other unusual objects from the Melrose site are high-temperature aluminosilicate spherules with partially melted accretion rims, reported for Melrose in Wu (13), displaying melting from the inside outward, in contrast to cosmic ablation spherules that melt from the outside inward. This characteristic was also observed in trinitite melt beads that have lechatelierite grains within the interior bulk glasses and partially melted to unmelted quartz grains embedded in the surfaces (22), suggesting that the quartz grains accreted within the hot plume. The heterogeneity of Melrose spherules, in combination with flow-oriented suessite and FeO droplets, strongly suggests that the molten host spherules accreted a coating of bulk sediment while rotating within the impact plume.

The minimum temperature required to melt typical bulk sediment is approximately 1,200 °C; however, for mullite and corundum solidus phases, the minimum temperature is >1,800°. The presence of suessite (Fe_3Si) and reduced native Fe implies a minimum temperature of >2,000 °C, the requisite temperature to promote liquid flow in aluminosilicate glass. Another high-temperature indicator is the presence of embedded, melted magnetite (melting point, 1,550 °C) (Fig. 14*D*), which is common in many SLOs and occurs as splash clumps on spherules at Melrose (*SI Appendix*, Fig. S23). In addition, lechatelierite is common in SLOs and glass spherules from Melrose; the minimum temperature for producing schlieren is >2,000 °C.

Trinity nuclear site, New Mexico. YDB objects are posited to have resulted from a cosmic airburst, similar to ones that produced Australasian tektites, Libyan Desert Glass, and Dakhleh Glass. Melted material from these sites is similar to melt glass from an atomic detonation, even though, because of radioactive materials, the means of surface heating is somewhat more complex

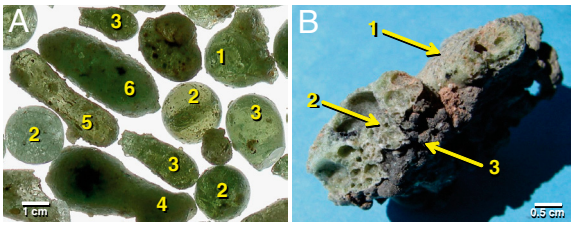

Fig. 15. Trinity detonation. (*A*) Assortment of backlit, translucent trinitite shapes: accretionary (no. 1), spherulitic (no. 2), broken teardrop (no. 3), bottle-shaped (no. 4), dumbbell (no. 5), elongated or oval (no. 6). (*B*) Edge-on view of a pancake trinitite with smooth top (no. 1), vesiculated interior (no. 2), and dark bottom (no. 3) composed of partially fused rounded trinitite objects incorporated with surface sediment.

(*SI Appendix*). To evaluate a possible connection, we analyzed material from the Alamogordo Bombing Range, where the world's first atomic bomb was detonated in 1945. Surface material at Trinity ground zero is mostly arkosic sand, composed of quartz, feldspar, muscovite, actinolite, and iron oxides. The detonation created a shallow crater (1.4 m deep and 80 m in diameter) and melted surface sediments into small glass beads, teardrops, and dumbbell-shaped glasses that were ejected hundreds of meters from ground zero (Fig. 15*A*). These objects rained onto the surface as molten droplets and rapidly congealed into pancake-like glass puddles (*SI Appendix*, Fig. S24). The top surface of this ejected trinitite is bright to pale grey-green and mostly smooth; the interior typically is heavily vesiculated (Fig. 17*B*). Some of the glassy melt was transported in the rising cloud of hot gases and dispersed as distal ejecta.

Temperatures at the interface between surface minerals and the puddled, molten trinitite can be estimated from the melting behavior of quartz grains and K-feldspar that adhered to the molten glass upon impact with the ground (*SI Appendix*, Fig. S22). Some quartz grains were only partly melted, whereas most other quartz was transformed into lechatelierite (26). Similarly, the K-feldspar experienced partial to complete melting. These observations set the temperature range from 1,250 °C (complete melting of K-feldspar) to >1,730 °C (onset of quartz melting). Trinitite samples exhibit the same high-temperature features as observed in materials from hard impacts, known airbursts, and the YDB layer. These include production of lechatelierite from quartz (T = 1,730–2,200 °C), melting of magnetite and ilmenite to form quench textures ($T \geq$ 1,550 °C), reduction of Fe to form native Fe spherules, and extensive flow features in bulk melts and lechatelierite grains (Fig. 16). The presence of quenched magnetite and native iron spherules in trinitite strongly suggests extreme oxygen fugacity conditions over very short distances (Fig. 17*B*); similar objects were observed in Blackville SLOs (Fig. 10*A*). Other features common to trinitite and YDB objects include accretion of spherules/beads on larger objects, impact microcratering, and melt draping (Figs. 16 and 17).

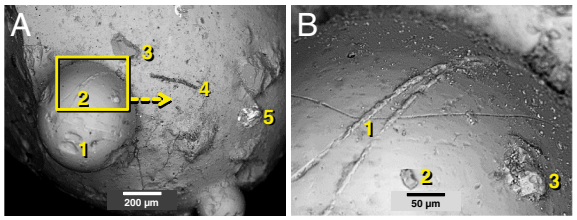

Fig. 16. Trinitite produced by debris cloud interactions. (*A*) Trinitite spherule showing accreted glass bead with impact pits (no. 1); melt drapings (no. 2); and embedded partially melted quartz grain (no. 3), carbon filament (no. 4), and melted magnetite grain (no. 5). (*B*) Enlarged image of box in *A* showing melt drapings (no. 1), and embedded partially melted quartz grain (no. 2) and melted magnetite grains (no. 3). See Fig. 9*D* for similar YDB melt drapings.

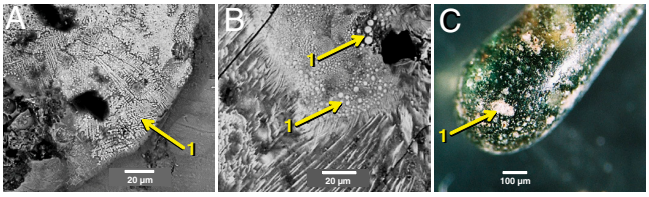

Fig. 17. Trinity: characteristics of high-temperature melting. (*A*) SEM-BSE image of bead in trinitite that is mostly quenched, dendritic magnetite (no. 1). (*B*) Melt beads of native Fe in etched glass (no. 1). (*C*) Heavily pitted head of a trinitite teardrop (no. 1) resulting from collisions in the debris cloud.

The Trinity nuclear event, a high-energy airburst, produced a wide range of melt products that are morphologically indistinguishable from YDB objects that are inferred to have formed during a high-energy airburst (*SI Appendix*, Table S1). In addition, those materials are morphologically indistinguishable from melt products from other proposed cosmic airbursts, including Australasian tektites, Dakhleh Glass, and Tunguska spherules and glass. All this suggests similar formation mechanisms for the melt materials observed in of these high-energy events.

Methods

YDB objects were extracted by 15 individuals at 12 different institutions, using a detailed protocol described in Firestone et al. (1) and Israde-Alcántara et al. (4). Using a neodymium magnet (5.15 × 2.5 × 1.3 cm; grade N52 NdFeB; magnetization vector along 2.5-cm face; surface field density = 0.4 T; pull force = 428 N) tightly wrapped in a 4-mil plastic bag, the magnetic grain fraction (dominantly magnetite) was extracted from slurries of 300–500 g bulk sediment and then dried. Next, the magnetic fraction was sorted into multiple size fractions using a stack of ASTM sieves ranging from 850–38 µm. Aliquots of each size fraction were examined using a 300× reflected light microscope to identify candidate spherules and to acquire photomicrographs (Fig. 1), after which candidate spherules were manually selected, tallied, and transferred to SEM mounts. SEM-EDS analysis of the candidate spherules enabled identification of spherules formed through cosmic impact compared with terrestrial grains of detrital and framboidal origin. From the magnetic fractions, SLO candidates >250 µm were identified and separated manually using a light microscope from dry-sieved aliquots and weighed to provide abundance estimates. Twelve researchers at 11 different universities acquired SEM images and obtained >410 analyses. Compositions of YDB objects were determined using standard procedures for SEM-EDS, electron microprobe, INAA, and PGAA.

Conclusions

Abundance peaks in SLOs were observed in the YDB layer at three dated sites at the onset of the YD cooling episode (12.9 ka). Two are in North America and one is in the Middle East, extending the existence of YDB proxies into Asia. SLO peaks are coincident with peaks in glassy and Fe-rich spherules and are coeval with YDB spherule peaks at 15 other sites across three continents. In addition, independent researchers working at one well-dated site in North America (8) and one in South America (10–12) have reported YDB melt glass that is similar to these SLOs. YDB objects have now been observed in a total of eight countries on four continents separated by up to 12,000 km with no known limit in extent. The following lines of evidence support a cosmic impact origin for these materials.

Geochemistry. Our research demonstrates that YDB spherules and SLOs have compositions similar to known high-temperature, impact-produced material, including tektites and ejecta. In addition, YDB objects are indistinguishable from high-temperature melt products formed in the Trinity atomic explosion. Furthermore, bulk compositions of YDB objects are inconsistent with known cosmic, anthropogenic, authigenic, and volcanic materials, whereas they are consistent with intense heating, mixing, and quenching of local terrestrial materials (mud, silt, clay, shale).

Morphology. Dendritic texturing of Fe-rich spherules and some SLOs resulted from rapid quenching of molten material. Requisite temperatures eliminate terrestrial explanations for the 12.9-kyr-old material (e.g., framboids and detrital magnetite), which show no evidence of melting. The age, geochemistry, and morphology of SLOs are similar across two continents, consistent with the hypothesis that the SLOs formed during a cosmic impact event involving multiple impactors across a wide area of the Earth.

Lechatelierite and Schlieren. Melting of SLOs, some of which are >80% SiO_2 with pure SiO_2 inclusions, requires temperatures from 1,700–2,200 °C to produce the distinctive flow-melt bands. These features are only consistent with a cosmic impact event and preclude all known terrestrial processes, including volcanism, bacterial activity, authigenesis, contact metamorphism, wildfires, and coal seam fires. Depths of burial to 14 m eliminate modern anthropogenic activities as potential sources, and the extremely high melting temperatures of up to 2,200 °C preclude anthropogenic activities (e.g., pottery-making, glass-making, and metal-smelting) by the contemporary cultures.

Microcratering. The YDB objects display evidence of microcratering and destructive collisions, which, because of the high initial and differential velocities required, form only during cosmic impact events and nuclear explosions. Such features do not result from anthropogenesis or volcanism.

Summary. Our observations indicate that YDB objects are similar to material produced in nuclear airbursts, impact crater plumes, and cosmic airbursts, and strongly support the hypothesis of multiple cosmic airburst/impacts at 12.9 ka. Data presented here require that thermal radiation from air shocks was sufficient to melt surface sediments at temperatures up to or greater than the boiling point of quartz (2,200 °C). For impacting cosmic fragments, larger melt masses tend to be produced by impactors with greater mass, velocity, and/or closeness to the surface. Of the 18 investigated sites, only Abu Hureyra, Blackville, and Melrose display large melt masses of SLOs, and this observation suggests that each of these sites was near the center of a high-energy airburst/impact. Because these three sites in North America and the Middle East are separated by 1,000–10,000 km, we propose that there were three or more major impact/airburst epicenters for the YDB impact event. If so, the much higher concentration of SLOs at Abu Hureyra suggests that the effects on that settlement and its inhabitants would have been severe.

ACKNOWLEDGMENTS. We thank Malcolm LeCompte, Scott Harris, Yvonne Malinowski, Paula Zitzelberger, and Lawrence Edge for providing crucial samples, data, and other assistance; and Anthony Irving, Richard Grieve, and two anonymous reviewers for useful reviews and comments on this paper. This research was supported in part by US Department of Energy Contract DE-AC02-05CH11231 and US National Science Foundation Grant 9986999 (to R.B.F.); US National Science Foundation Grants ATM-0713769 and OCE-0825322, Marine Geology and Geophysics (to J.P.K.); US National Science Foundation Grant OCD-0244201 (to D.J.K.); and US National Science Foundation Grant EAR-0609609, Geophysics (to G.K.).

1. Firestone RB, et al. (2007) Evidence for an extraterrestrial impact 12,900 years ago that contributed to the megafaunal extinctions and the Younger Dryas cooling. *Proc Natl Acad Sci USA* 104:16016–16021.
2. Haynes CV, Jr (2008) Younger Dryas "black mats" and the Rancholabrean termination in North America. *Proc Natl Acad Sci USA* 105:6520–6525.
3. Kennett DJ, et al. (2009) Shock-synthesized hexagonal diamonds in Younger Dryas boundary sediments. *Proc Natl Acad Sci USA* 106:12623–12628.
4. Israde-Alcántara I, et al. (2012) Evidence from central Mexico supporting the Younger Dryas extraterrestrial impact hypothesis. *Proc Natl Acad Sci USA* 109: E738–E747.
5. Melott AL, Thomas BC, Dreschhoff G, Johnson CK (2010) Cometary airbursts and atmospheric chemistry: Tunguska and a candidate Younger Dryas event. *Geology* 38:355–358.
6. Surovell TA, et al. (2009) An independent evaluation of the Younger Dryas extraterrestrial impact hypothesis. *Proc Natl Acad Sci USA* 104:18155–18158.
7. Pinter N, et al. (2011) The Younger Dryas impact hypothesis: A requiem. *Earth-Sci Rev* 106:247–264.
8. Fayek M, Anovitz LM, Allard LF, Hull S (2012) Framboidal iron oxide: Chondrite-like material from the black mat, Murray Springs, Arizona. *Earth Planet Sci Lett* 319–320:251–258.
9. Haynes CV, Jr, et al. (2010) The Murray Springs Clovis site, Pleistocene extinction, and the question of extraterrestrial impact. *Proc Natl Acad Sci USA* 107:4010–4015.
10. Mahaney WC, et al. (2010) Evidence from the northwestern Venezuelan Andes for extraterrestrial impact: The black mat enigma. *Geomorphology* 116:48–57.
11. Mahaney WC, et al. (2011) Fired glaciofluvial sediment in the northwestern Andes: Biotic aspects of the black mat. *Sediment Geol* 237:73–83.
12. Mahaney WC, Krinsley D (2012) Extreme heating events and effects in the natural environment: Implications for environmental geomorphology. *Geomorphology* 139–140:348–359.
13. Wu Y (2011) Origin and provenance of magnetic spherules at the Younger Dryas boundary. Thesis (Dartmouth College, Hanover, NH).
14. Pigati JS, et al. (2012) Accumulation of "impact markers" in desert wetlands and implications for the Younger Dryas impact hypothesis. *Proc Natl Acad Sci USA* 109:7208–7212 .
15. French BM (1998) *Traces of Catastrophe. LPI Contribution* No. 954 (LPI, Houston), pp 102–103.
16. Chao ETC (1967) Shock effects in certain rock forming minerals. *Science* 156:192–202.
17. Wasson J (2003) Large aerial bursts: An important class of terrestrial accretionary events. *Astrobiology* 3:163–179.
18. Osinski GR, et al. (2008) The Dakhleh Glass: Product of an impact airburst or cratering event in the Western Desert of Egypt? *Meteorit Planet Sci* 43:2089–2107.
19. Kirova OA, Zaslavskaya NI (1966) Data characterizing the dispersed matter as recovered from the area of fall of the Tunguska meteorite. *Meteoritika* 27:119–127.
20. Hermes RE, Strickfaden WB (2005) A new look at trinitite. *J Nucl Weap* 2:2–7.
21. Moore AMT, Hillman GC, Legge AJ (2000) *Village on the Euphrates* (Oxford University Press, New York).
22. Eby N, Hermes R, Charnley N, Smoliga JA (2010) Trinitite: The atomic rock. *Geol Today* 26:181–186.
23. Taylor S, Lever JH, Harvey RP (2000) Numbers, types, and compositions of an unbiased collection of cosmic spherules. *Meteorit Planet Sci* 35:651–666.
24. Doyle LJ, Hopkins TL, Betzer PR (1976) Black magnetic spherule fallout in the eastern Gulf of Mexico. *Science* 194:1157–1159.
25. Glass BP, Senftle FE, Muenow DW, Aggrey KE, Thorpe AN (1987) Atomic bomb glass beads: Tektite and microtektite analogs. *Proceedings of the Second International Conference on Natural Glasses*, ed J Konta (Charles University, Prague), pp 361–369.
26. Grieve RAF, Pillington M (1996) The significance of terrestrial impact craters. *AGSO J Aust Geol Geophy* 16:399–420.
27. Stöffler D, Langenhorst F (1994) Shock metamorphism of quartz in nature and experiments: I. Basic observations and theory. *Meteorit Planet Sci* 31:6–35.
28. Rutherford MJ, Devine JD, III (2008) Magmatic conditions and processes in the storage zone of the 2004–2006 Mount St. Helens dacite. *US Geological Survey Professional Paper 1750*.
29. Philpot CW (1965) *Temperatures in a Large Natural-Fuel Fire* (US Forestry Service, Pacific Southwest Forest and Range Experimental Station, Berkeley) , Research Note PSW-90.
30. Gimeno-Garcia E, Andreu E, Rubio JL (2004) Spatial patterns of soil temperatures during experimental fires. *Geoderma* 118:17–38.
31. Thy P (1995) Implications of prehistoric glassy biomass slag from east-central Botswana. *J Archaeol Sci* 22:629–637.
32. Beretta M (2009) *The Alchemy of Glass: Counterfeit, Imitation, and Transmutation in Ancient Glassmaking* (Science History Publications, Sagamore Beach).
33. Wasson JT, Moore K (1998) Possible formation of Libyan Desert Glass by a Tunguska-like aerial burst. *Meteorit Planet Sci* 33(Suppl):A163–A164.
34. Walter LS (1965) Coesite discovered in tektites. *Science* 147:1029–1032.
35. Kyte F, et al. (2010) Accretionary growth on impact spherules. *Meteorit Planet Sci* 45 (Suppl S):A113–A113.
36. Prasad MS, Khedekar VD (2003) Impact microcrater morphology on Australasian microtektites. *Meteorit Planet Sci* 38:1351–1371.
37. Mirsa S, et al. (2010) Geochemical identification of impactor for Lonar Crater, India. *Meteorit Planet Sci* 44:1001–1018.
38. Rietmeijer FJM, et al. (2008) Origin and formation of iron silicide phases in the aerogel of the Stardust mission. *Meteorit Planet Sci* 43:121–134.
39. Longinelli A, et al. (2011) Delta ^{18}O and chemical composition of Libyan Desert Glass, country rocks, and sands: New considerations on target material. *Meteorit Planet Sci* 46:218–227.
40. Winkler HGF (1979) *Petrogenesis of Metamorphic Rocks* (Springer, New York).
41. US Geological Survey (2001) (USGS, Reston). *Geochemistry of Soils in the US from the PLUTO Database* (USGS, Reston, VA).

Very High-Temperature Impact Melt Products as Evidence for Cosmic Airbursts and Impacts 12,900 years ago

SUPPORTING INFORMATION: IMAGES

HYPERLINKS:

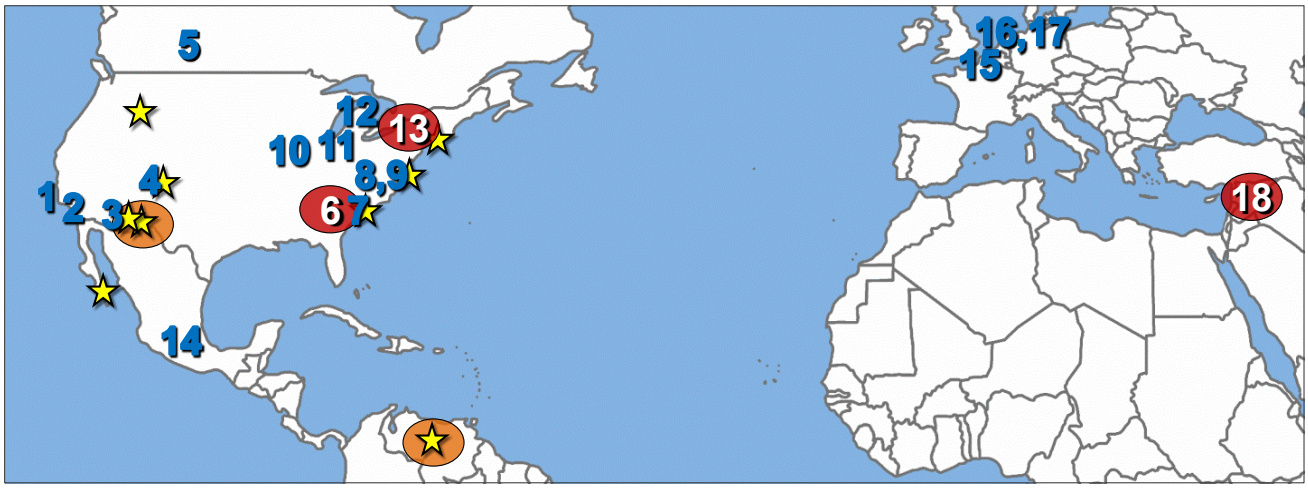

Figure S1. Site Map for 18 numbered sites in this study (described below), spanning about 12,000 km of the Northern Hemisphere. Currently, there is no known limit to the YDB impact field.

SLOs and spherules were observed at the three numbered sites in red circles: (#6) Blackville, South Carolina; (#13) Melrose, Pennsylvania; and (#18) Abu Hureyra, Syria.

Impact-related spherules without SLOs were observed at the other sites numbered in blue as follows: (#1) Arlington Canyon, California; (#2) Talega, California; (#3) Murray Springs, Arizona; (#4) Blackwater Draw, New Mexico; (#5) Chobot, AB, Canada; (#7) Topper, South Carolina; (#8) Barber Creek, North Carolina; (#9) Kimbel Bay, North Carolina; (#10) Big Eddy, Missouri; (#11) Sheriden Cave, Ohio; (#12) Gainey, Michigan; (#14) Cuitzeo, Mexico; (#15) Lommel, Belgium; (#16) Ommen, Netherlands; and (#17) Lingen, Germany.

Independent research. Also shown are 9 sites (yellow stars) investigated by 7 independent groups. SLOs were found at two sites, marked with a star in orange circle: Venezuela (Mahaney *et al.*, 2011) and Arizona (Fayek *et al.*, 2008, 2011). Impact-related YDB microspherules without SLOs were reported in the YDB layer in Montana (Baker *et al.*, 2008); Arizona (Haynes *et al.*, 2010); Mexico (Scruggs *et al.*, 2010); New Mexico, Maryland, South Carolina (LeCompte *et al.*, 2010); and Pennsylvania (Wu *et al.*, 2011).

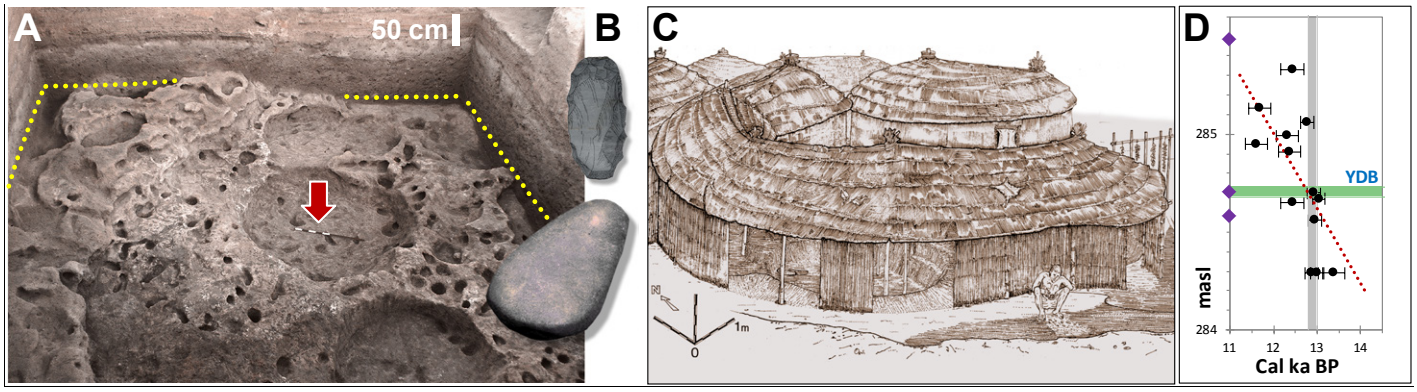

Figure S2. Abu Hureyra, Syria. A) This site is located on an archaeological mound, or "tell," about 14 km west of Al Thawra, Syria (lat/long: 35.8667°N, 38.4000°E)**.** The site was excavated shortly before being flooded by the filling of Lake Assad in 1974. Sediment samples and archeological collections are curated at the University College London, but the site remains submerged >25 m below the lake surface. Trench E, 7×7 m square (shown above) displayed circular floor depressions that are all that remains of pit-houses used by inhabitants at 12.9 ka. The YDB layer is represented by the yellow dotted line. **B)** A 60-cm grinding stone (bottom), found inside the pit-house at red arrow, dates to the YDB, and was used to process food grains, when the villagers began cultivating plants including a domesticated variety of rye (Moore *et al.*, 1986, 2000; Moore and Hillman, 1992; Hillman *et al.*, 2001). At center top is an illustration of an 8-cm flaked stone tool from approximately the same level as the grindstone. **C)** Illustration of thatched pit-houses used at 12.9 ka by hunter-gatherers in a village covering approximately 2000 m^2. **D)** Linear interpolation is used to develop an age-depth model based on 13 accelerator mass spectrometry (AMS) radiocarbon dates from Moore *et al.* (2000) (red dotted line) (**SI Table 2**). The vertical gray bar represents 12.9 ± 0.1 ka, and the purple diamonds represent sediment sampling locations. The green bar shows the depth of the peaks in SLOs and spherules in Level 445 (see Figure S3), a 3-cm-thick layer centered at 284.7 above sea level (asl) from 284.69 and 284.72 m asl at 4.1 m below surface (mbs) (**Figure S3)**. Based on linear interpolation, the YDB layer is within the 12.9-ka age range.

Abu Hureyra Site; Stratigraphy and the YDB. Much of northern Syria consists of calcareous Mediterranean, steppe, and desert soils, all of which are enriched in CaO and SiO_2. This site is near the Euphrates River on well-developed, unconsolidated limey, silty sand, atop massive limestone deposits. Six samples of bulk sediment were examined over a 3.02-m interval from 287.6 to 284.58 m asl, as shown in **Figure S3**, exhibiting an average composition of SiO_2 at 31 weight percentage (wt%), CaO at 26 wt%, FeO^T at 12 wt%, and Al_2O_3, at 11 wt% (**SI Table 4**). The six samples display negligible compositional differences, except for the presence of higher carbon content from charcoal and ash in Level 445, excavated from just outside a pit-house (**Figure S3)**. All such YD-aged pit-houses at Abu Hureyra and their immediate environs contained a dark charcoal-rich layer indicating extensive burning that the excavators previously attributed to residue from cooking fires (Moore *et al.*, 2000), but which is also consistent with broader-scale biomass burning at 12.9 ka. Level 445 was a 3-cm-thick layer (yellow dotted line in **Figure S2A**), centered at 4.1 mbs or 284.7 m asl, relative to a local reference elevation. In addition to an abundance peak in charcoal, Level 445 contained major peaks in spherules (595/kg) and SLOs (15.8 g/kg; the highest of any site investigated), consistent with being the YDB layer.

The palynological and macrobotanical record at the site demonstrates that Level 445 coincides with major climatic change, previously interpreted to represent the onset of the Younger Dryas cooling episode (Moore *et al.*, 2000; Hillman *et al.*, 2001). At that time the regional environment of Abu Hureyra abruptly changed from a moist woodland-steppe to an arid, treeless steppe. This change is reflected by the sudden decline in abundance of charred seed remains of several major groups of food: (a) a decline of approximately 100% in seeds of food plants, such as wild pears and cherries, found in an oak-dominated park-woodland, which disappeared from the Abu Hureyra area at the YD onset; (b) a decline of approximately 70% in seeds of some legumes; and (c) a decline of approximately 60% in grains of wild ryes and wheat (Hillman *et al.* 2001). Altogether, changes in more than 150 species of plants reflect the major effects of this abrupt climatic change from warmer, moister conditions of the Bølling-Allerød episode to cooler, dryer condition at the onset of the YD at 12.9 ka. This climatic change coincides with deposition of SLOs and impact-related spherules in the YDB layer at Abu Hureyra.

Lateral Distribution of SLOs. To examine the lateral extent of the SLOs at Abu Hureyra, we sampled about 4.5 m away in the stratum above the YDB layer (levels 402-406) and observed about 0.23 g/kg of SLOs. This indicates that the SLOS are not limited to just one small area of the excavation trench.

Chronology and the YDB layer. We have adopted the chronology for Trench E of Moore *et al.* (2000), who acquired AMS radiocarbon dates on charcoal and charred bones, seeds, and grains (SI Table 2). Those authors collected non-contiguous samples in Trench E from various locations across 1.66 m of sediment ranging from about 284.24 to 285.90 m asl. For those samples, 13 AMS ^{14}C dates were acquired, ranging from 11.45 ± 0.30 ^{14}C kiloannum before present, or ka BP (13.37 ± 0.30 calibrated

kiloannum before present, or cal ka BP) to 10.60 ± 0.20 ^{14}C ka BP (12.43 ± 0.27 cal ka BP) (**SI Table 2**; Moore *et al.*, 2000). Based on linear interpolation of 13 ^{14}C dates, the 3-cm-thick proxy-rich YDB layer at Level 445 at 284.7 m asl (**Figure S3**) dates to 12.9 ± 0.15 ka, consistent with the age of the YDB at other sites.

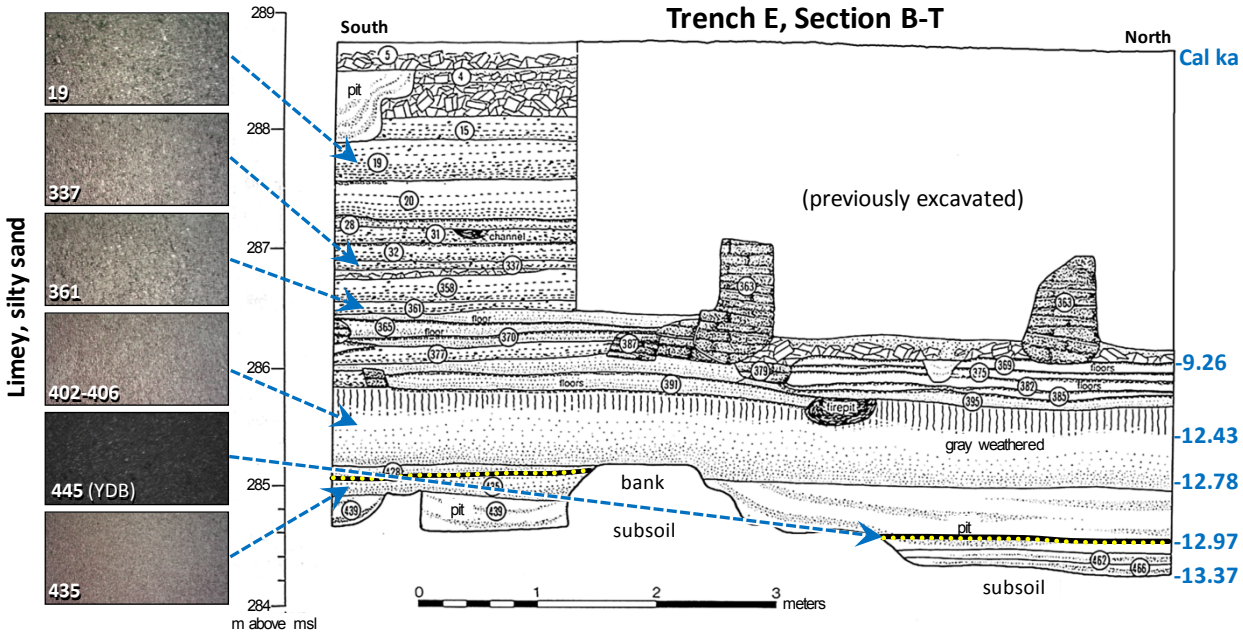

Figure S3. Cross-section diagram, matching the far wall of Trench E, shown in **Figure S2A.** "Bank" in this diagram corresponds to the highest point of the floor in the far wall in **Figure S1A.** Photomicrographs at left show colors of bulk sediment from the samples analyzed. Arrows point to the position of each sample in stratigraphic profile. The uniquely dark, charcoal-rich Level 445 (yellow dotted line, equivalent to yellow line in **Figure S2A**) displays peaks in SLOs and spherules. The YDB layer marking the onset of YD cooling at 12.9 ka is shown relative to the scale at right displaying five radiocarbon dates in cal ka BP, listed in **SI Table 2**.

Archaeological Importance of Abu Hureyra Site. This site in the Euphrates Valley in northern Syria is significant because it documents how and when hunter-gatherers in Western Asia began to cultivate domesticated plants, a fundamental step towards transforming human societies in the region during subsequent millennia (Moore *et al.*, 2000). Abu Hureyra is at present the oldest known site in the world demonstrating the transition from hunting-gathering to cultivation. Most final Epipalaeolithic hunter-gatherer and early Neolithic agricultural sites in Western Asia were located in separate places because of the different ecological requirements of these contrasting ways of life, and this has made it difficult to trace the course of the transition. Abu Hureyra, however, was inhabited relatively continuously from the Late Glacial into the early Holocene because it offered resources appropriate for both groups. The site's unusually lengthy occupation (6 kyrs from 13.4 to 7.5 ka) spanned major changes in climate and vegetation that are clearly visible in the archaeological record from the site and are connected to world-wide abrupt environmental adjustments during the Pleistocene-Holocene transition.

At the onset of the Bølling-Allerød episode at 14.6 ka, during what is called Phase 1 at Abu Hureyra, the climate across Western Asia, as elsewhere, began to ameliorate as temperatures rose and rainfall increased (Renssen *et al.* 2001; Robinson *et al.* 2006). This change stimulated an expansion of open woodland and grassland from the Mediterranean coast eastwards into the interior, creating highly favorable conditions for Late Glacial hunter-gatherers, whose numbers increased as a consequence (Moore *et al.,* 2000). The foragers who established the settlement at Abu Hureyra were attracted by an unusual array of resources, because the site lay at the edge of the Euphrates floodplain, giving easy access to two environmental zones, the river valley bottom and the woodland-steppe beyond, both important for the wild plant foods they offered. Furthermore, the site lay on a gazelle migration route that offered a rich seasonal meat source for the inhabitants. This abundance of edible wild plants and animals enabled the inhabitants to live at the site year-round, and therefore, they became sedentary hunter-gatherers for a few centuries.

During Phase 2 at Abu Hureyra, the beginning of which coincides with drier and cooler climate at the onset of the Younger Dryas at 12.9 ka, the vegetation around the site altered markedly as open woodland was replaced by arid steppe. This sudden change is documented in the plant remains recovered from the site itself and, more generally, in regional pollen core sequences (Moore and Hillman, 1992). Across large areas of Western Asia, patterns of settlement and economy among contemporary hunter-gatherer groups were disrupted. At Abu Hureyra, however, the inhabitants adopted farming at 12.9 ka while continuing to exploit wild plant and animal foods. Their crops included rye, lentils, and einkorn wheat (literally "single grain"), enabling them to maintain year-round occupation of the village.

In the following millennia, the villagers developed a

mature farming system from this nascent agricultural economy. They added more crops to the mix, including barley, bread wheat, and chickpeas, and also the main species of domestic animals, first, sheep and goats and then later, cattle and pigs. Sedentary village life supported by productive farming enabled the population to increase, such that in its later stages, Abu Hureyra had several thousand inhabitants and covered up to 16 hectare. The effects of this new way of life are clearly recorded archaeologically, including evidence for increased population size, the reorganization of the village layout, and new forms of houses. Also, the hard work required for growing and processing food was reflected in the skeletons of the people buried on site.

The adoption of plant cultivation at Abu Hureyra was caused by the convergence of several factors, one of which was the increase in the number of hunter-gatherers across the region, occasioned by an ameliorating environment towards the end of the Pleistocene. However, the catalyst for the ultimate adoption of plant cultivation was the rapid onset of the Younger Dryas and the disruption it caused. Only by adopting plant cultivation could the already-sedentary inhabitants of Abu Hureyra remain in place and maintain their settlement. We can now identify the Younger Dryas cooling event, felt widely across the planet, as a causal mechanism for the changes at Abu Hureyra, including the beginnings of domesticated plant cultivation.

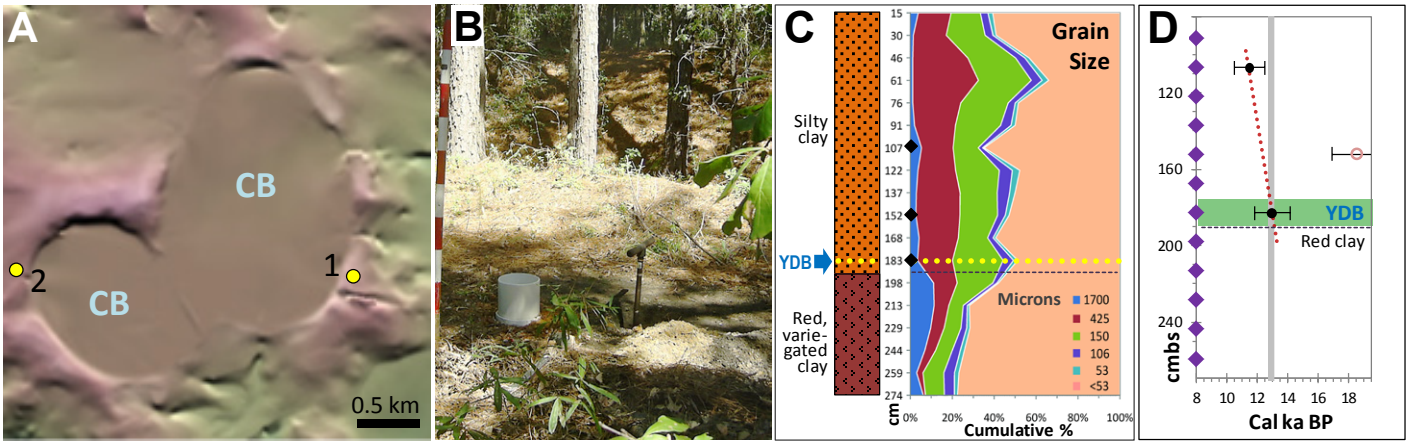

Figure S4. Blackville, SC. Core #1. A) The sampling site is about 3.2 km WNW of the town of Blackville (lat/long: 33.361545°N, 81.304348°W). The digital elevation model shows area topography, including several Carolina Bays (CB). Eighteen samples were acquired by coring from the widest and thickest part of the rim of a bay (core #1). **B)** Photo of sampling location with handle of core auger visible. **C)** Lithostratigraphy of section and sediment grain size distribution. Optically stimulated luminescence (OSL) sample depths in cm below surface (cmbs) are denoted by black diamonds; top of clay section is denoted by black dashed line. **D)** OSL dates place the onset of the YD at 12.9 ka in the sample centered at 183 cmbs (174 to 190 cm). Linear interpolation is used to develop an age-depth model (red dotted line) based on two OSL dates (**SI Table 2**). The vertical gray bar represents 12.9 ± 0.1 ka, and sediment sample locations are represented by purple diamonds. The green bar shows the depth of the peaks in SLOs and spherules in the 15-cm sample centered at 183 cmbs. Based on linear interpolation, the YDB layer is within the 12.9-ka age range.

Blackville Site. Stratigraphy and the YDB layer in Core #1. According to USGS maps (Horton and Dicken, 2001), the geologic profile for Blackville includes unconsolidated Quaternary alluvium over ~1-million-year-old Miocene marine clay. At the site, the surficial sediments are eolian and alluvial sediments comprised of variable loamy to silty red clays down to 190 cmbs. Immediately beneath 190 cmbs, there is massive, variegated, red clay, interpreted to be a paleosol that predates bay rim formation. There is an unconformity at this level, supported by the sharp increase from approximately 50% to 80% in fine-grained sediments (<53 μm), which increase with depth beginning at 190 cmbs and continuing to 274 cmbs (**Figure S4C**). Eighteen contiguous 15-cm-thick core samples of bulk sediment were examined from the surface to 274 cmbs, showing an average composition in the YDB layer of SiO_2 at 61 wt%, FeO^T at 10 wt%, and Al_2O_3 at 21 wt% (**SI Table 4**). Eleven samples were examined for SLOs and spherules, revealing a peak in SLOs (0.06 g/kg) and spherules (525/kg) in the 15-cm-thick interval centered at 183 cmbs (**SI Tables 2 & 3**).

Lateral Distributions of SLOs. At Blackville, we sampled the same stratigraphic level about 10 m away from the first location and observed about 0.02 g/kg of SLOs, comparable to abundances in core #1 (0.06 g/kg). This indicates that the SLOS are not limited to just one small area of the site. To further investigate the local distribution of YDB objects, Scott Harris extracted core #2 from an adjacent Carolina Bay rim 2.2 km to the west (lat/long: 33.364134°N, 81.328086°) and recovered 19 samples down to 163 cmbs. As in core #1, the sediments were mostly variable loamy to silty red clays, unconformably overlying massive red clay at 110 cmbs. We observed a broad peak in spherules (180/kg) from 80 to 100 cmbs, significantly lower in abundances than in core #1 (525/kg). No SLOs were observed. These results show a) that abundances of spherules are widespread in the area, but vary significantly over short distances, and b) that SLOs have highly variable local distribution and are absent in some places.

Chronology and the YDB layer. Because of a dearth of datable charcoal and because of sediment mixing

by deep-rooted plants, a recognized problem in this region (Casson and Feathers, 2001), radiocarbon dating of the YDB layer was not possible. Consequently, OSL dating of three samples was undertaken with the limited objective of testing whether the age of the layer containing SLOs and spherules is consistent with an age of 12.9 ka. Limitations of the OSL method include wide uncertainties of >1000 years, typically larger than for ^{14}C dating. The dating methodology required multiple small aliquots comprised of approximately100 quartz grains for each sample (Murray and Wintle, 2000). Standard practice was used at the OSL laboratory (IIRMES, California State University Long Beach) to obtain an average age for the sediment samples (Feathers, 2003).

OSL dating was conducted on three samples, including one centered at 183 cmbs in the layer containing peaks in SLOs and spherules. The dates obtained were 12.96 ± 1.19 ka at 183 cmbs, 18.54 ± 1.68 ka at 152 cmbs, and 11.5 ± 1.03 ka at 107 cmbs at 1σ probability (**SI Table 1**). The OSL age of 12.96 ka for the 183-cm, proxy-rich layer corresponds to the YDB age of 12.9 ka ± 010 ka, as published by Firestone *et al.* The two dates at 107 and 183 cmbs were used to generate an age-depth model, excluding the sample at 152 cmbs because of the large magnitude of the age reversal, i.e., older sediments lying stratigraphically higher than younger sediments. The age of the proxy-rich layer is consistent with the YDB age at other sites.

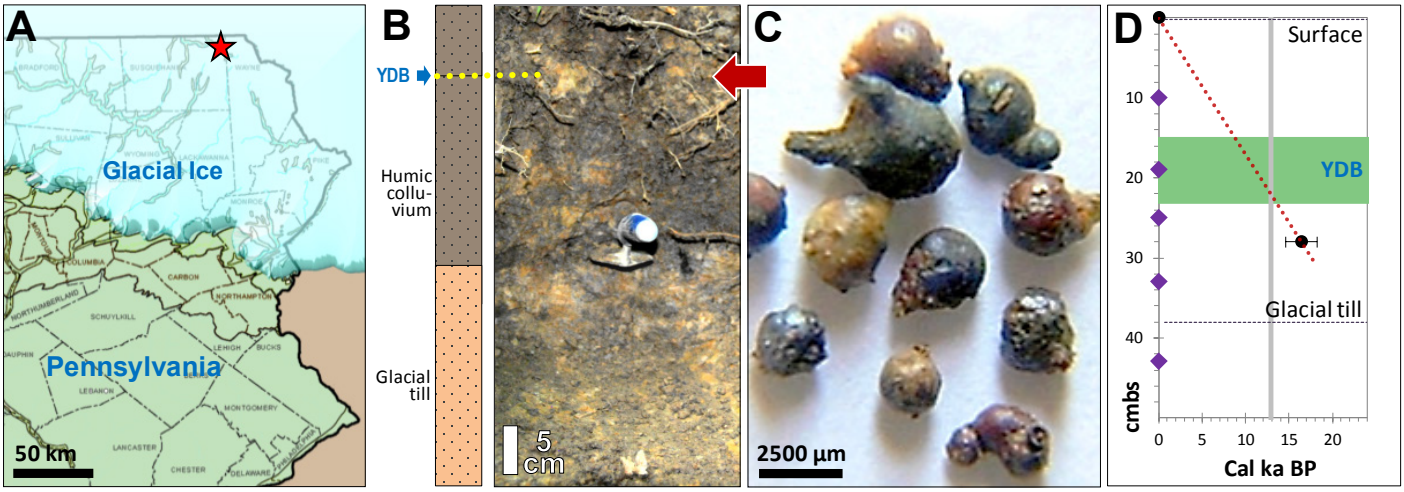

Figure S5. Melrose, PA. **A)** Area map showing location of the site (red star) about 1 km SW of the town of Melrose in northeastern PA (lat/long: 41.925350°N, 75.510066°W). The map shows the extent of glacial advance of the Laurentide Ice Sheet at approximately 25 ka (Fullerton *et al.* 2003) and began to retreat rapidly after 18 ka (Colgan *et al.*, 2003). **B)** Photo of exploratory trench showing lighter-colored glacial till (diamicton; below trowel), overlain by darker humic colluvium (photo credit: Malcolm LeCompte). The YDB is located in the colluvium in an 8-cm-thick layer from 15 to 23 cmbs, centered at 19 cmbs. **C)** Photomicrographs of subrounded SLOs ranging from about 800 to 5000 µm recovered from the YDB layer. These objects display evidence of melting at >2000°C, including lechatelierite (main paper, **Fig. 5C**), schlieren (**Fig. 16B**), impact pitting (**Fig. 6A**), and melt drapings (**Fig. 16D**) that conclusively rule out an origin by anthropogenesis, volcanism, or authigenesis. **D)** Linear interpolation is used to develop an age-depth model (red dotted line) based on one OSL date at 28 cmbs and the inferred age of surface sediments (**SI Table 2**). The vertical gray bar represents 12.9 ± 0.1 ka, and sediment sample locations are represented by purple diamonds. The green bar shows the depth of the peaks in SLOs and spherules in the 8-cm sample centered at 19 cmbs. Based on linear interpolation, the YDB layer is within the 12.9-ka age range.

Melrose site. Stratigraphy and the YDB layer. During the Last Glacial Maximum, the Melrose area in NE Pennsylvania lay beneath 0.5 to 1 km of glacial ice that reached maximum extent at approximately 25 ka and began to retreat rapidly after ~18 ka (Colgan *et al.*, 2003). According to the USGS (Berg *et al.*, 1980), the general geologic profile for Melrose is unconsolidated Quaternary alluvium over Pleistocene glacial till over the Devonian Catskill formation, comprised of sandstone, siltstone, shale, and mudstone. At this site, a shallow reconnaissance trench was excavated, and five contiguous samples were taken from 5 cmbs down to a depth of 48 cmbs. The sedimentary profile consists of fine-grained, humic colluvium down to 38 cmbs, resting on well-defined end-Pleistocene glacial till (diamicton, Figure S5B), comprised of 40 wt% angular clasts >2 mm in diameter. Bulk sediment showed an average composition of SiO_2 at 56 wt%, FeO^T at 11 wt%, and Al_2O_3 at 19 wt% (**SI Table 4**). Major abundance peaks in SLOs (0.8 g/kg) and spherules (3100/kg) occurred in an 8-cm-thick interval at 19 cmbs from 15 to 23 cmbs about 15 cm above the till, consistent with emplacement after 18 ka when the ice sheet retreated.

Lateral Distribution of SLOs. At Melrose, we sampled the same stratigraphic level above glacial till about 28 m away from the original sampling location. We found SLOs in about the same abundance (approximately 0.5 g/kg) as at the main site. To investigate whether SLOs are distributed more widely, we examined a forested site 28 km SSE from Melrose (41.698N, 75.347W). The site was selected because it was known to have been glaciated

(Fullerton *et al.* 2003), the topography was similar to that at Melrose, and the site is currently undisturbed by agricultural activities. Inspection revealed the sediment to be humic colluvium, containing angular clasts consistent with reworked glacial material. We extracted one 15-cm-thick sample across the interval from 15 to 30 cmbs, spanning the same 8-cm-thick interval as the YDB layer at Melrose (15 to 23 cm). Processing revealed that the sample contained >0.5 g/kg of SLOs up to 2 mm in diameter compared to 0.8 g/kg at Melrose, along with 2500 spherules/kg compared to 3100/kg. These results indicate that for these two sites a) abundances of SLOs and spherules are similar even though separated by 28 m and up to 28 km, and b) SLOs in the area are not limited to the Melrose site, although there are insufficient data to determine the extent of coverage.

Chronology and the YDB layer. Because of a dearth of datable charcoal at Melrose and because of sediment mixing by deep-rooted plants, as at Blackville, it was not possible to acquire direct radiometric dating of the sedimentary profile. Instead, we collected a sample for OSL dating at 28 cmbs, 5 cm below the layer containing peaks in SLOs and spherules (see approaches described earlier for the Blackville site). The sample yielded an OSL date of 16.4 ± 1.6 ka (**SI Table 2**), and assuming a modern age for the surface layer, then linear interpolation dates the proxy-rich YDB layer centered at a depth of 19 cmbs to 12.9 ± 1.6 ka. This date is supported by its location relative to the glacial till known to date to <18 ka (Colgan *et al.,* 2003) and is consistent with a YDB age.

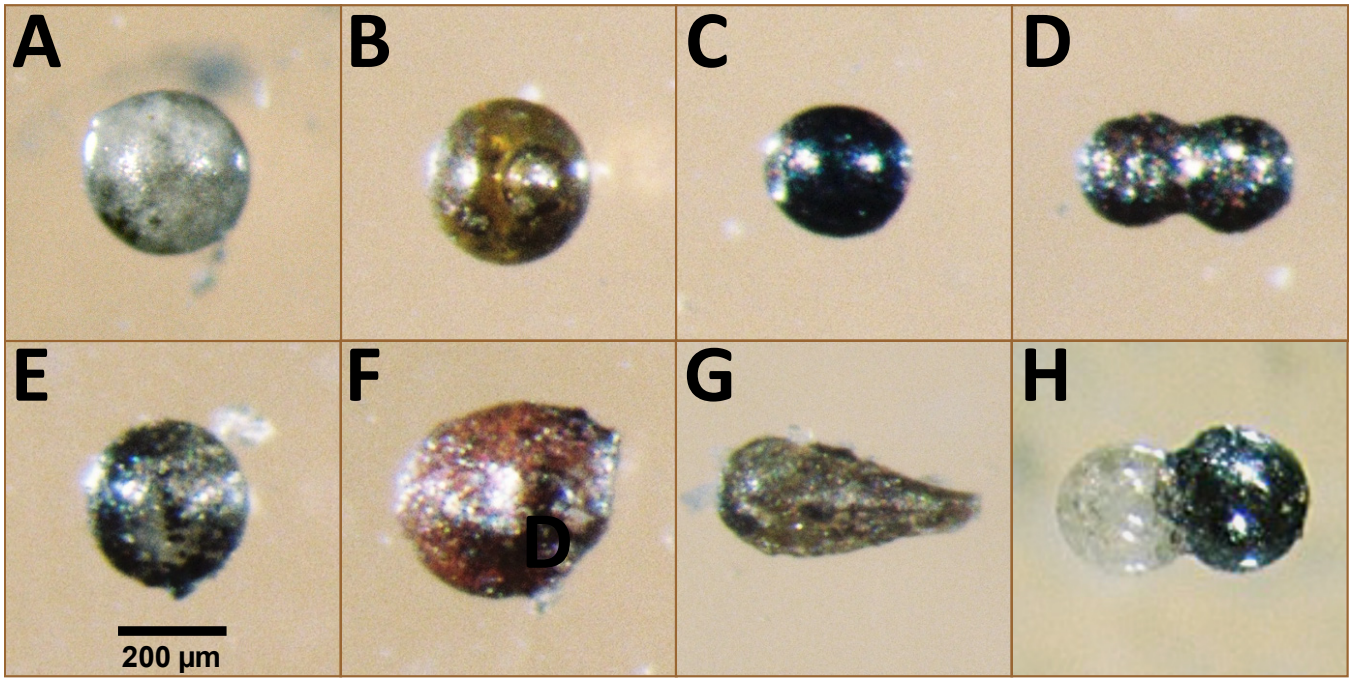

Figure S6. Light photomicrographs of magnetic and glassy spherules from Melrose, PA. Shapes include spherules, ovals, teardrops, and dumbbells. Colors include clear, gray, red, brown, and black. Note spherule **B** contains a large bubble. Both dumbbells (**D** and **H**) indicate fusion of molten or semi-plastic spherules. Note that dumbbell **H** consists of two dissimilar accretionary spherules, one clear (Si-rich) and the other opaque (Fe-rich).

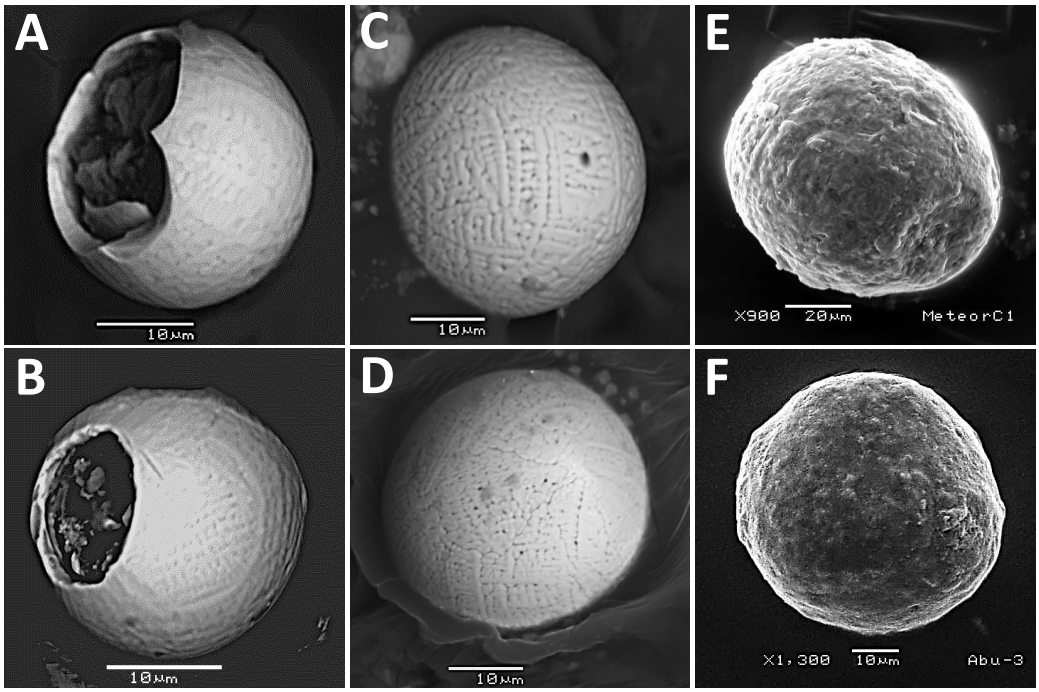

Figure S7. SEM images comparing YDB spherules with those of known impact events. **A)-B) KPg vs. YDB.** These images compare a spherule from the 65-Ma KPg boundary at Knudsens Farm, Canada with one from the YDB at Lake Cuitzeo, Mexico. These images are similar to those previously published of KPg spherules (Grachev *et al.*, 2008) and geochemically match other YDB spherules. **C)-D) Tunguska vs. YDB.** These images compare a spherule from the Tunguska, Siberia airburst of 1908 with one from the YDB at Lingen, Germany. Even though the Tunguska impactor did not produce a crater (Kulik, 1940), researchers have reported chemical traces of the impactor (Kolesnikov, 2010) and an abundance of spherules that formed during this event (Florenskiy, 1965). **E)-F) Meteor Crater vs. YDB.** These images compare a Fe-Ca-Si spherule from Meteor Crater, Arizona that formed in carbonate-rich rock with a Fe-Ca-Si spherule from Abu Hureyra, Syria that was also formed from carbonate-rich rock.

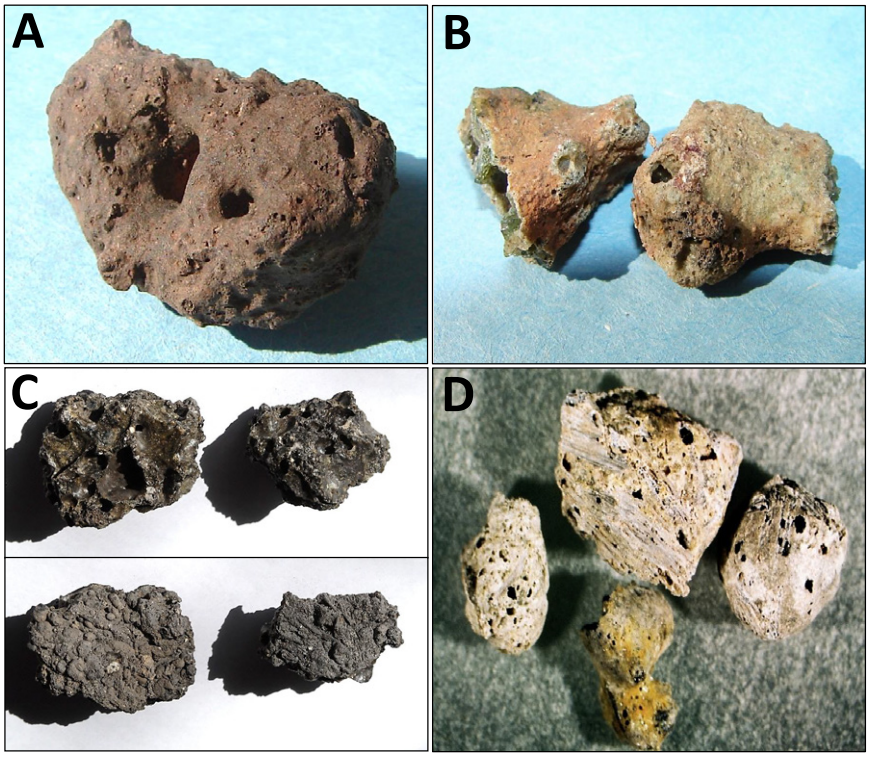

Figure S8. Light photomicrographs of high-temperature melt-glass. **A) Meteor Crater** SLO, width = 27 mm. **B) Trinity nuclear test, New Mexico, 1945**; yield 20 kilotons (kt). Glass known as trinitite; width =28 mm. **C) Soviet-era nuclear test, 1953;** material from Semipalatinsk, Kazakhstan. SLOs called "Stalinite" are from nuclear airburst with yield of 400 kt, TNT equivalent. Upper row formed facing up; lower row is down side of same objects. Width = 5.5 cm for largest. **D) Abu Hureyra** SLOs, width = 1 cm.

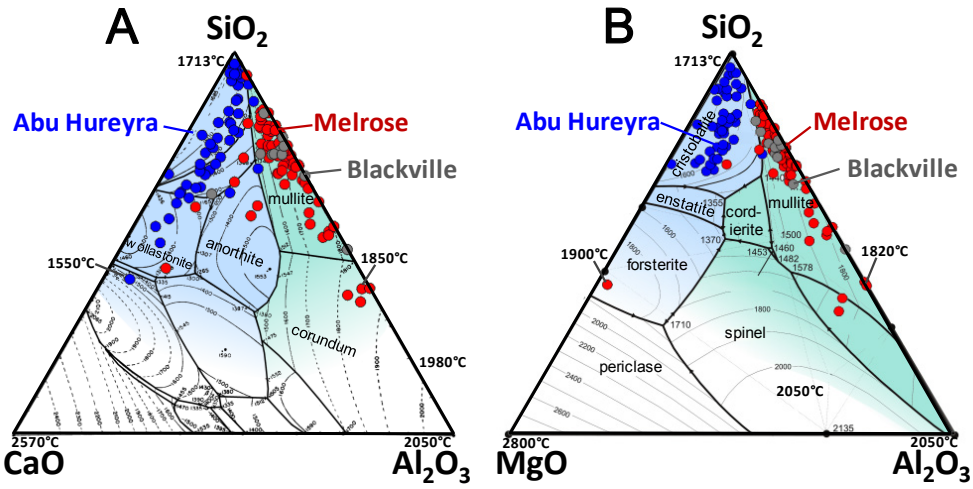

Figure S9. Temperatures. Ternary diagrams for estimated maximum temperatures of YDB objects. Key temperatures are displayed at each diagram corner and adjacent to the highest temperature sample for each group. The temperatures displayed are estimates only, because YDB objects contain significant amounts of iron (range: 0 to 100 wt%; mean: 55 wt%), which melts at lower temperatures. Overall, based on the temperature data here and in **Fig. 3D**, YDB objects belong to three main mineral groupings: 1) iron-rich, 2) aluminosilicate, and 3) Mg-and-Ca-aluminosilicate.

Ca-Silicate Sub-groups /Temperatures (Figure S9A). Using the standard CaO-Al_2O_3-SiO_2 (CAS) system, this ternary diagram indicates that YDB objects fall into two main groups, calcium-silicates and aluminosilicates. YDB objects from Abu Hureyra (blue dots) fall mostly in the CaO-SiO_2 group with liquidus temperatures up to 1700°C. Samples from Melrose (red dots) and Blackville, SC (gray dots) are mostly in the Al_2O_3-SiO_2 group that forms at temperatures up to 1850°C. Only a few YDB examples from Melrose and Blackville fall within the CaO-SiO_2 group.

Mg-Silicate Sub-groups/Temperatures (Figure S9B). The MgO-Al_2O_3-SiO_2 system shows that few Mg-rich silicate rocks are represented in YDB objects. Abu Hureyra (blue dots) falls mostly in the MgO-SiO_2 group, although Melrose (red dots) has several YDB objects that fall within the forsterite mineral region with melt temperatures of 1900°C. For the Al_2O_3-SiO_2 group, several Melrose YDB objects have maximum temperatures of 1820°C to 2050°C and fall within the mullite and corundum regions respectively, whose crystals have been observed using SEM.

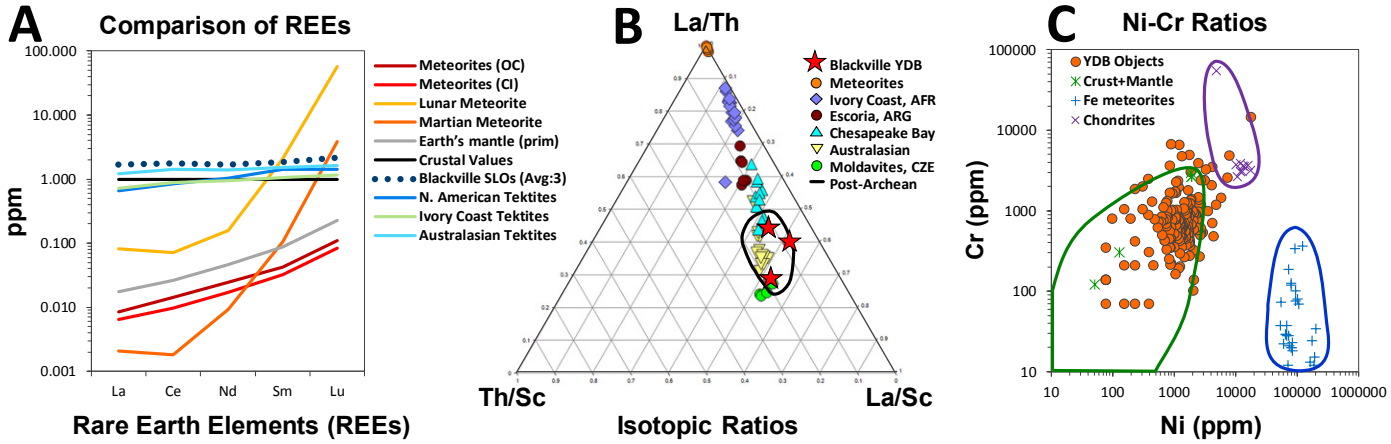

Figure S10. YDB objects derived from terrestrial precursors.

Crust-normalized rare-earth elements (REE) (Figure S10A). This graph compares values of REEs from Blackville SLOs to various other materials. REE compositions indicate SLOs from Blackville are compositionally comparable to tektites and to Earth's upper continental crust. SLOs are highly dissimilar to approximately 90% of all meteorites (OC, CI, Lunar, and Martian), and to material originating in Earth's mantle. This confirms that the YDB objects are terrestrial in origin, rather than cosmic. [Data sources: YDB from Firestone *et al.,* 2007, 2010. Meteorites from Lodders and Fegley, 1998; Gnos *et al.,* 2004; and Taylor *et al.*, 2002. Tektite data from Koeberl and Glass, 1988; Luetke *et al.*, 2008; and Lee *et al.*, 2004. Crust and mantle data from Taylor and McClennan, 1985]

Ratios of thorium, lanthanum, and scandium (Figure S10B). This ternary diagram further confirms that ratios for Blackville YDB objects are dissimilar to those for meteorites (Data: YDB from Firestone *et al.,* 2007, 2010.

Meteorites from Lodders and Fegley, 1998; Newsom, 1995). They are also geochemically unlike impact-related tektites from the Ivory Coast (Data: Koeberl, 2007), impact-related melt-rocks, or escoria, from Argentina (Data: Schultz *et al.*, 2006), and most Chesapeake Bay tektites (Data: Poag *et al.*, 2004; Koeberl *et al.*, 1988). On the other hand, the values overlap Australasian tektites (Data: Amare and Koeberl, 2006), and Czech Moldavites (Data: Koeberl *et al.*, 1988), indicating a terrestrial origin. Also, SLO values fall within the black-circled area that represents post-Archean upper continental crust (<2.5 Ga), including surface sediments, riverine deposits, shales, mudstones, and clays (Data: Taylor and McClennan, 1985). YDB object compositions are inconsistent with Archean sediments (>2.5 Ga) (Data: Taylor and McClennan, 1985), suggesting that likely source-materials were <2.5 Ga in age.

Chromium-nickel ratios (Figure S10C). This binary diagram compares nickel (Ni) and chromium (Cr) abundances in YDB objects with terrestrial material and meteorites. YDB objects are highly dissimilar to known iron meteorites (blue line), and a few fall in the typical ranges for chondrites (purple line). On the other hand, nearly all are within the range of terrestrial rocks and sediments (green line). (Data: terrestrial values from McDonough, 1998; chondrite data from Lodders *et al.*, 1998; and iron meteorite data from Daode *et al.*, 1996.]

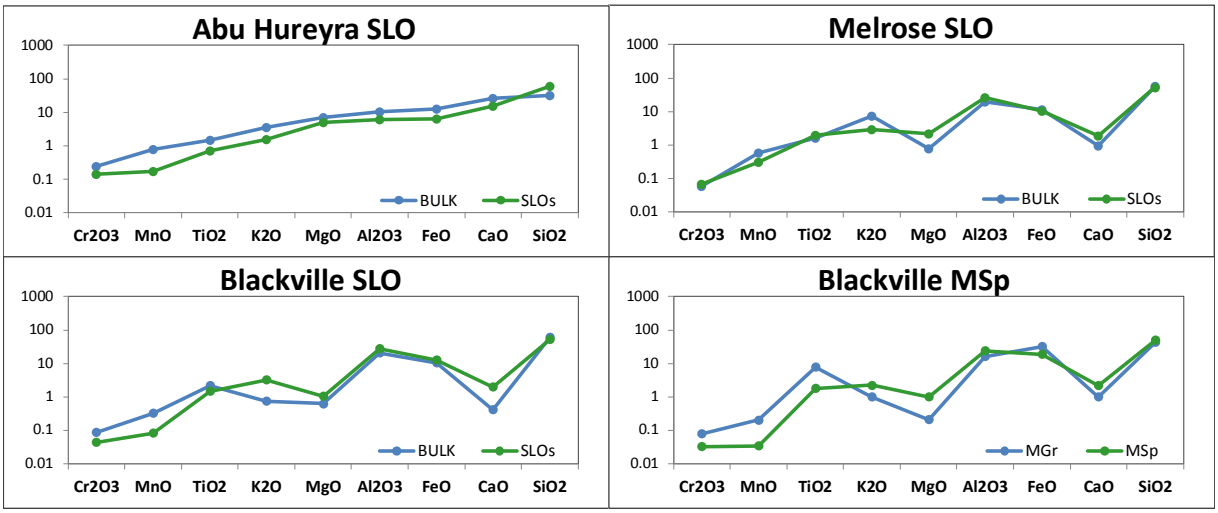

Figure S11. Major Oxides. Percentages of major oxides for Abu Hureyra, Melrose, and Blackville are plotted comparing SLOs (green) with bulk sediment (blue). SLOs analyzed with SEM-EDS compare favorably to bulk sediment analyzed with neutron activation analyses (NAA) and prompt gamma activation analyses (PGAA) (Firestone *et al.*, 2007, 2010) within a range of approximately ±4×. The lower right panel demonstrates that Blackville spherules (MSp, green) compare closely to the site's magnetic grains (MGr, blue) and to SLOs shown in lower left panel. These results suggest that for each site, the SLOs and spherules could have formed from melted local sediment. In addition, the results demonstrate that SLOs and spherules from eastern North America are geochemically similar to each other, but dissimilar to SLOs found at Abu Hureyra in Syria.

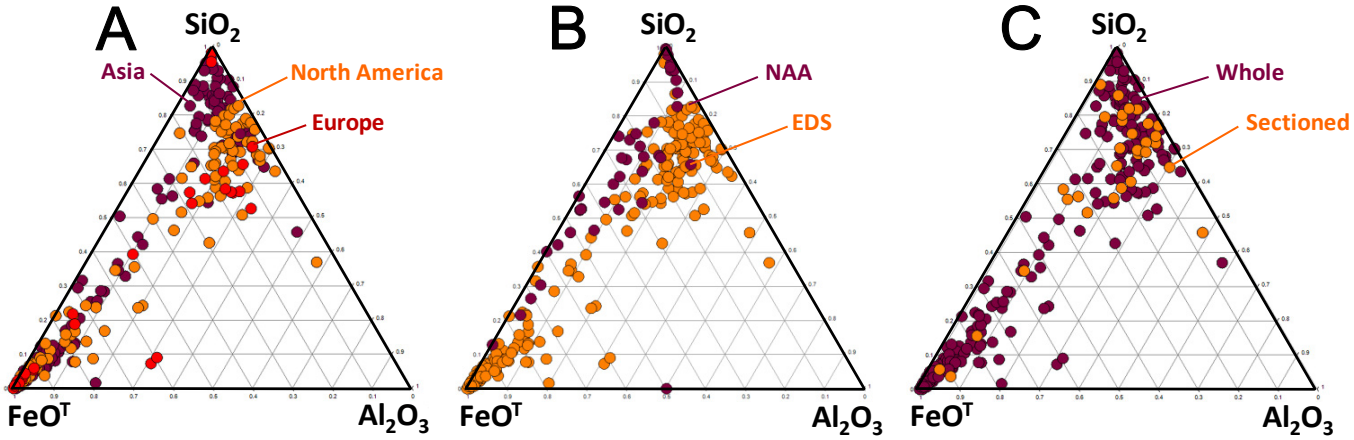

Figure S12. Comparative Analyses of Datasets. A comparison of major elemental percentages (Fe, Al, and Si): **A) Different continents:** YDB objects are indistinguishable by continent. **B) C) EDS vs. NAA;** for six sites (Blackville, Blackwater Draw, Gainey, Lommel, Topper, and Murray Springs), we have neutron activation analysis (NAA) for bulk sediment (YDB from Firestone *et al.,* 2007, 2010), along with elemental analyses using SEM-EDS for YDB objects. The results show no significant difference in composition, suggesting that YDB objects are derived from local sediments. **C) Whole or sectioned YDB objects** are geochemically similar, indicating that the accuracy of analyses appears unaffected by method of preparation.

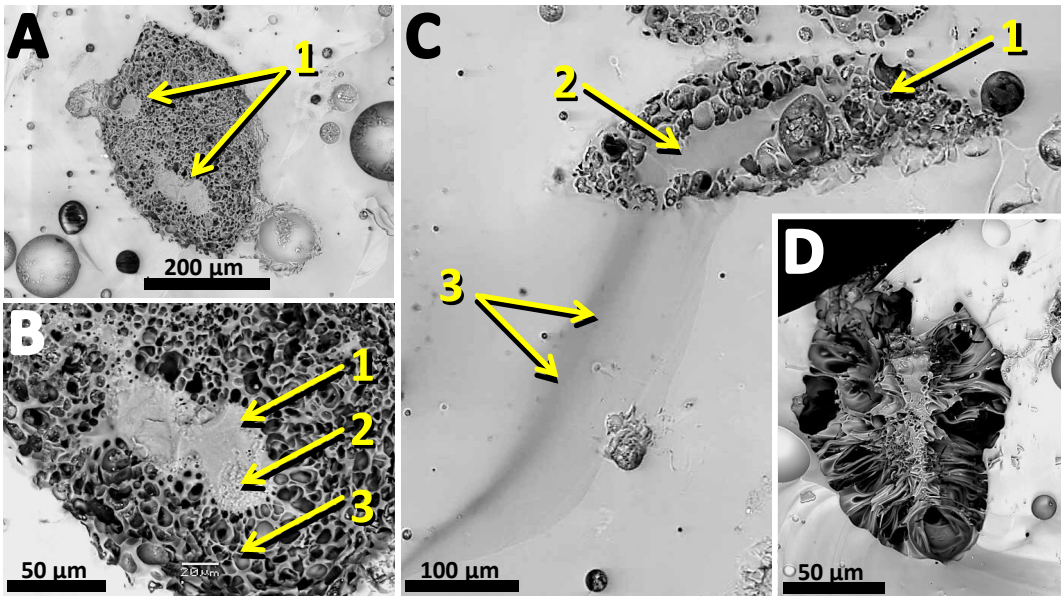

Figure S13. **Melting and evaporation of quartz** in Muong Nong layered tektite glass from the Australasian tektite field. **A)** Residual quartz and non-vesiculated silica (lechatelierite) regions of a boiled quartz grain at #1. **B)** Close-up shows non-vesiculated silica glass at #1, partially melted quartz at #2, and frothy silica glass (boiled quartz) at #3. **C**) Frothy silica glass at #1 with non-vesiculated silica glass core at #2 (SiO_2 = 99 wt%) that has leaked into and formed a long streak within the lighter gray tektite glass matrix at #3 (SiO_2 = 74 wt%). **D)** Completely boiled quartz grain. These four examples suggest minimum temperatures of 2230°C, the boiling point of quartz.

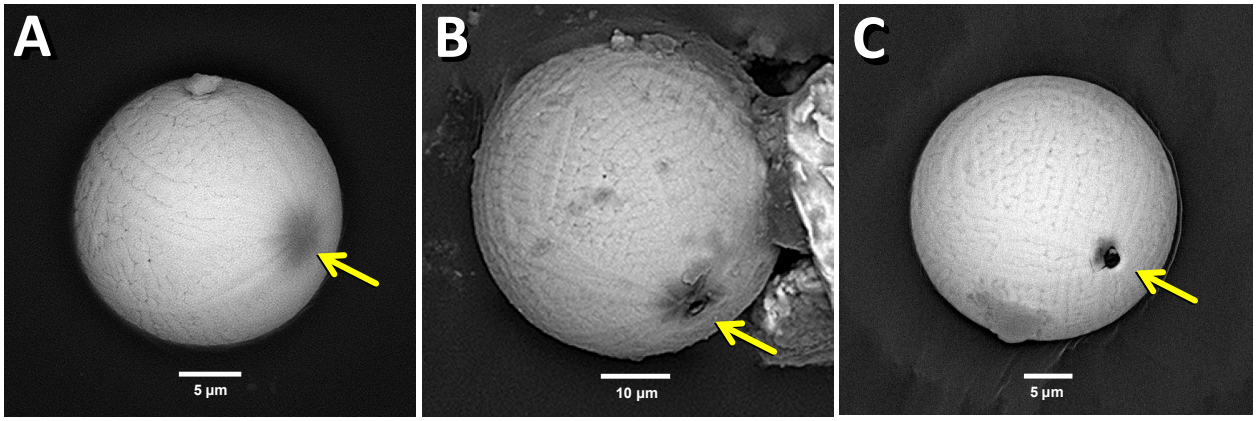

Figure S14. Carbon-rich impactors. A) Blackwater Draw: craterless non-penetrating impact by low-velocity carbon particle onto a magnetic spherule. **B) Kimbel Bay:** moderately-high-velocity impact (<5 km/sec.) by carbon impactor that penetrated a hollow magnetite-rich spherule, creating a raised rim; crater is 2 µm. YDB spherules frequently have large central vesicles for unknown reasons. There is no evidence that the small impacting spherule exited the larger spherule or survived the impact. **C) Blackwater Draw**: another moderately-high-velocity impact by a carbon impactor that penetrated a hollow magnetite-rich spherule, dimpling and penetrating the host material without forming a raised rim; entry hole is 2 µm.

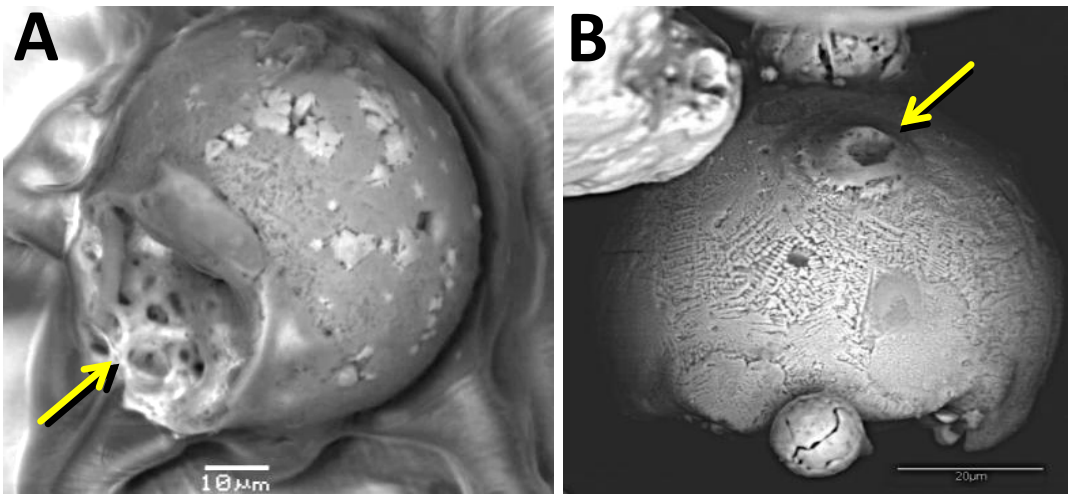

Figure S15. Collisional YDB spherules. A) Lommel. Spherule with hercynite (bright areas) and sillimanite crust (dull, lath-shaped). This spherule exhibits an impact crater (arrow) or a vapor pressure blow-out, revealing aluminosilicate and silica (lechatelierite) interior glasses. **B)** Potential YDB spherule with splash-form impact at arrow that has magnetite quench-crystals on the surface (LeCompte *et al.*, 2010, 2011). Note pit caused by the impact, surrounded by a splash apron with a raised impact rim beyond it, similar to cratering observed by Prasad and Khedekar (2003) and Prasad *et al.* (2010).

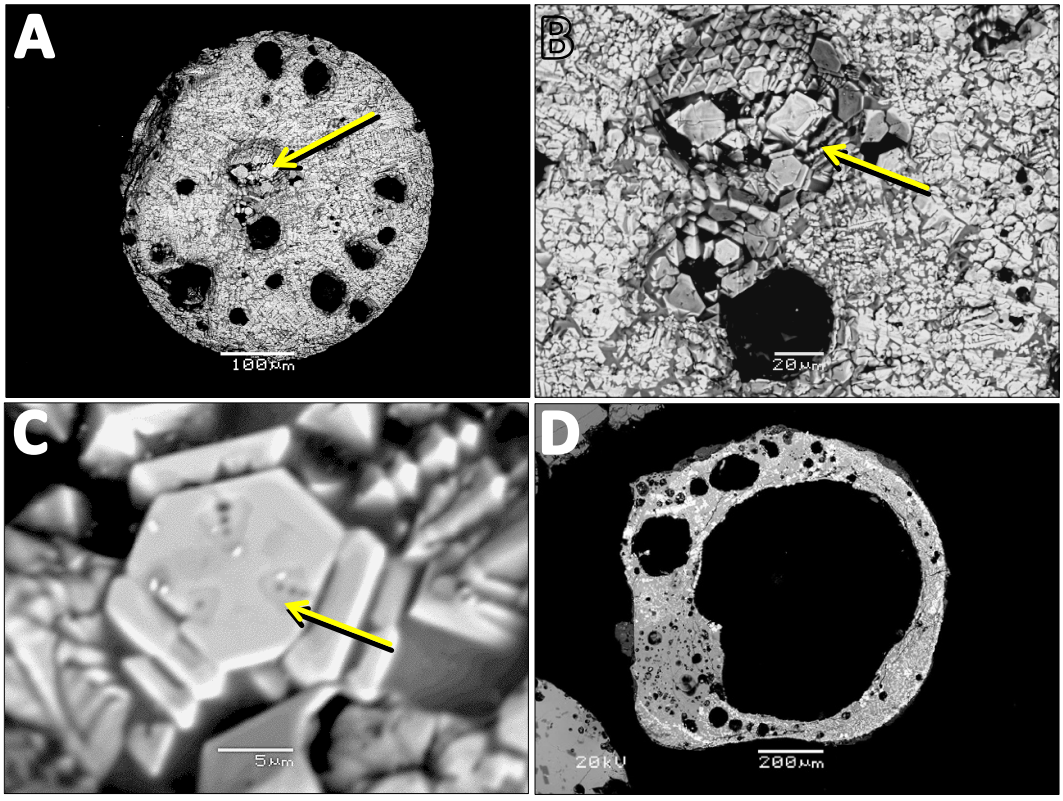

Figure S16. Melrose site, aluminum-rich hematite. A) Spherule displaying vesicles and bubbles with an inclusion comprised of >85 vol.% Al-hematite (arrow) surrounded by aluminosilicate glass. **B) Bubbled interior** of same spherule showing Al-hematite platelets (arrow). **C) Hexagonal platelets** of same spherule, containing trigonal inclusions of Al_2O_3-rich material (arrow). **D) Thin section** of a hollow high temperature spherule with high-density Al-hematite quench crystals and a partial rim of fused clays and quartz. Al_2O_3 contents range from 5.6 to 9.2 wt% for these specimens.

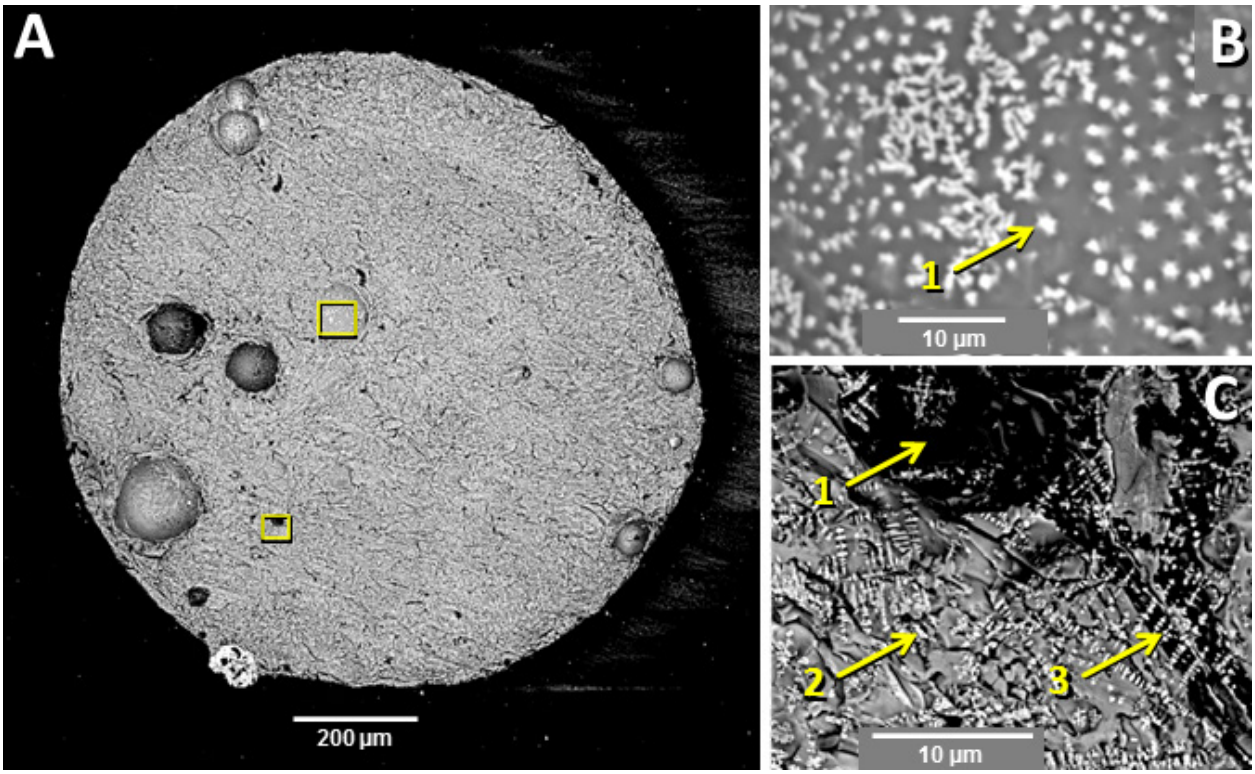

Fig. S17. Blackville. **A)** Overview of aluminosilicate spherule. **B)** Enlargement of upper box in **11A**, showing vapor-deposited magnetite on inside wall of bubble. **C)** Enlargement of lower box in **11A**, showing dark carbon inclusions (no. 1) and dendritic magnetite crystals (no. 2), some intergrown with dark, glassy carbon-rich areas, implying rapid cooling of non-equilibrium melt materials.

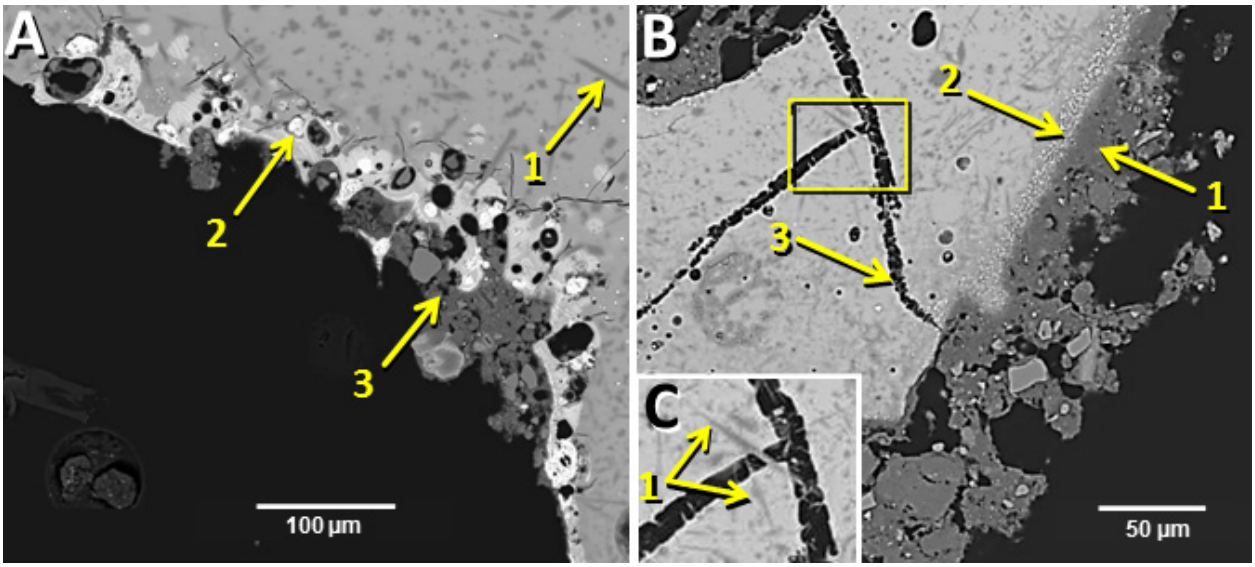

Fig. S18. SEM-BSE image of Blackville SLOs. A) Portion of aluminosilicate glass shard displaying spindle-like mullite quench crystals (no. 1), metallic Fe particles (no. 2), and a reaction rim with fused soil-like material (no. 3). Bright material in rim is quenched magnetite. Soil consists of kaolinite and illite clays, quartz, chlorite, iron oxides, and altered feldspar. **B)** SLO showing a reaction rim composed of soil (no. 1). Bright phase under the rim is hercynite spinel (no. 2); dark veins are glass-like carbon (no. 3). **C)** Inset box from **12B** shows mullite crystals (no. 1) intergrown with carbon-filled areas, indicating high-temperature crystallization.

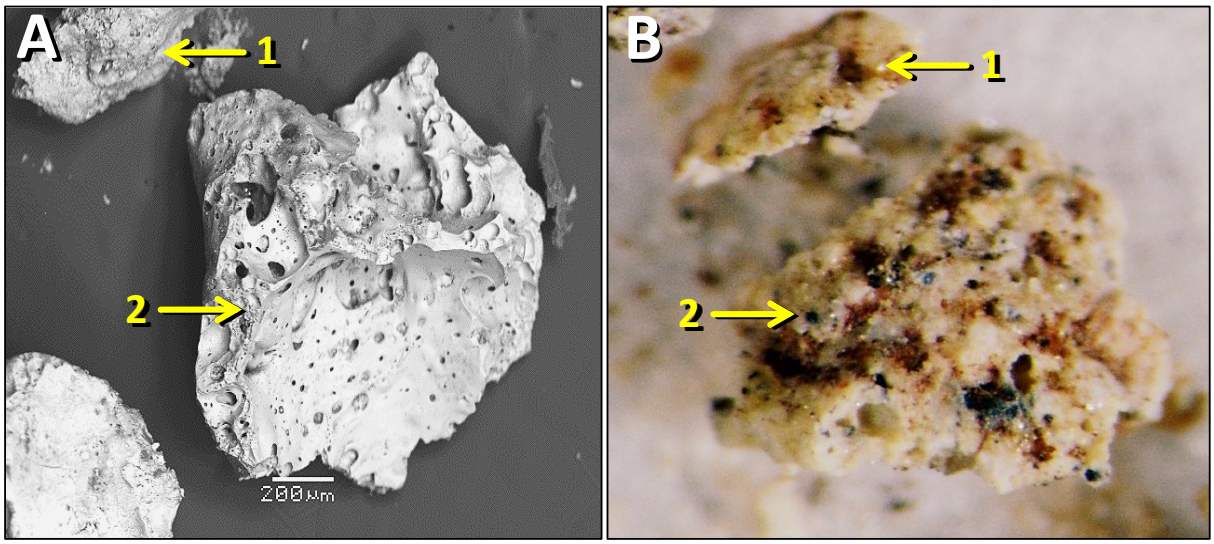

Figure S19. Abu Hureyra. **A) SEM-BSE image** of SLO exhibiting highly vesiculated texture of melted quartz, carbonate, and iron oxides. **B) Light microscope image** of the same grain, slightly rotated.

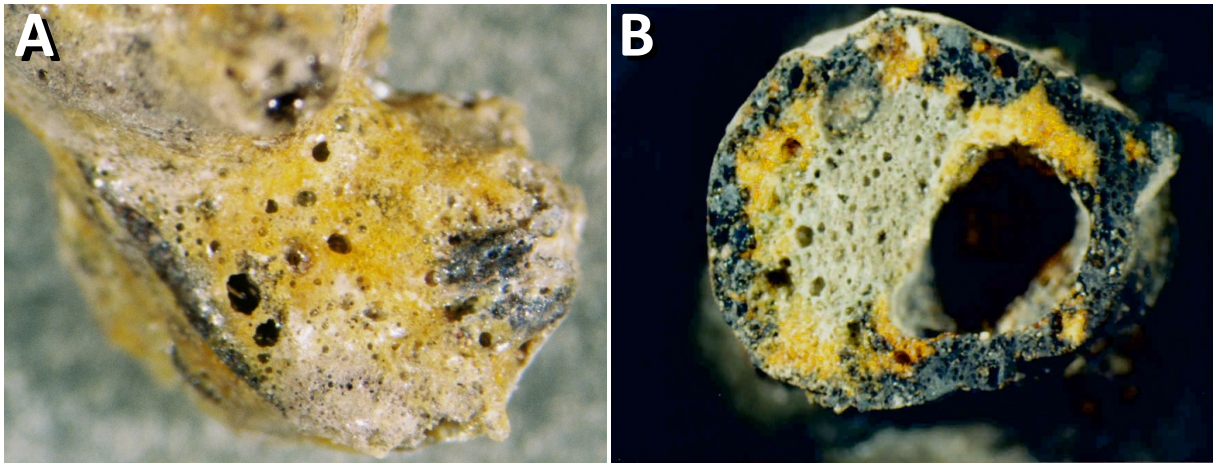

Figure S20. CaO-rich SLOs from the melting of carbonate and silica-rich precursor rocks. **A) Abu Hureyra** SLO; width is 3 mm. Yellow area is CaO-rich (CaO = 35.3 wt%); white to clear is lechatelierite; dark is FeO-rich. **B) Meteor Crater** SLO; width is 5 mm. Yellow is CaO-rich (CaO = 32.5 wt%); clear to gray is lechatelierite; dark is FeO-rich.

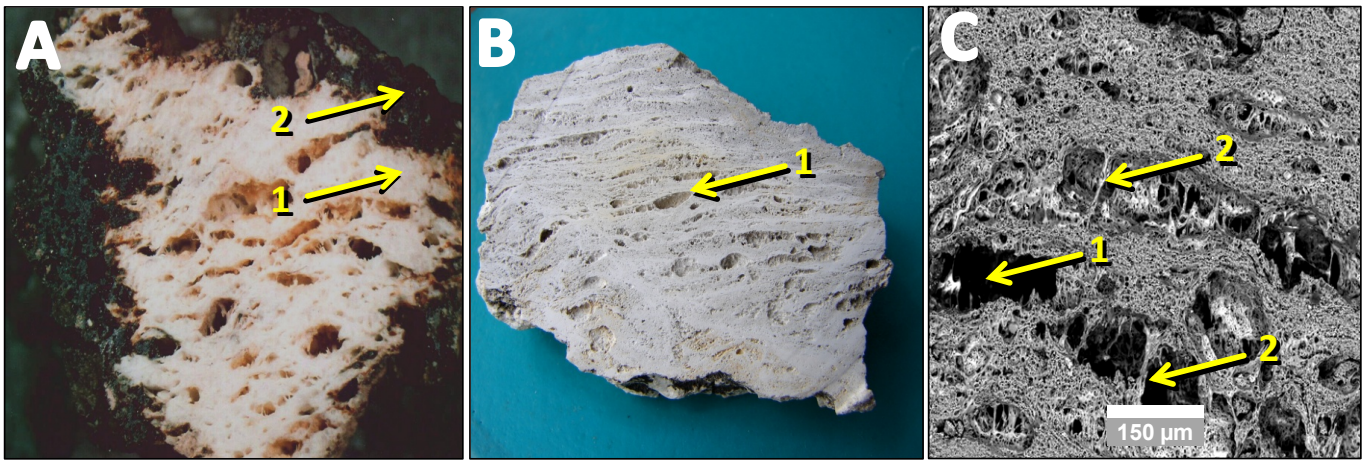

Figure S21. **A) Meteor Crater;** light-colored pumice-like lechatelierite (#1) covered by a dark Ca-rich carbonate melt (#2) that penetrates into lechatelierite voids (width of the impactite = 12 mm). **B**) **Haughton crater;** pumice-like lechatelierite (width = 72 mm) with pulled-apart texture (#1). **C**) **SEM-BSE image** of enlarged portion of **19B** that shows the high porosity level, pulled-apart texture (#1) and vesiculated taffy-like SiO_2 melt stringers (#2).

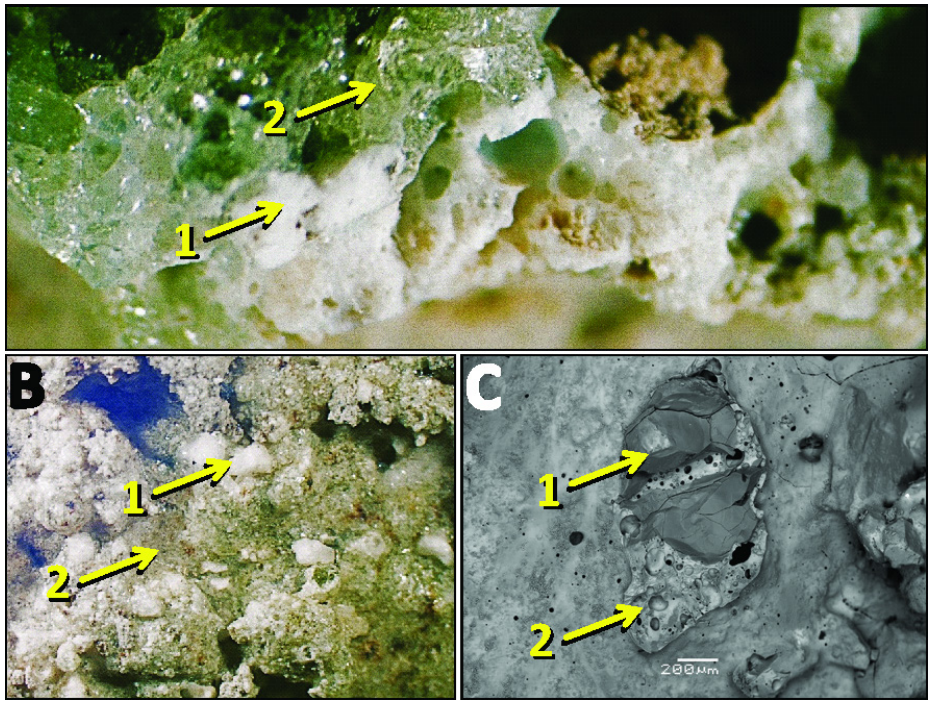

Fig. S22. Trinity: images of puddled trinitite fallback melt that shows melted to partially melted surface arkosic sand minerals. **A)** Edge-on image of trinitite green glass (width, 17mm); white is melted K-feldspar (no. 1); clear glass is melted quartz or lechatelierite (no. 2). **B)** Green trinitite shows embedded, melted K-feldspar (white, no. 1), and partially to fully melted quartz (no. 2) (width, 8 mm). The implied interface temperature between trinitite melt and arkosic sand is >1730ºC. **C)** SEM-BSE image showing unmelted quartz grain (no. 1) set in melted K-feldspar (no. 2) surrounded by trinitite. Implied temperature is >1200ºC, the melting temperature of K-feldspar, and <1730ºC, the melting temperature of quartz.

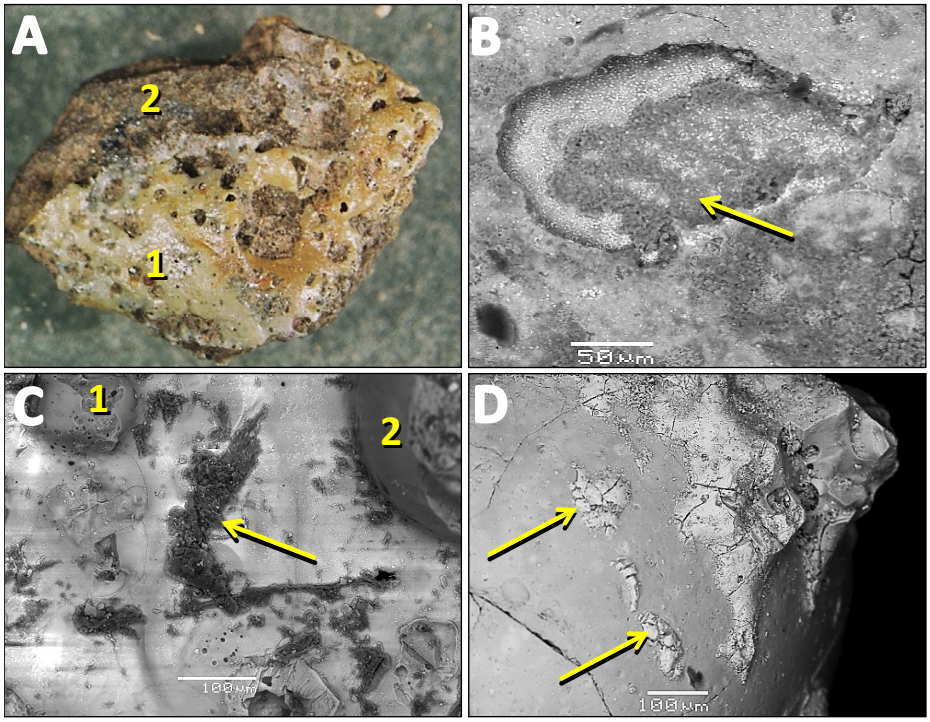

Figure S23. Molten splash-forms. A) Melrose. Fe-rich aluminosilicate melt splash (#1) on shale (#2); width = 3 mm. **B) Meteor Crater.** Molten splash on large SLO that contains tiny magnetite quench crystals and a mass of carbon in the interior (dark gray at arrow). **C) Trinitite** surface with splash-form carbon (dark gray at arrow) and two accreted spherules (#1, #2), formed through nuclear detonation. **D) Trinitite**. Clumpy melt splash on spherule with small puddles of lechatelierite (arrows), formed through nuclear detonation.

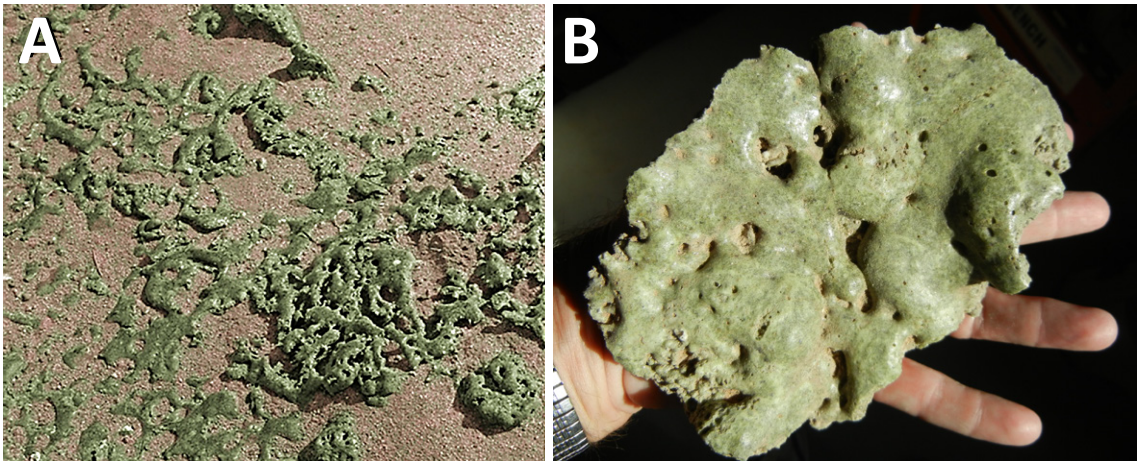

Figure S24. Pooled trinitite. A) Colorized photo of *in situ* trinitite on ground after the nuclear detonation. Width of view is about 50 cm. **B)** Large piece dubbed the "Green Monster" is about 18 cm long. Visible side was facing up on the ground.

NUCLEAR AND ET AIRBURSTS

The thousands of people who worked on the Manhattan project and tested the first atomic bomb at the Trinity Site probably did not anticipate that their efforts would later serve as a real-time experiment for the study of catastrophic cosmic aerial impact bursts. The ET impact events proposed to have produced Libyan Desert Glass (LDG), the Australasian tektites, Dakhleh glass, and Tunguska glass are probable aerial bursts. Wasson (1998, 2003) investigated the characteristics of some of these glasses, the Australasian tektites and LDG glass, and found these glasses to be inconsistent with crater-forming impacts, and yet, as we have also found, are very similar to the formation and characteristics of trinitites**.** The most significant are: A) Layered glasses that formed as pools of melt from the raining of droplets from the hot impact plume. B) These layered glasses melted at very high temperatures and are nearly devoid of unmelted materials. The temperature of the glasses was >2000°C and melting was evenly distributed throughout, in contrast to heterogeneous melt breccia and suevite-like products from crater-forming impacts that sustained lower initial temperatures (Wasson and Moore, 1998). C) Tektites, LDG, and trinitites were produced from surface sediment precursors, not deep-seated rocks.

Although Dakhleh, Tunguska, and the YDB sites lack large-scale layered glasses, these inferred aerial bursts did produce splash or spin-form glasses (spherules, teardrop, dumbbell, etc.) similar to tektites and trinitites, all of which formed by spinning and cooling in an impact plume (Elkins-Tanton *et al.,* 2003). Whether or not massive layered glasses are produced depends on several factors, the most important of which is the burst altitude (Vasilyev, 1998; Boslough and Crawford, 2007). The most intense heating would come from a blast that is very near the Earth's surface, e.g., the Trinity detonation at 20 kt of energy 30 m above the ground. In contrast, the air burst energy for Tunguska was orders of magnitude greater, but the burst altitude was much higher at 5-10 km (Svetsov, 2006), thus the thermal damage was significantly less, although Tunguska tektites have been reported (Kirova *et al.*, 1966). A comparison of other plume products from these impact events is given in **SI Table 1.**

HEATING: Impact vs. Atomic

Nuclear airbursts heat the atmosphere and surface soils by kinetic energy, as well as by intense gamma and beta nuclear radiation. This contrasts with a kinetic airburst during a cosmic impact, which mostly heats by thermal to micro-wave radiation. A breakdown of the approximate energy released by fission in a nuclear detonation is as follows:

MeV kinetic energy of fission fragments	165
Instantaneous gamma rays	7
Kinetic energy of neutrons	5
Beta particles from product decay	7
Gamma rays from product decay	6
Neutrinos from product decay	10
TOTAL (MeV):	200

For both types of events, the post-heating processes are similar (e.g., lofting, collisions, and entrainment), because, regardless of whether a detonation is the result of chemical, nuclear, or kinetic airburst, the thermal effects are much the same. During all types of airbursts, thermal radiation is released and a flash-heating event of 1000's of degrees C is generated, followed by an overpressure wave and finally an underpressure wave.

Another major difference among the two types of events is that nuclear detonations are static, whereas the aerial burst from an impacting body is dynamic with momentum and delivers the heat to the surface at high velocity. The radiation heat that fluxes to the ground increases with increasing velocity of the impactor. So, in comparing an atomic detonation with a cosmic airburst with equivalent energy in terms of TNT, a cosmic airburst delivers a greater thermal radiation flux to the surface and, hence, has greater melting efficiency. However, it does not change the melting and quenching effects on the melted surface soil, i.e., glass formed from temperatures >2000°C will have the

same characteristics regardless of the mechanism.

FULGURITES

Lechatelierite is present in two types of lightning-generated melt material. 1) Subsurface fulgurites form when cloud-to-ground lightning melts mostly unconsolidated sediment. 2) Exogenic fulgurites, which are much rarer, form when very high-energy lightning melts unconsolidated sediment or rocks, such as on mountaintops (French, 1998; Wasilewski P and Kletetschka G, 1999; Carter, *et al.* 2010; Walter, 2011)

SUBSURFACE FULGURITES are hollow, glassy tubes usually up to 1-2 cm in diameter with walls several millimeters thick (Sponholz *et al.* 1993, 2004), but rare ones range up to approximately 15 cm in diameter and may form branches of melt material extending several meters underground. For these fulgurites, the lightning typically affects only a few cm of ground around the subsurface fulgurite (Walter, 2011). The inner surface of the tube is highly polished and comprised of fully melted grains that have flowed together completely to form vesicular lechatelierite. From the smooth inside surface outward, the fulgurite displays a gradation from a) fully melted highly reflective glass to b) partially melted grains and glass to c) unmelted grains fused to glass forming a rough, sandy outer surface (Sponholz *et al.* 1993, 2004). This morphology is distinctive and easily recognized.

EXOGENIC FULGURITES appear as vesicular glassy spherules and droplets that are usually less that 5 cm in diameter. They are formed by the most energetic of lightning strikes that create a subsurface fulgurite and then, eject melted glass up to a meter away (Walter, 2011).

GEOCHEMISTRY. Analyses of fulgurites indicate that they are comprised of typical surficial sediments rapidly heated to >2300°C, then rapidly cooled, resulting in reduced (oxygen-deficient) glass (Sheffer *et al.* 2006). Most fulgurites are enriched in SiO_2 (>70 wt%) and depleted in FeO (<8 wt%) (Walter, 2011; Carter *et al.* 2010). Because fulgurites form from terrestrial sediments and rocks, they closely resemble melted material from cosmic impact events and nuclear airbursts (Sheffer *et al.* 2006). However, there are recognizable differences, as follows:

1) Collisional Damage. Fulgurites form in high-temperature, lower-energy events, which eject low-velocity melted particles that are incapable of causing collisional damage to other particles (Prasad and Khedekar, 2003). This is unlike high-velocity cosmic impacts/airbursts and nuclear detonations that can cause considerable collisional damage.

2) Ultrastructure. Subsurface fulgurites, the most common variety, are easily recognized when encountered in a sedimentary profile because of their tube-like shape. Their walls tend to be only several millimeters thick, and so, they can break into smaller pieces. However, they are still recognizable because their inner surfaces typically are shiny and their outer surfaces are rough and coated with fused sand grains. YDB SLOs do not display this morphology.

3) Lateral Distribution of Glass (SLOs). At Abu Hureyra, we sampled about 4.5 m away in the stratum above the YDB layer and observed SLOs in both places. At Blackville, two samples approximately 10 m apart displayed glass as SLOs. At Melrose, two samples 28 m apart displayed melted glass. The results from the three sites indicate that the SLOS are not limited to just one small area of each site, but rather, range from 4.5 to 28 m apart. By comparison, exogenic fulgurites are not reported beyond a 1-m radius of a subsurface fulgurite (Walter, 2011). Thus, the YDB SLOs are not limited to just one confined area of each site, as would be the case with a lightning strike. This suggests that the observed glass from these three sites was not produced by lightning strikes.

4) Rarity of Glass in Sedimentary Column. Of the 18 sites investigated, some spanning a range of >16,000 years, we did not observe any fulgurites or fragments of them. The only glassy material (SLOs) that we found was morphologically different and displayed large peaks in the 12.9-ka YDB layer with low quantities in adjacent layers. Strata that were remote from the YDB contained no or few pieces of impact-type glass or SLOs.

Even though fulgurites are accepted to be rare in sedimentary profiles, it has been proposed by Pigati *et al.* (2010) that they and other YDB-like proxies, such as spherules and iridium, might become concentrated on deflational surfaces or under the wetland-related black layers or mats. One could speculate that this might occur in relation to extreme weather conditions at the onset of Younger Dryas cooling episode. Eight of our sites have such black layers (Arlington Canyon, CA; Blackwater Draw, NM; Chobot, AB, Canada; Lake Cuitzeo, Mexico; Gainey, MI; Murray Springs, AZ; Sheriden Cave, OH; and Talega, CA). Of those eight sites, only one (Murray Springs) displays glass, but it is clearly not fulguritic, according to Fayek *et al.* (2012). Also, at Murray Springs, we sampled several stratigraphically separated black mat layers that were younger than the YDB-related mat layer, and none of those contained fulgurites, glass, or spherules. Four other sites have charcoal-related black layers (Lingen, Germany; Lommel, Belgium; Ommen, Netherlands; and Abu Hureyra, Syria), and of those, only Abu Hureyra displays glass as SLOs that are morphologically unlike fulgurites. Thus, at these twelve sites with black layers, not one fulgurite tube or fragment was observed in the YDB, or in strata above it and below it. These observations indicate that fulgurites are not common at our collection sites and suggest that they are not concentrated by black mat layers.

In conclusion, high-temperature lechatelierite melt-glass is only known to result from lightning strikes, atomic detonations, and cosmic impacts. The available evidence does not support an origin of YDB glass by lightning and instead, supports an impact origin.

TABLES

SI Table 1. Comparison of high-temperature proxies from various sources: YDB, Trinity detonation (TRIN), Meteor Crater (METC), Australasian tektite field (AUST), and Tunguska (TUNG). The range of proxies reported is nearly identical for all events. [References: B=Bunch *et al.* (2012); C=Chao *et al.* (1962); F=Florenskiy *et al.* (1963); K=Kirova *et al.* (1966); P=Prasad *et al.* (2003); and Z=Zbik (1984).]

	YDB	TRIN	METC	AUST	TUNG
Magnetic spherules	B	B	B*	C	F
Silicate spherules	B	B	B	P	K
Melted glass (SLOs)	B	B	B	B	K
Lechatelierite	B	B	B	B	K
Micro-craters	B	B	B	P	Z
Melt drapings/splash	B	B	B	P	Z
Spherule accretions	B	B	B	P	Z
Carbon-to-Si accretions	B	B	B	n/a	n/a

Note: *Rich in Ni-Fe from impactor. Rich in Fe from target.
"n/a" = not tested

SI Table 2. Site information and dates. Age-depth models were established for Abu Hureyra using 13 AMS ^{14}C dates and for Blackville and Melrose using OSL dating. Dates for the three sites were graphed using linear interpolation (**SI Figs. 2, 4, 5)**, and in each case, the intersection of the YD onset at 12.9 ka coincided the depth of the peaks in YDB proxies. The column "YDB?" indicates the dates closest to the YDB layer.

Site	Lat/Lon	Elev. (m)	Lab	Depth	Level	RCYBP	±	Cal BP	±	YDB?	Type	Material	Reference
Abu Hureyra	35.8667°N	310	OxA-170	285.33	405	10600	200	12430	270	--	AMS	Charred grain	Moore, et al. 2000
	38.4000°E	--	OxA-407	285.13	419	10050	180	11680	320	--	AMS	Charred bone	Moore, et al. 2000
	--	--	OxA-386	285.12	420	10800	160	12780	140	--	AMS	Charred grain	Moore, et al. 2000
	--	--	OxA-473	284.95	425	10000	170	11610	290	--	AMS	Charred bone	Moore, et al. 2000
	--	--	OxA-397	284.91	430	10420	140	12310	240	--	AMS	Charred grain	Moore, et al. 2000
	--	--	OxA-434	284.91	430	10490	150	12370	230	--	AMS	Charred bone	Moore, et al. 2000
	--	--	OxA-171	284.72	457	10600	200	12430	270	--	AMS	Charred grain	Moore, et al. 2000
	--	--	UCIAMS-105429	284.70	445	11070	40	12932	176	**Yes**	AMS	Charcoal	This paper
	--	--	BM-1718R	284.67	447	11140	140	13040	150	**Yes**	AMS	Charcoal	Moore, et al. 2000
	--	--	OxA-430	284.56	460	11020	150	12940	130	**Yes**	AMS	Charred bone	Moore, et al. 2000
	--	--	OxA-172	284.29	470	10900	200	12870	160	**Yes**	AMS	Charred seed	Moore, et al. 2000
	--	--	OxA-468	284.29	470	11090	150	13000	160	**Yes**	AMS	Charred bone	Moore, et al. 2000
	--	--	OxA-883	284.29	470	11450	300	13370	300	--	AMS	Charred grain	Moore, et al. 2000
Blackville	33.361545°N	98	LB862	107	--	--	--	11500	1030	--	OSL	Quartz grains	This paper*
	81.304348°W	--	LB861	152	--	--	--	18540	1680	--	OSL	Quartz grains	This paper*
	--	--	LB859	183	--	--	--	12960	1190	**Yes**	OSL	Quartz grains	This paper*
Melrose	41.925350°N	419	LB860a	28	--	--	--	16400	1600	**Yes**	OSL	Quartz grains	This paper*
	75.510066°W	--	--	--	--	--	--	--	--	--	--	--	--

*OSL Dating by: IIRMES laboratory, California State University Long Beach.

SI Table 3. Abundances of Proxies. This table shows midpoint depth in cm relative to YDB, thickness of layers, magnetic grain (MGr) abundances in g/kg, spherules (MSp) in #/kg, and SLOs in g/kg.

Abu Hureyra, SYR					Blackville, SC					Melrose, PA				
Cm	Thick	MGr	MSp	SLO	Cm	Thick	MGr	MSp	SLO	Cm	Thick	MGr	MSp	SLO
290	5.00	--	--	0.04	76	15	1.20	190	0.00	9	10	6.96	310	0.76
78	5.00	129	0	0.23	61	15	1.10	115	0.01	0	8	2.71	3110	0.80
0	5.00	74	595	15.76	46	15	1.10	90	0.00	-6	5	4.18	1190	0.05
-12	5.00	182	0	0.02	30	15	0.10	70	0.04	-14	10	11.06	70	0
					15	15	1.30	205	0.03	-24	10	0.66	210	0
					0	15	1.30	525	0.06					
					-15	15	1.70	0	0.00					
					-30	15	4.00	0	0.00					
					-46	15	4.40	2	0.00					
					-61	15	1.40	0	0.00					
					-76	15	1.40	5	0.00					

SI Table 4. Average oxide abundances for SLOs, spherules, and bulk sediment in wt% by site. Crustal abundances are also listed. Some bulk sediment values from Firestone *et al.* (2007, 2010).

Type	SITE	Al_2O_3	CaO	Cr_2O_3	FeO^T	K_2O	MgO	MnO	Na_2O	NiO	P_2O_5	SiO_2	SO_3	TiO_2
SLOs	Abu Hureyra	5.97	15.17	0.14	6.30	1.53	5.06	0.17	1.17	0.05	3.76	59.44	0.54	0.69
	Blackville	27.66	1.92	0.04	12.56	3.13	1.02	0.08	0.51	0.15	0.25	51.13	0.11	1.45
	Melrose	25.92	1.90	0.07	10.13	2.87	2.12	0.31	0.83	0.09	0.30	53.16	0.4	1.92
	SLOs AVG:	**19.85**	**6.33**	**0.08**	**9.66**	**2.51**	**2.73**	**0.18**	**0.84**	**0.10**	**1.44**	**54.58**	**0.35**	**1.35**
	Crustal Values	**15.42**	**4.00**	**0.01**	**5.34**	**3.10**	**2.77**	**0.08**	**3.33**	**0.00**	**0.17**	**65.16**	**0.00**	**0.63**
Spherules	Abu Hureyra	8.97	10.06	0.03	11.51	2.58	4.85	0.29	1.56	0.06	1.55	56.94	0.93	0.66
	Blackville	22.85	1.80	0.00	21.39	2.44	1.05	0.04	0.24	0.05	0.19	49.00	0.00	0.96
	Melrose	21.06	1.50	0.12	32.00	1.70	0.63	0.11	0.86	0.11	0.49	39.80	0.39	1.24
	Spher. AVG:	**17.63**	**4.45**	**0.05**	**21.63**	**2.24**	**2.18**	**0.15**	**0.89**	**0.07**	**0.74**	**48.58**	**0.44**	**0.95**
	Crustal Values	**15.42**	**4.00**	**0.01**	**5.34**	**3.10**	**2.77**	**0.08**	**3.33**	**0.00**	**0.17**	**65.16**	**0.00**	**0.63**
Bulk Sed	Abu Hureyra	10.51	25.70	0.24	12.42	3.49	6.88	0.77	1.00	0.02	2.02	31.37	4.10	1.48
	Blackville	20.61	0.41	0.09	10.22	0.74	0.00	0.32	0.00	0.00	2.26	61.27	1.88	2.20
	Melrose	19.13	0.93	0.06	11.36	7.23	0.79	0.59	0.08	0.00	1.12	56.28	0.80	1.65
	Bulk AVG:	**17.63**	**4.45**	**0.05**	**21.63**	**2.24**	**2.18**	**0.15**	**0.89**	**0.07**	**0.74**	**48.58**	**0.44**	**0.95**
	Crustal Values	**15.42**	**4.00**	**0.01**	**5.34**	**3.10**	**2.77**	**0.08**	**3.33**	**0.00**	**0.17**	**65.16**	**0.00**	**0.63**

SI Table 5. DATA SOURCES for TERNARY DIAGRAMS of cosmic, anthropogenic, volcanic, and impact-related materials. Materials are shown by type, sampling location, number of sites, number of analyses per site, and references. Note: "Micromet." equals "micrometeorites."

TYPE	LOCATION or TYPE	SITES	ANAL.	REFERENCE
ANTHROPOGENIC				
Spherules	USA	1	42	This paper
Fly ash	AUS	27	6	Provis, 2009
	AUS		14	Ward, 2006
	BUL		3	Shoumkova, 2006
	CAN, JAP, USA, UK, FRA		5	Gikunoo, 2004
	CHN		2	Gao, 2004
	CHN		3	Yijin, 2004
	CZE		1	Sulc, 2009
	EST		1	Marini, 2009
	IND		11	Chandra, 2009
	IND		9	Mandal, 2006
	IND		25	Natarajan, 2007
	IND		2	Sivakumar, 2009
	ISR, CHN, USA, GER, JOR		10	Oymael, 2007
	JAP, PHL, THA		6	Yamada, 2001
	NLD		1	Nugteren, 2009
	NZL, AUS		2	Keyte, 2004
	POL		12	Jablonska, 2003
	POL		10	Uscinowicz, 2009
	S.AFR		1	Muriithi, 2009
	SPN		13	Acosta, 1997
	SPN, NLD, GRE, ITA		23	Towler, 2002
	TWN		1	Wang, 2003
	UK		5	Snelson, 2007
	USA		7	Bhatty, 2001
	USA		2	Giere, 2003
	USA		19	Jewell, 2009
	USA		5	McKeen, 1998
	USA		13	White, 2005
	USA, TUR, POL, PRT, CHN, ITA, SPN, EGY, IND		13	Rawlings, 2006
	TOTAL ANTHROPO:	**28**	**267**	
VOLCANIC				
Glass	Atlantic, Pacific, Indian, Carib.	193	10026	Melson, 2002
Spherules	Pacific	2	57	Melson, 1988
	Pacific		119	Vallier, 1977
Tephra	Andean volcanoes (3)	10	19	Kilian, 2003
	Crater Lake		21	Bruggman, 1993
	Glacier Peak, St. Helens		8	Carrara, 1992
	Glacier Peak, St. Helens		124	Hallett, 2001
	Iceland		31	Wastegard, 2001
	Laacher See		17	Worner, 1984
	Minoan tephra		183	Weiss, 1993
	St. Helens		2	Fiacco, 1993
	Toba; Pacific Ocean		24	Mascarenhas, 2006
	TOTAL VOLCANIC:	**205**	**10631**	

TYPE	LOCATION or TYPE	SITES	ANAL.	REFERENCE
COSMIC				
Spherules	Antarctica	3	20	Engrand, 1999
	Antarctica		71	Genge, 1997
	Antarctica		20	Genge, 1998
	Antarctica		14	Rochette, 2008
	Antarctica		279	Taylor, 2000,2002
	Antarctica		14	Rochette, 2008
	Atlantic Ocean		45	Dekov, 2007
	Greenland		8	Maurette, 1986
Micromet.	Antarctica	80	21	Engrand, 1999
	Antarctica		86	Genge, 1997
	Antarctica		78	Kurat, 1994
	Meteorites, misc.		77	Genge, 1999
	TOTAL COSMIC:	**83**	**733**	
IMPACTS				
Ejecta	KPg	2	15	Bauluz, 2004
	KPg		12	Koeberl, 1992
	Rio Cuarto		3	Bland, 2002
Spherules	Lonar Crater, IND	3	40	Misra, 2009
	Nuussuaq, Greenland		79	Jones, 2005
	Tunguska, Russia		13	Dolgov, 1973
	Tunguska, Russia		4	Glass, 1969
Tektites	Australasian tektite field	7	6	Amare, 2006
	Australasian tektite field		2	Chalmers,1976
	Australasian tektite field		47	Folco, 2008
	Australasian tektite field		48	Glass, 1990
	Australasian tektite field		47	Glass, 2004
	Australasian tektite field		16	Glass, 2006
	Australasian tektite field		19	Koeberl, 1992
	Australasian tektite field		30	Lee, 2004
	Australasian tektite field		11	Son, 2005
	Bahia Blanca, Argentina		2	Schultz, 2004
	Chesapeake Bay crater		2	Glass, 1990
	Chesapeake Bay crater		28	Glass, 1998
	Chesapeake Bay crater		130	Kelly, 2004
	Chesapeake Bay crater		16	Koeberl, 1998
	Chesapeake Bay crater		7	Koeberl, 2001
	Chesapeake Bay crater		46	McHugh, 1996
	Chesapeake Bay crater		18	McHugh, 1998
	Chesapeake Bay crater		7	Povenmire, 1994
	Chesapeake Bay crater		3	Povenmire, 1997
	Darwin glass		18	Koeberl, 1990
	Lake Botsumtwi crater		1	Glass, 1990
	Lake Botsumtwi crater		5	Koeberl, 2006
	Lake Botsumtwi crater		194	Koeberl, 2007
	Lake Botsumtwi crater		30	Luetke, 2008
	Ries crater--moldavites		1	Glass, 1990
	Ries crater--moldavites		118	Trnka, 2002
	Zhamanshin crater		4	Zolensky, 1991
	TOTAL IMPACT:	**12**	**1018**	

REFERENCES

Acosta A, Aineto M, Iglesias I, Romero I, Rincon JM. (2001) Physico-chemical characterization of slag waste coming from IGCC thermal power plant. *Mater Lett,* 50: 246-250.

Amare K and Koeberl C. (2006) Variation of chemical composition in Australasian tektites from different localities in Vietnam. *Meteoritics & Planetary Science* 41, Nr 1, 107–123.

Baker DW, Miranda PJ, Gibbs KE. (2008) Montana Evidence for Extra-Terrestrial Impact Event That Caused Ice-Age Mammal Die-Off. American Geophysical Union, Spring Meeting 2008, abstract #P41A-05.

Bauluz B, Peacor DR, and Hollis CJ.(2004) TEM study of meteorite impact glass at New Zealand Cretaceous-Tertiary sites: evidence for multiple impacts or differentiation during global circulation? *Earth and Planetary Science Letters* 219, 209-219.

Berg TM, *et al.* (1980) Geologic map of Pennsylvania: Pennsylvania Geological Survey, 4th ser., Map 1, 2nd ed., 3 sheets, scale 1:250,000.

Bhatty JI, Gadja J, Miller FM. (2001) Commercialization of High-Carbon Fly Ash in Cement Manufacture; Report No. 00-1/3 1A-1; Illinois Clean Coal Institute: Canterville, IL.

Bland PA, *et al.* (2002) A Possible Tektite Strewn Field in the Argentinian Pampa. *Science* 296, 1109.

Boslough MBE and Crawford DA (2007) Low altitude airbursts and the impact threat. Proc. Hypervelocity Imp. Sym.

Bruggman PE, Bacon CR, Mee JS, Pribble ST, Siems DF. (1993) Chemical Analyses of pre-Mazama Silicic Volcanic Rocks, Inclusions, and Glass Separates, Crater Lake, Oregon. USGS. Open-file Report 93-314.

Carrara PE and Trimble DA. (1992) A Glacier Peak and Mount Saint Helens J volcanic ash couplet and the timing of deglaciation in the Colville Valley area, Washington: *Canadian Journal of Earth Sciences*, v. 29, no. 11, p. 2397-2405.

Carter EA, Hargreaves MD, Kee TP, Pasek MA, Edwards HGM. (2010) A Raman spectroscopic study of a fulgurite. *Phil. Trans. R. Soc. A*, 368, 3087-3097.

Casson MA and Feathers JK. (2001) The Application of Luminescence Dating to Cultural Resource Management. Society for American Archaeology, New Orleans, LA.

Chalmers RO, Henderson EP, Mason B. (1976) Occurrence, Distribution, and Age of Australian Tektites. *Smithsonian Contributions To The Earth Sciences,* Number 17.

Chandra A, Kumar S, and Kumar S. (2004) Investigations on fly ash Resistivity of varieties of Coals used in Indian power plants. Proceeding, 9th International Conference on Electrostatic Precipitation, Mpumalanga, South Africa B-05.

Chao ECT, Adler I, Dwornik EJ, Littler J. (1962) Metallic spherules in tektites from Isabella, the Philippine Islands. *Science* 135, 97–98.

Colgan PM, Mickelson DM, & Cutler PM. (2003) Ice-Marginal Terrestrial Landsystems: Southern Laurentide Ice Sheet, in Evans, D.A. and Rea, B.R., (eds.), *Glacial Landsystems*, Edwin Arnold, London, 111-142.

Daode W and Yongheng C. (1996) The chemical compositions of Antarctic iron meteorites and their classification. *Advances in Polar Science* 1996, 7(1) 41-49.

Dekov VM, *et al.* (2007) Cosmic spherules from metalliferous sediments:A long journey to the seafloor. *N. Jb. Miner. Abh.,* Vol.183/3, p. 269–282.

Dolgov YA, Vassil'ev AN, Shugurova NA, Lavrent'ev YG, L'vov YA. (1973) The composition of the microscopic spherules from the fallsite of the Tunguska meteorite. *Meteoritika*, 2, 147-149.

Elkins-Tanton LT, Aussillous P, Bico J, Quere D, and Bush JWM. (2003) A laboratory model of splash-form tektites. Meteoritics & Planetary Science 38, Nr 9, 1331–1340.

Engrand C, Deloule E, Robert F, Maurette M, Kurat G. (1999) Extraterrestrial water in micrometeorites and cosmic spherules from Antarctica: An ion microprobe study. *Meteoritics & Planetary Science* 34, 773-786.

Fayek M, Anovitz LM, Allard LF, Hull S, Haynes, CV Jr. (2012) Framboidal iron oxide: chondrite-like material from the black mat, Murray Springs, Arizona. *Earth and Planetary Science Letters*, 319-320, 251-258.

Fayek M, Hull S, Anovitz L, Haynes CV Jr, Bergen L. (2008) Evidence of impact material and the extinction of the mega-fauna 12,900 years ago. American Geophysical Union, Fall Meeting 2008, abstract #PP13C-1469.

Feathers JK. (2003) Use of luminescence dating in archaeology. *Measurement Science and Technology* 14:1493-1509.

Ferraro D and Bergin K. (2007) *Talega Site Report.* Viejo California Associates, Mission Viejo, CA.

Fiacco RJ J., Palais JM, Germani MS, Zielinski GA, and Mayewski PA. (1993) Characteristics and possible source of a 1479 A.D. volcanic ash layer in a Greenland ice core. *Quaternary Research* 39, 267–273.

Firestone RB, *et al.* (2007) Evidence for an extraterrestrial impact 12,900 years ago that contributed to the megafaunal extinctions and the Younger Dryas cooling. Proc Natl Acad Sci USA 104:16016–16021.

Firestone RB, *et al.* (2010) Analysis of the Younger Dryas Impact Layer. Journal of Siberian Federal University. Engineering & Technologies 1 (2010 3) 30-62.

Florenskiy KP. (1963) Preliminary Results From The 1961 Combined Tunguska Meteorite Expedition. Tenth Conference on Meteorites in May 1962, *Meteoritica*, Vol. XXIII.

Folco L, *et al.* (2008) Microtektites from Victoria Land Transantarctic Mountains. *Geology*, Vol. 36, No. 4, 291-294.

Forman S. (2002) OSL Dating and Topper. Paper presented at the Allendale-Topper Conference, Columbia, South Carolina.

French BM. (1998) Traces of Catastrophe. LPI Contribution No. 954, 102-103.

Fullerton DS, Bush CA, Pennell JN. (2003) Surficial deposits and materials in the eastern and central United States (east of 102 degrees west longitude) *U.S. Geological Survey Geologic Investigations Series, I-2789*, Edition: 1.0, U.S. Geological Survey, Denver, CO.

Gao L-X, Yao Y, and Wang L. (2004) Research on sintered fly ash aggregate of high strength and low absorption of water. Proceedings of International workshop on Sustainable development and Concrete Technology, 151-157.

Genge M and Grady M. (1998) Melted micrometeorites from Antarctic ice with evidence for the separation of immiscible Fe-Ni-S liquids during entry heating. *Meteoritics &Planetary Science* 33, 425-434.

Genge M and Grady M. (1999) The fusion crusts of stony meteorites: Implications for the atmospheric reprocessing of extraterrestrial materials. *Meteoritics & Planetary Science* 34, 341-356.

Genge MJ, Grady M, and Hutchison R. (1997) The textures and compositions of fine-grained Antarctic micrometeorites: Implications for comparisons with meteorites. *Geochimica et Cosmochimica Acta*, Vol. 61, No. 23, 5149-5162.

Giere R, Carleton LE, and Lumpkin GR. (2003) Micro- and nanochemistry of fly ash from a coal-fired power plant. *American Mineralogist*, Volume 88, pages 1853–1865.

Gikunoo E. (2004) *Effect of Fly Ash Particles on the Mechanical Properties and Microstructure of Aluminium Casting Alloy A535.* Thesis, Department of Mechanical Engineering, University of Saskatchewan, CAN.

Glass BP and Koeberl C. (2006) Australasian microtektites and associated impact ejecta in the South China Sea and the Middle

Pleistocene supereruption of Toba. *Meteoritics & Planetary Science* 41, Nr 2, 305–326.

Glass BP, Huber H, and Koeberl C. (2004) Geochemistry of Cenozoic microtektites and clinopyroxene-bearing spherules. *Geochimica et Cosmochimica Acta* 69, 3971-4006.

Glass BP. (1969) Silicate Spherules from the Tunguska Impact Area: Electron Microprobe Analysis, *Science* 164, 547-549.

Glass BP. (1990) Tektites and microtektites: key facts and inferences. In: Nicolaysen LO and Reimold WU (Editors), *Cryptoexplosions and Catastrophes in the Geological Record, with a Special Focus on the Vredefort Structure*. 171: 393-404.

Glass, BP and Koeberl C. (1999) Ocean Drilling Project Hole 689B spherules and upper Eocene microtektites and clinopyroxene-bearing spherule strewn fields. *Meteoritics & Planetary Science 34*, 197-208.

Gnos E, *et al.* (2004) Pinpointing the Source of a Lunar Meteorite: Implications for the Evolution of the Moon. *Science*, Vol. 30530, 657-659.

Grachev AF, Korchagin OA, Tselmovich VA, Kollmann HA. (2008) Cosmic dust and micrometeorites in the transitional clay layer at the Cretaceous-Paleogene boundary in the gams section (Eastern Alps): Morphology and chemical composition. Izvestiya, *Physics of the Solid Earth*, Vol. 44, No. 7, 555–569.

Hallett DJ, Mathewes RW, and Foit FF Jr. (2001) Mid-Holocene Glacier Peak and Mount St Helens We tephra layers detected in lake sediments from southern British Columbia using high resolution techniques. *Quaternary Research*, 55: 284-292.

Haynes CV Jr, *et al.* (2010a) The Murray Springs Clovis site, Pleistocene extinction, and the question of extraterrestrial impact. *Proc Natl. Acad. Sci. USA*, 107(9), 4010-4015.

Hillman G, Hedges R, Moore A, Colledge S, and Pettitt P. (2001) New evidence of Lateglacial cereal cultivation at Abu Hureyra on the Euphrates. *The Holocene* 11, 4, 383-393.

Horton, JW, and Dicken CL. (2001) Preliminary Geologic Map of the Appalachian Piedmont and Blue Ridge, South Carolina Segment: U.S. Geological Survey, Open-File Report 01-298, CD.

Jablonska M and Smola-Danielowska D. (2003) Aluminosilicate particles in fly ash and atmospheric dust. Mineralogical Society of Poland special papers 22, 82-89.

Jewell RB and Rathbone RF. (2009) Optical Properties of Coal Combustion Byproducts for Particle-Size Analysis by Laser Diffraction. *Coal Combustion and Gasification Products*, Vol. 1, 1-7.

Jones AP, *et al.* (2005) Are there signs of a large Paleocene impact, preserved around Disko Bay, West Greenland?: Nuussuaq spherule beds origin by impact instead of volcanic eruption?, in Kenkmann, T., Hörz, F., and Deutsch, A., eds., Large meteorite impacts III: *Geological Society of America Special Paper* 384.

Kelly DC and Elkins-Tanton LT. (2004) Bottle-green microtektites from the South Tasman Rise: Deep-sea evidence for an impact event near the Miocene/Pliocene boundary. *Meteoritics & Planetary Science* 39, Nr 12, 1921–1929.

Keyte LM, Lukey GC, and van Deventer JSJ. (2004) The Effect of Coal Ash Composition on Properties of Wastebased Geopolymers. International Symposium of Research Students on Material Science and Engineering, Chennai, India.

Kilian R, Hohner M, Biester H, Wallrabe-Adams HJ, and Stern CR. (2003) Holocene peat and lake sediment tephra record from the southernmost Chilean Andes (53-55°S). *Revista Geológica de Chile*, Vol. 30, No. 1, p. 23--37.

Kirova OA and Zaslavskaya NI. (1966) Data characterizing the dispersed matter as recovered from the area of fall of the Tunguska meteorite. *Meteoritika*, 27, 119-127.

Koeberl C (2007) The geochemistry and cosmochemistry of impacts. In: *Treatise of Geochemistry*, Vol. 1 (ed. A. Davis), Elsevier, p. 1.28.1 -1.28.52.

Koeberl C and Glass BP. (1988) Chemical composition of North American microtektites and tektite fragments from Barbados and DSDP Site 612 on the continental slope off New Jersey. *Earth and Planetary Science Letters,* 87, 286 292.

Koeberl C and Sigurdsson H. (1992) Geochemistry of impact glasses from the K/T boundary in Haiti: Relation to smectites, and a new type of glass. *Geochimica et Cosmochimica Acta* 56, 2113- 2129.

Koeberl C, Brandstätter F, Niedermayr G, and Kurat G. (1988) Moldavites from Austria. Meteoritics 23, 325-332.

Koeberl C, *et al.* (2006) Uppermost Impact Fallout Layer in a Drillcore at the Bosumtwi Impact Crater (Ghana): A Preliminary Study. 37th Annual Lunar and Planetary Science Conference, March 13-17, 2006, League City, Texas, abstract no.1552.

Koeberl C, Kruger FJ, and Poag CW. (2001) Geochemistry of surficial sediments near the Chesapeake Bay impact structure and the search for source rocks of the North American Tektites. *Lunar and Planetary Science* XXXII.

Koeberl C. (1992) Geochemistry and origin of Muong Nong-type tektites. *Geochimica et Cosmochimica Acta* 56, 1033-1064.

Koeberl C. (1998) Identification of meteoritical components in impactites. In: *Meteorites: Flux with Time and Impact Effects;* Grady, M.M., Hutchison, R., McCall, G.J.H., and Rothery, D.A., (Eds.), Geological Society of London, Special Publication 140, 133-152.

Koeberl C. (2007) The geochemistry and cosmochemistry of impacts. In: *Treatise of Geochemistry*, Vol. 1 (ed. A. Davis), Elsevier, p. 1.28.1 -1.28.52, doi:10.1016/B978-008043751-4/00228-5.

Koeberl C., 1990. The geochemistry of tektites, an overview. In: L.O. Nicolaysen and W.V. Reimold (Editors), Cryptoexplosions and Catastrophes in the Geological Record, with a Special Focus on the Vredefort Structure. *Tectonophysics*, 171: 405-422.

Kolesnikov EM, Kolesnikova NV. (2010) Traces of cometary material in the area of the Tunguska impact (1908). *Solar System Research* 44, 110-121.

Kulik LA. (1940) The meteorite expedition to Podkamennaya Tunguska in 1939. *Comptes Rendus De L Academie Des Sciences De L Urss* 28, 596-600.

Kurat G, Koeberl C, Presper T, Brandstätter F, Maurette M. (1994) Petrology and geochemistry of Antarctic micrometeorites. *Geochimica et Cosmochimica Acta,* vol. 58, Issue 18, 3879-3904.

LeCompte MA, Goodyear AC, Demitroff M, Batchelor D, Mooney C. (2010) An Independent Review of the Younger Dryas Extraterrestrial Impact Hypothesis and its Recent Re-Evaluation by Surovell *et al.* 21st Biennial Meeting of the American Quaternary Association (AMQUA). Laramie, Wyoming.

Lee MY, Chen C-H, Wei K-Y, Iizuka Y, Carey S. (2004) First Toba supereruption revival. *Geology* 32, 61–64.

Lodders K and Fegley B. (1998) *The Planetary Scientist's Companion*. Oxford Univ. Press, Oxford, 314-316.

Luetke S, Deutsch A, Berndt J, Langenhorst F. (2008) Trace Elements in Ivory Coast Tektites, Microtektites, and Fallback Particles of the Lake Bosumtwi Impact Crater, Ghana: A LA-ICP-MS Study. 39th Lunar and Planetary Science Conference, (Lunar and Planetary Science XXXIX), held March 10-14, 2008 in League City, Texas. LPI Contribution No. 1391., p.1613.

Mahaney WC, *et al.* (2010b) Evidence from the northwestern Venezuelan Andes for extraterrestrial impact: The black mat enigma. *Geomorphology*, v. 116, iss. 1-2, p. 48-57.

Mahaney WC, *et al.* (2011a) Fired glaciofluvial sediment in the northwestern Andes: Biotic aspects of the Black Mat. *Sedimentary Geology*. 237, (1-2), 73-83.

Mahaney WC, *et al.* (2011b) Notes on the black mat sediment, Mucunuque Catchment, northern Mérida Andes, Venezuela. *Journal of Advanced Microscopic Research*, vol. 6, no. 3.

Mahaney WC, Krinsley D, Kalm V (2010a) Evidence for a cosmogenic origin of fired glaciofluvial beds in the northwestern Andes: Correlation with experimentally heated quartz and feldspar. *Sedimentary Geology*, v. 231, iss. 1-2, p. 31-40.

Mandal A and Sengupta D. (2006). An assessment of soil contamination around coal- based thermal power plant in India, *Environmental Geology*, 51 (3) 409-420.

Marini F and Raukas A. (2009) Lechatelierite-bearing microspherules from semicoke hill (Kiviõli, Estonia): contribution to the contamination problem of natural microtektites. *Oil Shale* 26(3), 415-423.

Mascarenhas-Pereira, MBL, Nath BN, Borole DV, Gupta SM. (2006) Nature, source and composition of volcanic ash in sediments from a fracture zone trace of Rodriguez Triple Junction in the Central Indian Basin. *Marine Geology,* vol.229, 79–90.

Maurette M, Hammer C, Reeh N, Brownlee DE, Thomsen HH. (1986) Placers of cosmic dust in the blue ice lakes of Greenland. *Science* (ISSN 0036-8075), vol. 233, Aug. 22, 1986, p. 869-872.

McDonough WF. (1998). Earth's core. *In: Encyclopedia of geochemistry.* Marshall, C.P. and Fairbridge, R.W. (Editors), Kluwer Academic Publishers, Dordrecht. 151-156.

McHugh CMG, *et al.* (1996) Upper Eocene tektites of the New Jersey continental margin, Site 904. In: Mountain G. S., Miller K. G., Blum P., Poag C. W. and Twichell D. C. (eds). Proceedings of the Ocean Drilling Program, Scientific Results. United States Government Printing Office, Washington, D.C. USA. 150: 241-265.

McHugh CMG., Snyder SW, Miller KG. (1998) Upper Eocene ejecta of the New Jersey continental margin reveal dynamics of Chesapeake Bay impact. *Earth and Planetary Science Letters.* 160 (3-4): 353-367.

McKeen RG, Lenke LR, Pallachulla KK. (1998), Mitigation of Alkali Silica Reactivity in New Mexico. Materials Research Center, University of New Mexico, Albuquerque, NM.

Melson WG, O'Hearn T, and Jarosewich E. (2002) A data brief on the Smithsonian Abyssal Volcanic Glass Data File. *Geochemistry Geophysics Geosystems*, Vol. 3 No. 4, 10.

Melson WG, O'Hearn T, Fredriksson K. (1988) Composition and Origin of Basaltic Glass Spherules in Pelagic Clay from the Eastern Pacific. *Marine Geology*, 83 (1988) 253-271.

Misra S, *et al.* (2009) Geochemical identification of impactor for Lonar crater, India. *Meteoritics & Planetary Science*, vol. 44, Issue 7, p.1001-1018.

Mittlefehldt DW. (2004). Achondrites. In: *Treatise on Geochemistry*. Holland, H.D. and Turekian, K.K. (Editors), Elsevier, Amsterdam. 291-324.

Moore AMT and Hillman GC. 1992. The Pleistocene to Holocene transition and human economy in Southwest Asia: the impact of the Younger Dryas. *American Antiquity* 57, 3, 482-494.

Moore AMT, *et al.* (1986) Radiocarbon accelerator (AMS) dates for the epipaleolithic settlement at Abu Hureyra, Syria. *Radiocarbon* 28(3): 1068-1076.

Moore AMT, Hillman GC, and Legge AJ. (2000) *Village on the Euphrates*. Oxford University Press: New York, 585 pages.

Muriithi GN, Gitari MW, Petrik LF. (2009) Brine Remediation using Fly Ash and Accelerated Carbonation. In: Water Institute of Southern Africa & International Mine Water Association: Proceedings, International Mine Water Conference, 671-679.

Murray AS and Wintle AG. (2000) Luminescence dating of quartz using an improved single-aliquot regenerative-dose protocol. *Radiation Measurements* 32 (1): 57-73.

Nataraja MC, Jayaram MA, Raikumar, CN. (2007) Inductive Classifying Artificial Network for Fly Ash Type Categorization. *Engineering Letters,* 14:1, EL_14_1_28.

Newsom HE. (1995) Composition of the Solar System, Planets, Meteorites, and Major Terrestrial Reservoirs. In *Global earth physics, a handbook of physical constants.* Edited by Thomas J. Ahrens. American Geophysical Union, AGU reference shelf Series, vol no 1, 159-189.

Nugteren HW, Butselaar-Orthlieb VCL, Izquierdo M. (2009) High Strength Geopolymers Produced from Coal Combustion Fly Ash. *Global NEST Journal*, Vol 11, No 2, 155-161.

Oymael S. (2007) Suitability of Oil Shale Ash as a Constituent of Cement. Oil Shale, Vol. 24, No. 1, 45–58.

Poag CW, Koeberl C, and Reimold WU. (2004) *The Chesapeake Bay Crater: Geology and Geophysics of a Late Eocene Submarine Impact Structure.* New York: Springer, 522 pages.

Povenmire H, Chance S. (1997) Tektite from Jenkins County, Georgia. 28th Annual Lunar and Planetary Science Conference, March 17-21, 1997, Houston, TX, p. 1135.

Povenmire H, Glass BP, Strange RL. (1994) Discovery and description of a Muong Nong-type Georgia tektite. Abstracts of the Lunar and Planetary Science Conference. 25th: 1101-1102.

Pigati, JS, *et al*. (2012) Accumulation of "impact markers" in desert wetlands and implications for the Younger Dryas impact hypothesis. *Proc. Natl. Acad. Sci. USA* (in press).

Prasad MS and Khedekar VD. (2003) Impact microcrater morphology on Australasian microtektites. *Meteoritics & Planetary Science* v.38, 1351-1371.

Prasad MS, Roy SK, Gupta A. (2010) Changes in abundance and nature of microimpact craters with distance from the proposed source crater location. Meteorit Planet Sci, 45, 6, 990-1006.

Provis JL, Duxson P, Harrex RM, Yong C-Z, Van-Deventer SJ. (2009) Valorisation of fly ashes by geopolymerisation. *Global NEST Journal* 11 (2) : 147-154.

Rawlings, RD, Wu, JP, Boccaccini, AR.(2006) Glass-ceramics: Their production from wastes-a review. J Materials *Science* 41 (3) 733 - 761.

Renssen H, Isarin RFB, Vandenberghe J. (2001) Rapid climatic warming at the end of the last glacial: new perspectives. *Global and Planetary Change* 30, 1-2, 155-165.

Robinson SA, Black S, Sellwood BW, Valdes PJ. (2006) A review of palaeoclimates and palaeoenvironments in the Levant and Eastern Mediterranean from 25,000 to 5000 years BP: setting the environmental background for the evolution of human civilisation. *Quaternary Science Reviews* 25, 13-14, 1517-1541.

Rochette P. (2008) Micrometeorites from the Transantarctic Mountains. *Proc Natl. Acad. Sci. USA* November 25, 2008 vol. 105 no. 47 18206-18211.

Schultz P. (2004) The Quaternary impact record from the Pampas, Argentina. *Earth and Planetary Science Letters* 219 (2004) 221-238.

Schultz PH, *et al.* (2006) The record of Miocene impacts in the Argentine Pampas. *Meteoritics & Planetary Science* 41: 749-771.

Scruggs, MA, Raab LM, Murowchick JS, Stone MW, Niemi TM. (2010) Investigation of Sediment Containing Evidence of the Younger Dryas Boundary (YPB) Impact Event, El Carrizal, Baja California Sur, Mexico. *Geological Society of America Abstracts with Programs*, Vol. 42, No. 2, p. 101.

Sheffer AA, Dyar MD, Sklute EC (2006) Lightning strike glasses as an analog for impact glasses: 57Fe Mössbauer Spectroscopy of Fulgurites. 37th Annual Lunar and Planetary Science Conference, March 13-17, 2006, League City, Texas, abstract no.2009.

Shoumkova AS. (2006) Physico-Chemical Characterization and Magnetic Separation of Coal Fly Ashes from "Varna," "Bobov Dol" And "Maritza-Istok I" Power Plants, Bulgaria: Physico-Chemical Characteristics. *Journal of the University of Chemical Technology and Metallurgy,* 41, 2, 175-180.

Simons DL, Shott MJ, Wright HT. (1984) The Gainey site: variability in a Great Lakes Paleo-Indian assemblage. *Archaeology of Eastern North America* 12, 266-279.

Sivakumar G, Mohanraj K, and Barathan S. (2009) Dielectric Study on Fly Ash Blended Cement. *E-Journal of Chemistry,* 6(1), 231-236.

Snelson DG, Kinuthia JM, Davies P, Chang S-R. (2007) Sustainable road construction in the United Kingdom: Combined use of waste tyres and PFA. The 9th International Conference, Modern Building Materials, Structures and Techniques, 168-173.

Son TH, Koeberl C. (2005) Chemical variation within fragments of Australasian tektites. Meteoritics & Planetary *Science* 40, Nr 6, 805–815.

Sponholz B, Baumhauer R, and Felix-Henningsen P. (1993) Fulgurites in the southern Central Sahara, Republic of Niger, and their palaeoenvironmental significance. The Holocene, 3,2, 97-104.

Sponholz B. (2004) Fulgurites as palaeoclimatic indicators—the proof of fulgurite fragments in sand samples. In Paleoecology of Quaternary Drylands, Lecture Notes in Earth Sciences, Felix-Henningsen P (ed), Springer, Berlin/Heidelberg, 102, pp. 73–78.

Sulc R. (2009) Effect of Water Ratio in Fly-Ash Concrete on the Process of Alkali Activation. In Mlady vedec [CD-ROM]. Košice: Technická universita v Košiciach, Stavebná fakulta.

Svetsov VV. (2006) Thermal radiation on the ground from large aerial bursts caused by Tunguska-like impacts. LPSC 37th, 1553.

Taylor LA, *et al.* (2002) Martian meteorite Dhofar 019: A new shergottite. *Meteoritics & Planetary Science* 37, 1107–1128.

Taylor S. (2002) Micrometeorites from the South Pole water well. Boulder, CO, USA: National Snow and Ice Data Center.

Taylor SR and McLennan SM. (1985) *The continental crust: Its composition and evolution.* Oxford: Blackwell Scientific Publications, 312 pages.

Towler MR, *et al.* (2002) Modelling of the glass phase in fly ashes using network connectivity theory. International Workshop on Novel Products from Combustion Residues, 240-245.

Trnka M and Houzar S. (2002) Moldavites: a review. *Bulletin of the Czech Geological Survey,* Vol. 77, No. 4, 283–302.

Uścinowicz G. (2009) Micro-scale magnetic grains from shallow water sediments of the Gulf of Gdańsk. *Journal of Oceanography and Hydrobiology*. Vol. XXXVIII, No.4, 21-30.

USGS. (2001) Geochemistry of soils in the US from the PLUTO database: U.S. Geological Survey, Reston, VA.

Vallier T, Bohrer D, Moreland G, McKee EE. (1977) Origin of basalt microlapilli in lower Miocene pelagic sediment, northeastern Pacific Ocean. *Geol. Soc. Am. Bull.,* 88: 787-796.

van Geel B, Coope GR, and van der Hammen T. (1989) Palaeoecology and stratigraphy of the Lateglacial type section at Usselo (the Netherlands). *Rev. Palaeobot. Palynol.* 60: 25-129.

Vasilyev NV. (1998) The Tunguska Meteorite problem today. Planetary and Space Sciences, v.46, no.2/3, p.129-150.

Walter M. (2011) An Exogenic Fulgurite Occurrence in Oswego, Oswego County, New York. Rocks and Minerals, Vol. 86, 3, 264-270.

Wang JW and Cheng TW. (2003) Production geopolymer materials by coal fly ash. Proceedings of the 7th International Symposium on East Asian Resources Recycling Technology, Tainan, Taiwan.

Ward CR, French DH, Jankowski J, Riley KW, Li Z. (2006) Use of coal ash in mine backfill and related applications. Research report, Cooperative Research Centre for Coal in Sustainable Development, Australia, 62.

Wasilewski P, and Kletetschka G. (1999) Lodestone - Natures Only Permanent Magnet, what it is and how it gets charged, Geophysical Research Letters 26(15), 2275-227.

Wasson J. (2003) Large aerial bursts; an important class of terrestrial accretionary events. *Astrobiology*, 3(1): 163-179.

Wasson JT and Moore K. (1998) Possible formation of Libyan Desert Glass by a Tunguska-like aerial burst. *Metoritics and Planet. Sci* 33, A163.

Wastegård S, Bjorck S, Grauert M, Hannon GE. (2001) The Mjauvøtn tephra and other Holocene tephra horizons from the Faroe Islands: a link between the Icelandic source region, the Nordic Seas, and the European continent. *The Holocene* 11,1 (2001) 101–109.

Weiss H, *et al.* (1993) The Genesis and Collapse of Third Millennium North Mesopotamian Civilization. *Science*, Vol. 261, 995-1003.

White DJ, Harrington D, Thomas Z. (2005) Fly ash soil stabilization for non-uniform subgrade soils, Volume I: Engineering properties and construction guidelines. Iowa State University, Ames, IA: Center for Transportation Research and Education Iowa State University.

Winkler HGF. (1979) *Petrogenesis of Metamorphic Rocks.* Springer-Verlag, New York, 334 pages.

Wittke JH, *et al.* (2012) High-temperature, Iron-rich Microspherules from Three Continents: Evidence for an ET Impact at the Younger Dryas Onset (12.9 ka). *Proc Natl. Acad. Sci. USA* (in review).

Wörner G and Schmincke H-U. (1984) Mineralogical and chemical zonation of the Laacher See tephra sequence (East Eifel, FRG). *Journal of Petrology,* Vol. 25, Part 4, 805-835.

Wu Y. (2011) *Origin and Provenance of Magnetic Spherules at the Younger Dryas Boundary*. Thesis, Dartmouth College, NH.

Yamada K, *et al.* (2001) Removal of Phosphate from Aqueous Solution by Crystallization Using Coal Fly Ash. 2001 International Ash Utilization Symposium, Center for Applied Energy Research, University of Kentucky, Paper #7.

Yijin L, Shiqiong Z, Jian Y, Yingli G. (2004) The Effect of Fly Ash on the Fluidity of Cement Paste, Mortar, and Concrete. Proceedings of the International Workshop on Sustainable Development and Concrete Technology Beijing, China.

Zbik M. (1984) Morphology of the Outermost Shells of the Tunguska Black Magnetic Spherules. *J. Geophys. Res.,* vol. 89, B605-B611.

Zolensky, ME, Koeberl, C. (1991) Why are blue zhamanshinites blue? Liquid immiscibility in an impact melt. *Geochimica et Cosmochimica Acta* (ISSN 0016-7037), vol. 55, May 1991, p. 1483-1486.